MODEL PREDICTIVE CONTROL FOR PERMANENT MAGNET SYNCHRONOUS MOTOR DRIVES WITH IMPROVED TECHNIQUES TO MINIMIZE CURRENT RIPPLES

MODEL PREDICTIVE CONTROL FOR PERMANENT MAGNET SYNCHRONOUS MOTOR DRIVES WITH IMPROVED TECHNIQUES TO MINIMIZE CURRENT RIPPLES

BY

GUANGHAN ZHAO, B.SC.

A THESIS
SUBMITTED TO THE SCHOOL OF GRADUATE STUDIES
IN PARTIAL FULFILLMENT OF THE REQUIREMENTS
FOR THE DEGREE OF
MASTER OF APPLIED SCIENCE

McMaster University

Master of Applied Science (2019) McMaster University
(Electrical and Computer Engineering) Hamilton, Ontario, Canada

TITLE: **Model Predictive Control for Permanent Magnet Synchronous Motor Drives with Improved Techniques to Minimize Current Ripples**

AUTHOR: Guanghan Zhao
B. Sc., (Automation)
Southeast University, Nanjing, China

SUPERVISOR: Ali Emadi, Professor
Ph. D. (Texas A&M University)
IEEE Fellow
Canada Excellence Research Chair in Hybrid Powertrain

NUMBER OF PAGES: XIV, 121

To My Parents

ABSTRACT

Permanent Magnet Synchronous Motor (PMSM) is widely used in many industrial applications such as electric vehicles, industrial robotics and servo machines due to the merits of low volume, light weight, high efficiency, and high power density, etc. Finite Control Set Model Predictive Control (FCSMPC), as an advanced and promising control scheme, has attracted more and more attention in its use for PMSM drives due to its notable advantages like fast dynamic response, the ability of multi-variable control and the flexibility to include multiple constraints. However, the FCSMPC scheme suffers from certain drawbacks of large current ripples, which will lead to unexpected torque ripples and noise in the PMSM drive system. This thesis presents two FCSMPC methods for PMSM drives with improved techniques to minimize the current ripples.

First, an improved FCSMPC with integrated duty cycle and finite virtual voltage vector technique is proposed. The finite control set is expanded by introducing six symmetrically positioned virtual voltage vectors in addition to the six original active voltage vectors while the selected optimal non-zero voltage vector is applied in the regulated proportion of the sampling period according to an efficiently calculated duty ratio. By combining the concept of duty cycle and finite virtual voltage vector in the proposed technique, the control accuracy is distinctly improved while the current ripples are effectively reduced for the FCSMPC-controlled PMSM drives.

Second, an improved FCSMPC with continuous virtual voltage vector technique is proposed. At each sampling interval, the proposed technique applies a continuous virtual voltage vector that is realized by at most two suboptimal basic non-zero voltage vectors and one null voltage vector in proper duty cycle ratios. The continuous virtual voltage vector eliminates the error between the reference current and the actual current at each sampling instant and therefore achieves significant current ripple reduction for the FCSMPC-controlled PMSM drives.

The effectiveness of both proposed techniques is validated with the reference 5 KW IPMSM drives test bench under different conditions. Additionally, to better evaluate the effectiveness of the proposed techniques on reducing the current ripple, two conventional techniques are introduced and implemented with the reference IPMSM drives under the same conditions. It is found in the experimental results that the FCSMPC with the proposed techniques achieve better steady-state performance and much lower current ripples while maintaining similar transient responses as compared to the basic FCSMPC and the FCSMPC with conventional techniques.

ACKNOWLEDGEMENTS

First of all, I would like to express my sincerest gratitude to my supervisor, Dr. Ali Emadi, for offering me the opportunity to join in the world's leading academic research program and to work in the top team with so many brilliant engineers and researchers. His invaluable guidance, suggestions, and encouragement have always been the warm force that inspired me throughout my Master's study.

I would like to give my special thanks to Dr. Nalakath Shamsuddeen. He provided me with numerous insights and helped me forward to the right direction during my research. Thanks for all his patience, suggestions and support.

Moreover, this research was undertaken, in part, thanks to funding from Canada Excellence Research Chairs Program.

I am also grateful to my friends and lab colleagues, Zekun Xia, Jing Zhao, Rasul Tarvirdilu Asl, Parisa M. Shamsabadi, Alice Dong, Xueqing Wang, Dianxun Xiao, Gaoliang Fang and Yuhang Yang, etc. I will cherish the memory for all the great days I spent with them.

At last, I would like to express my profound gratitude and deepest love to my parents for their continuous support and endless love. They are the first and the best teachers in my life, who set the examples for me to be serious, hardworking and kind. I owe my achievement to their generous love and dedication.

CONTENT

LIST OF FIGURES

Chapter 1

INTRODUCTION

1.1 BACKGROUND AND MOTIVATION

Electric machine, as a key apparatus for the mutual conversion between the mechanic energy and electric energy, has played a more and more important role in the modern industry and daily life. According to relative statistics, the electric motor systems are currently the single largest electrical end use which accounts for 43% to 46% of the global electricity consumption [1] . Therefore, the researches on electric motors and the corresponding control techniques are directly relevant to the development, utilization and saving of the electric energy, which are increasingly import nowadays due to the power shortage.

Electric motors are categorized into two groups, direct current (DC) motors and alternating current (AC) motors. Moreover, the AC motors can be further divided into induction motors and synchronous motors according to the working principle and structures. In 1960s to 1970s, DC motor was widely adopted in various fields due to the advantages like wide speed and torque range and the ease of controlling the motor performance [2] . However, it suffers from certain drawbacks, such as the complex commutation structures with short

life, the abrasion and sparks happened with the commutations and the high requirement of maintenance [3] . These shortages severely limited the application of the DC motor. Specifically, they are not suitable to be used in explosive environment or high-speed operations [2] .

With the rapid development in control theories, power electronic techniques and the chip manufacturing in 1980s, the AC motor had been increasingly used in the industry. In contrast to the DC motors, AC motor requires no complex commutation structures, which provides higher reliability in normal use. Moreover, it enjoys the advantages of low cost and simple manufacturing, which attracts great attention of the modern industry. For the induction motors and conventional synchronous motors, the rotor field is generated by the rotor windings, which leads to the rotor power loss with the certain problem of heat dissipation. With the advent of the permanent magnet synchronous motors (PMSM), the effects of those drawbacks are effectively mitigated as the rotor windings are substituted by the permanent magnets. Since the permanent magnets are adopted for the rotor field excitation, the motor structure is simplified while the motor volume and weight are also effectively reduced without the rotor windings. Moreover, the motor efficiency is sufficiently improved without the rotor copper loss [4] [5] . Obviously, the reduction in motor volume and weight plus the higher efficiency will bring a lower cost in both manufacturing and normal operation of the PMSM as compared to other AC motors. Besides, the PMSM enjoys the distinctive merits of fast transient response, high power

density and high torque density [6] [7] , which make it more and more welcomed in various applications in modern industry and transportation [8] [9] . Moreover, the availability of low-cost power electronic devices and the improvement of PM characteristics will enable the use of PMSM even in more demanding applications [10] . Given to the wide applications of the PMSM nowadays and in the future, it is of great practical significance to study and explore the high-performance control strategies for the PMSM. To date, various control strategies have been proposed, among which the two classical theories are Field-Oriented Control (FOC) and Direct Torque Control (DTC) [7] .

FOC was proposed by Blaschke in 1971 [11] . Inspired by the control strategy of DC motor drives, FOC achieves the decoupled control of the flux and torque of AC motors by transforming the stator current vectors into two vertical components through coordinate transformation. It greatly simplifies the control of AC motors and has become the fundamental theory of various control strategies. However, FOC has problems at certain applications that require no overshoot and superior transient control performance since PI controller is normally adopted in the current control loop of the FOC. Moreover, finely tuned parameters are strictly required for the internal current loop, which is another drawback of FOC [12] .

The other classical control strategy is DTC, in which the applied voltage vector is selected directly from a heuristic switching table according to the comparison results between the reference torque and flux and the estimated torque and flux. In contrast to FOC, DTC

directly controls the torque and flux with no need of the complex coordinate transformation and therefore has the merits of low reliability to parameters, fast dynamic torque response and simple structure [13] [14] . However, it suffers from certain disadvantages such as high current and torque ripples and the difficulty to control torque at low speed [15] .

Model Predictive Control (MPC), as an advanced control scheme and a promising alternate for the two classical control methods, has emerged in recent 30 years [16] [17] [18] . It was initially developed in late 1970s for the process control such as petrochemical industry while not adopted in motor control which has fast dynamic response [19] [20] [21] [22] . With the rapid development of modern material and the chip industry in recent years, the computational capability has been effectively promoted, which makes it possible for the MPC to be applied in the AC drive system [6] . For the PMSM drives specifically, MPC exhibits satisfactory performance under complex working conditions, such us large torque with low speed, high power with high voltage and applications driven by multi-level power converters [23] [24] . As compared to continuous control set MPC, finite control set MPC (FCSMPC) is often preferred for the PMSM drives as it takes the full advantage of the discrete essence of the inverter, which results in lower computational burden [25] . The control concept of FCSMPC is simple and efficient. It utilizes the mathematical model of the PMSM to predict the state of the control variable (such as current, torque, flux, etc.) at next instant. Then, a cost function is built based on the error between the reference and the predicted control variable. Finally, the available control voltage which minimizes the cost

function is selected from a finite control set and will be applied through the power converters to the machine.

As compared to DTC, FCSMPC has relatively lower current ripples and torque ripples. As compared to FOC, FCSMPC achieves better dynamic response while avoids the strong reliability on the strictly tuned parameters for the internal current control loop [26] . Moreover, FCSMPC enjoys the distinct merits of the absence of cascaded control loops, the ability of multi-variable control and the flexibility to include multiple constraints [27] . Therefore, it has gained more and more attention in the application with PMSM drives [28] [29] [30] [31] [32] . However, FCSMPC suffers from certain drawbacks of large current ripples. The large current ripples will lead to large torque ripples and noise. Moreover, it decreases the control precision of PMSM drive system. Furthermore, it will cause large torque ripples of the motor, which will affect the control accuracy for the PMSM drives. Therefore, it is of great practical value to explore advanced techniques to reduce the current ripples of the FCSMPC-controlled PMSM drives.

1.2 CONTRIBUTIONS

The author has contributed a number of original developments in the current ripple minimization techniques for the FCSMPC-controlled PMSM drive system, which are listed as follows:

1. An integrated duty cycle and finite virtual voltage vector technique is proposed for the FCSMPC-controlled PMSM drives.

2. A continuous virtual voltage vector technique is proposed for the FCSMPC-controlled PMSM drives.

3. Comparative assessments between the proposed techniques and the conventional techniques are exhibited through experimental results for comprehensively evaluating the proposed techniques.

1.3 THESIS OUTLINE

This thesis presents two FCSMPC methods for PMSM drives with improved techniques to minimize the current ripples.

Chapter 2 introduces the general MPC, the finite control set (FCS) and the principle of the MPC with FCS (FCSMPC) for PMSM drives. Firstly, the definition, essential components and the basic principle of the general MPC is discussed while the classification of the MPC is carefully presented. Moreover, the concept and definition of the FCS is clearly depicted and firmly founded, which provides full knowledge base for FCSMPC. Furthermore, the FCSMPC for the PMSM drives is specifically discussed, where the prediction model of PMSM, the essential principle of FCSMPC and other relative problems are presented in details. Additionally, the mechanism of the current ripples produced by the FCSMPC is carefully analyzed and studied. The FCSMPC is experimentally tested in the reference

IPMSM drive system at the end of this chapter, where the current ripples will be clearly demonstrated. Moreover, the experimental setup is also specified in this chapter.

Chapter 3 presents the typical and conventional techniques for current ripple minimization. The FCSMPC with virtual voltage vectors and the FCSMPC with duty cycle control are introduced in two subsections. The principle of the two techniques and the mechanism on reducing the current ripples are explained in detail, while the drawbacks of each techniques are also presented explicitly in the corresponding subsection. Moreover, the FCSMPC with the two conventional techniques are experimentally implemented with the reference IPMSM drive system as the benchmark reference methods.

Chapter 4 proposes an improved FCSMPC method with integrated duty cycle and finite virtual voltage vector technique for PMSM drives. The principle of the proposed method is elaborated carefully in this chapter. Additionally, the mechanism of the proposed method on reducing the current ripples is analyzed in detail. Moreover, the proposed method is comparatively studied with the FCSMPC with the conventional techniques, where its benefits on the current ripple reduction are confirmed by the experimental results for the reference IPMSM drives. In the end of this chapter, a supplementary analysis is presented on the difference between the proposed optimal vector selection method and the quick selection method adopted in the conventional techniques, which further proves the higher accuracy of the proposed method.

Chapter 5 chapter proposes an improved FCSMPC method with continuous virtual voltage vector technique for high performance control of PMSM drives. The proposed method applies a continuous virtual voltage vector at each sampling interval, which reduces the current ripples by successfully eliminating the error between the reference value and the actual value of the current. The principle of the proposed method is presented in detail. Additionally, the mechanism of the proposed method on reducing the current ripples is analyzed explicitly. Moreover, the proposed method is comparatively studied with the FCSMPC with the conventional techniques, where its benefits on the current ripple reduction are confirmed by the experimental results for the reference IPMSM drives.

The thesis is concluded in Chapter 6 with suggested future work.

Chapter 2

MODEL PREDICTIVE CONTROL (MPC) AND FINITE CONTROL SET (FCS)

2.1 INTRODUCTION

The theory of the general MPC, the FCS and the MPC with FCS for PMSM drive will be fully discussed in this Chapter. First, the definition, essential components and the classification of the general MPC are introduced in 2.1. Then, the concept and definition of the FCS is clearly depicted and firmly founded in 2.2. Next, the MPC with the FCS (FCSMPC) for the PMSM drive is specifically discussed in 2.3. Moreover, the current ripples, as the main problem for the conventional FCSMPC, is presented and deeply analyzed, which provides a strong theoretical support for the further research in this thesis. Finally, the performance of the FCSMPC is tested through experiments on the reference IPMSM drive system, where the current ripple problem will be clearly demonstrated.

2.2 MODEL PREDICTIVE CONTROL (MPC)

For a clear definition, MPC is a model-based open-loop-optimal feedback control strategy [18] . It enjoys the distinct merits of quick dynamic response, the absence of cascaded control loops, the ability of multi-variable control and the flexibility to include multiple constraints [33] [34] . The most notable characteristic of MPC, which makes it distinctly different from other conventional control methods, is that the close loop control is achieved in a way of solving the online optimization problem. As compared to conventional FOC and DTC, MPC avoided the heavy parameter-tuning work without using the PI controller while presents promising control performance for the torque at low speed. The basic mechanism of the MPC is described as:

In every discrete control period, MPC solves an online open-loop optimization problem within the limited future control steps according to the measured output or the observed state of the control objective. The first control action of the optimal control sequence that is obtained from solving the optimization problem is applied to the plant system. Then, the MPC will repeat the process in the next discrete control interval by updating the optimization result with the updated measurement output or the observed state feedback [35] . The schematic diagram of a typical MPC scheme is shown in Fig. 2.1.

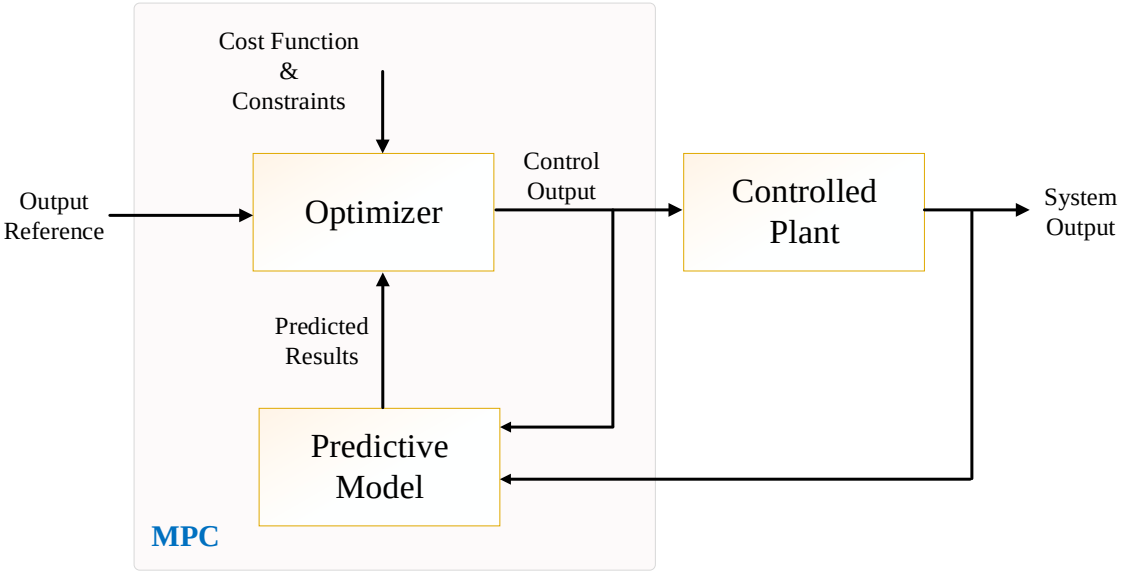

Fig. 2.1 The structure of a typical model predictive control scheme.

Based on this structure and concluded from different kinds of algorithms and implementation forms of MPC, it is found that the operation of MPC is conceptually consisted of the three basic components- Prediction model, Cost function and the Rolling optimization. By perceiving these three components separately, the general principle of MPC will be mapped clearly.

(a) Prediction Model

The prediction model is the accurate description of the control behaviors regarding the control system within the limited future steps, which is the basis of the MPC. Moreover, the prediction model can be built in any structures, such as impulse response, discrete transfer function and state space equations, as long as it can precisely project the

relationship of the input and output of the control system. The prediction model of the PMSM will be presented in 2.4.

(b) Cost Function

Different functions are adopted to estimate the corresponding control behaviors in different MPC algorithms. Normally, these functions are formulated as a cost function along with multiple constraints. The cost function is normally a quadratic function which should be able to evaluate the tracking error between the reference signal *y* and the future output $\hat{y}$ of the control system. Besides, some constraint conditions are normally added directly behind the cost function. The simplicity of embedding the constraints provides a sufficient freedom of achieving multiple control purposes. The general form of the cost function is expressed in a simple way as:

$$J(N_p) = \sum_{j=1}^{N_p} [\hat{y}(t+j|t) - y(t+j)]^2 \tag{2.1}$$

where N_p denotes the maximum predictive horizon. It is found that long prediction horizon N_p delivers a better steady-state performance. However, it slows down the dynamic response of the system and greatly increase the computational time and burden. In normal practice, N_p is usually adopted as 1 due to the high complexity of multi-predictive-step control with the limited digital computational ability. Moreover, solving the cost function is a complicated optimization problem consuming lots of computational resources, which makes it difficult to apply to the motor control system with fast dynamic response. To

simply the complex solving problem, J. Rodríguez proposed to transfer the optimization problem as an integral enumeration problem in 2004 by limiting the control input within the finite combinations of the inverter switching states, through which the optimization problem is solved by simple enumerations. This method is the so-called Finite Control Set Model Predictive Control, which will be elaborated further in the following content and more in details in 2.4.

(c) Rolling Optimization

In every control period, MPC solves the optimization problem of the cost function and seeks the optimal control sequence regarding the output tracking performance within the predictive horizon N_p while applies only the first of the optimal control sequence to the controlled system. Therefore, the rolling optimization of the MPC happens naturally as the online optimization process is carried out repeatedly with the sampling progressing forward. By constantly sampling and updating the operation state and tracking error of the control system, the rolling optimization process implies the close-loop control by revising the model-based prediction values and conducting the optimization in each sampling interval, which guarantees an effective correction on the control behavior under various complex control conditions.

With the knowledge of the general principle of MPC, its specific application on the PMSM drives can be discussed. An MPC-based control system for the PMSM drive is shown in Fig. 2.2, which is mainly constituted of three parts- PMSM, power converter and digital

controller. It is clearly seen in Fig. 2.2 that the output of the PMSM drive control system is consisted of stator currents, speed and rotor position, while the input is the stator voltage or the gate signals of the switches. Accordingly, the control objectives of the system could be designated as one of the system outputs while the control actions evaluated in the cost function is normally designated as the system input (i.e. stator voltage or the inverter gating signals).

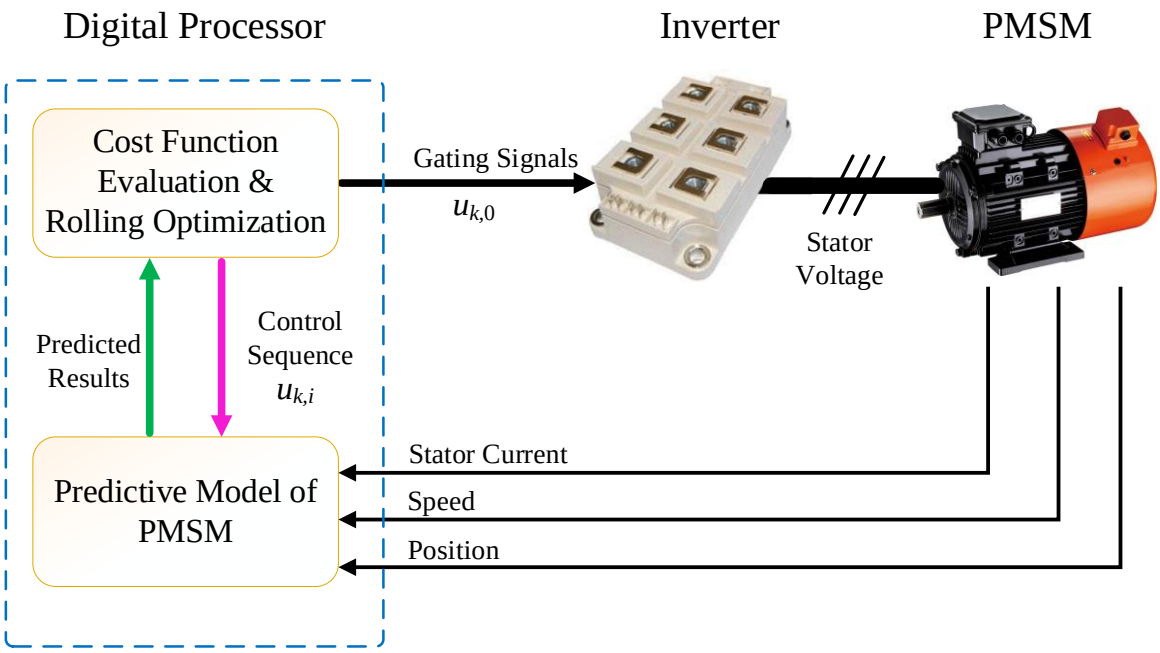

Fig. 2.2 The diagram of a typical MPC-based control system for PMSM drives.

According to the different control objectives mentioned before, the MPC strategies for the PMSM drives could be categorized as Model Predictive Current Control (MPCC) [36] [37] [38] [39] [40] , Model Predictive Torque Control (MPTC) [41] [42] [43] [44] [45] [46] ,

Model Predictive Speed Control [47] and Model Predictive Position Control [48] , etc. Among these methods, the more common used two are MPTC and MPCC. The MPTC is more accurate and effective than the DTC by selecting the best voltage vector minimizing the pre-defined cost function which is usually consisted of torque error and flux error. However, the optimal weighting factor which balances the torque and flux is difficult to obtain due to the lack of theoretical design procedure [49] , which forms the main drawback of this method. Moreover, the stator flux cannot be directly measured but has to be estimated using a flux estimator or observer, which makes the controller design even more complicated [50] . On the contrary, the weighting factor issue is naturally solved if the current control strategy is considered, while the stator current can be directly measured which adds more simplicity to this method. Based on this fact, the stator current is adopted as the control objective in the MPC strategy in this thesis.

According to the different characteristics of the control actions, the MPC strategies for the PMSM drives could be categorized as Continuous Control Set Model Predictive Control (CCSMPC) [51] [52] [53] and Finite Control Set Model Predictive Control (FCSMPC) [54] [55] [56] . CCSMPC includes all the possible continuous voltage vectors in its control set with the assistance of modulation techniques. Since the possible voltage vector candidates are with infinite angles and magnitudes, different optimization strategies have to be built up accordingly to obtain the optimal voltage vector, which is usually complicated consuming lots of computational resources. In contrast, the FCSMPC requires no

modulation but builds up a finite control input set that consists of eight switching states by embracing the discrete nature of the 2-level voltage source inverter, through which the optimal problem is solved by the simple enumerations on the pre-defined cost function, which greatly releases the computational burden and simplifies the control process as compared to the CCSMPC. For the sake of simplicity and practicality, the FCSMPC is considered in this thesis.

2.3 FINITE CONTROL SET (FCS)

The structure of the two-level voltage source inverter (2L-VSI) fed PMSM drive system is depicted in Fig. 2.3.

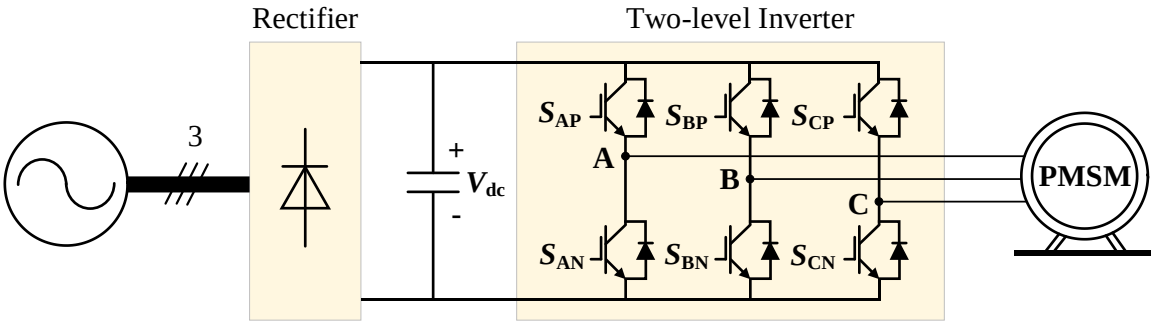

Fig. 2.3 The diagram of a 2L-VSI fed PMSM drive system.

In Fig. 2.3, V_{dc} represents the DC bus voltage. S_{AP} (S_{AN}), S_{BP} (S_{BN}) and S_{CP} (S_{CN}) denote the gating signals of the upper (lower) switches on phase-A, Phase-B and Phase-C of the two-level voltage source inverter, respectively. Moreover, the on-state of the corresponding

switch is represented by "1" while the off-state is denoted by "0". For example, "S_{AP}=1" represents that the upper switch on phase-A is enabled.

Since the switching states of the upper and lower switches on one phase are complementary to each other, there will be in total eight combinations of the switching states for the 2L-VSI, which can be represented by the vector S_i= [S_{AP} S_{BP} S_{CP}]^T (i=0, 1, …, 7). Among the eight combinations, there are six valid combinations (S_1~S_6) which could transmit the power from the DC bus to the machine. By transferring the output phase voltages corresponding to these six valid combinations into the space vector form, six magnitude-fixed and angle-fixed voltage vectors (denoted by V_1-V_6) could be obtained, which are defined as the active voltage vectors. The corresponding active voltage vectors with respect to the six valid switching combinations are demonstrated in Fig. 2.4.

Apart from the six valid switching combinations of the 2L-VSI, there are two switching combinations that fail to conduct the machine to the DC bus, i.e., the combinations (S_0 and S_7) which enable the three lower switches or the three upper switches of the inverter. Since the phase and the magnitude of the stator line voltage are both zero under these two circumstances, the voltage vectors that corresponds to these two combinations are defined as zero vectors or null vectors (denoted by V_0 and V_7).

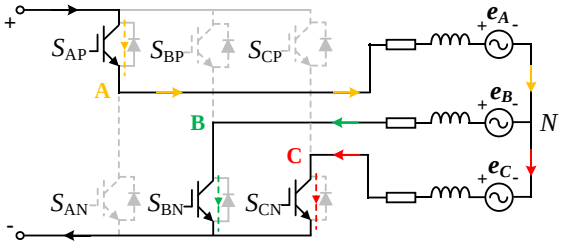

(a) S_1=[1 0 0]^T corresponding to V_1

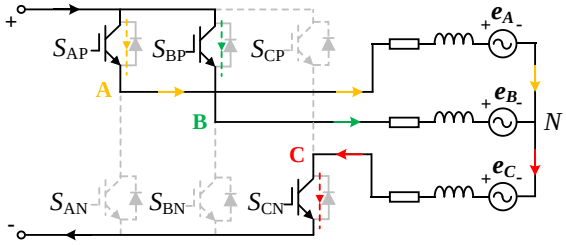

(b) S_2=[1 1 0]T corresponding to V_2

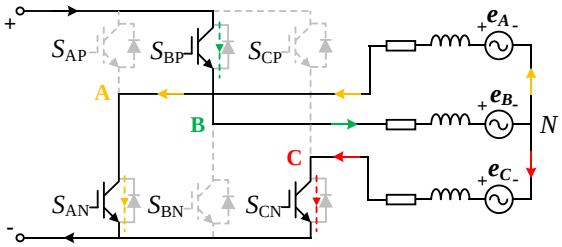

(c) S_3=[0 1 0]^T corresponding to V_3

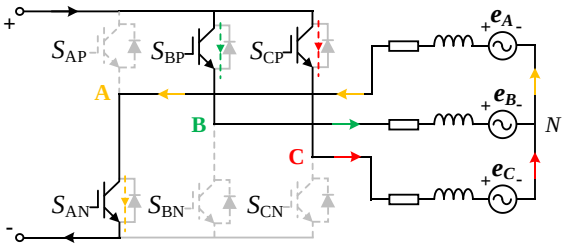

(d) S_4=[0 1 1]^T corresponding to V_4

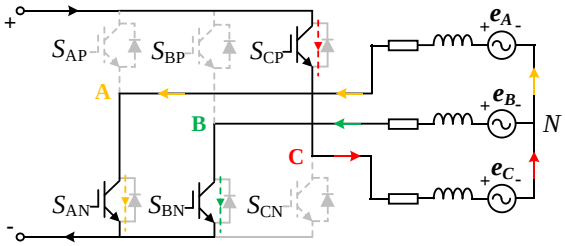

(e) S_5=[0 0 1]^T corresponding to V_5

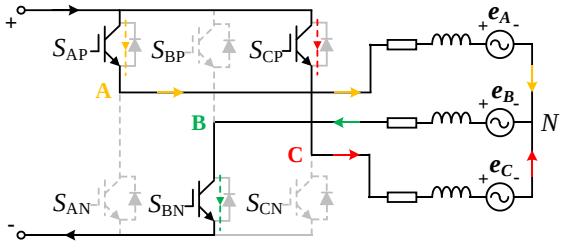

(f) S_6=[1 0 1]^T corresponding to V_6

Fig. 2.4 The valid switching combinations of a 2L-VSI.

The eight basic voltage vectors V_i (i=0, 1, …, 7) and the corresponding phase voltage v_{AN}, v_{BN}, v_{CN} with respect to the eight switching combinations S_i (i=0, 1, …, 7) are listed in Table 2.1.

Table 2.1 Basic voltage vectors and the corresponding switching states of the 2L-VSI

Basic voltage vectors V_i	Switching states S_i	v_{AN}	v_{BN}	v_{CN}
V_0	$[0 \quad 0 \quad 0]^T$	0	0	0
V_1	$[1 \quad 0 \quad 0]^T$	$\frac{2}{3}v_{dc}$	$-\frac{1}{3}v_{dc}$	$-\frac{1}{3}v_{dc}$
V_2	$[1 \quad 1 \quad 0]^T$	$\frac{1}{3}v_{dc}$	$\frac{1}{3}v_{dc}$	$-\frac{2}{3}v_{dc}$
V_3	$[0 \quad 1 \quad 0]^T$	$-\frac{1}{3}v_{dc}$	$\frac{2}{3}v_{dc}$	$-\frac{1}{3}v_{dc}$
V_4	$[0 \quad 1 \quad 1]^T$	$-\frac{2}{3}v_{dc}$	$\frac{1}{3}v_{dc}$	$\frac{1}{3}v_{dc}$
V_5	$[0 \quad 0 \quad 1]^T$	$-\frac{1}{3}v_{dc}$	$-\frac{1}{3}v_{dc}$	$\frac{2}{3}v_{dc}$
V_6	$[1 \quad 0 \quad 1]^T$	$\frac{1}{3}v_{dc}$	$-\frac{2}{3}v_{dc}$	$\frac{1}{3}v_{dc}$
V_7	$[1 \quad 1 \quad 1]^T$	0	0	0

With the coordinate transformation, the stator voltage of the machine under α-β frame can be calculated through:

$$\begin{bmatrix} v_\alpha \\ v_\beta \end{bmatrix} = \frac{2}{3}\begin{bmatrix} 1 & -\frac{1}{2} & -\frac{1}{2} \\ 0 & \frac{\sqrt{3}}{2} & -\frac{\sqrt{3}}{2} \end{bmatrix}\begin{bmatrix} v_{AN} \\ v_{BN} \\ v_{CN} \end{bmatrix} \tag{2.2}$$

where v_α and v_β denote the projection terms of the stator voltage on the α-axis and β-axis. By substituting the phase voltage v_{AN}, v_{BN} and v_{CN} from Table 2.1 into (2.2), the eight basic voltage vectors V_i (i=0, 1, …, 7) can be transformed into the eight basic voltage vectors v_i (i=0, 1, …, 7) on the α-β subspace. The basic voltage vectors v_i in α-β frame and the corresponding switching states are shown in Fig. 2.5. It should be noted that the all the

active voltage vectors have the same magnitude of $(2/3)V_{dc}$, while each two adjacent active vectors have 60 degrees phase shift.

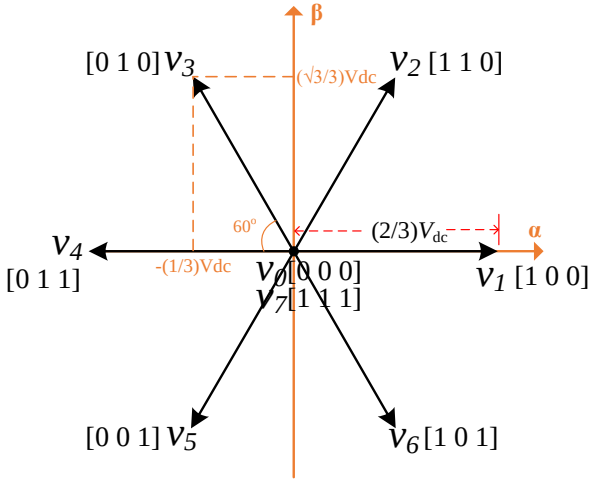

Fig. 2.5 The scheme of the basic voltage vectors in the stationary frame.

In conclusion, there are eight basic voltage vectors V_0~V_7 that corresponds to the eight switching combinations of the 2L-VSI, which could be further transformed into the vectors v_0~v_7 on the α-β subspace. The control set, that is built on the basis of the eight voltage vectors (including six active voltage vectors and two zero vectors), is defined as the Finite Control Set (FCS):

$$FCS=\{v_s=v_i|v_i=v_0, v_1, \ldots, v_7\} \tag{2.3}$$

The MPC, of which the control inputs adopt only the six active voltage vectors and the two zero voltage vectors, is defined as the MPC with FCS (FCSMPC), which will be elaborated in the following Section.

2.4 FCSMPC FOR PMSM DRIVES

2.4.1 PRINCIPLE OF FCSMPC

FCSMPC is one kind of MPC which utilizes the FCS as its control output pool. FCSMPC predicts the future value of the control objective under every single control voltage vector from the FCS through the prediction model of the control plant. The corresponding control output which minimizes the pre-defined cost function will be selected as the optimal control action. Since the FCSMPC adopts the discrete and finite control outputs provided by FCS, the principle of enumeration could be used to evaluate the control performance for each control voltage vector, which guarantees the optimal control under accurate prediction. As illustrated in 2.2, the FCSMPC could be classified into different categories according to the control objectives, such as torque or current, etc. In this section, the theory of the FCSMPC for current control on a PMSM drive is studied. Fig. 2.6 shows the diagram of a FCSMPC controlled PMSM drive system. It can be seen that the function blocks of the FCSMPC are mainly constituted of the prediction model of PMSM, enumeration of the voltage vectors and the cost function evaluation, which will be introduced in details in the following content.

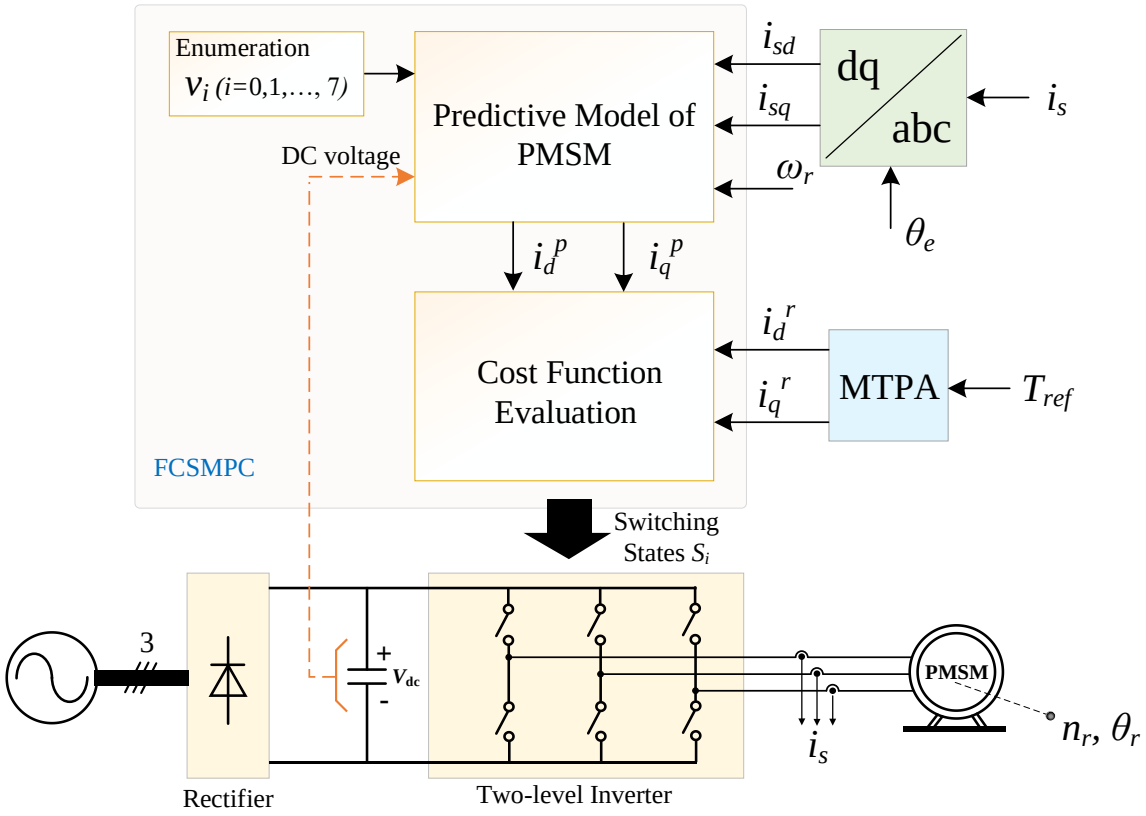

Fig. 2.6 The schematic diagram of an FCSMPC-controlled PMSM drive system.

The synchronous rotating frame (d-q frame) is established as shown in Fig. 2.7, where the d-axis is aligned with the permanent magnet flux linkage Ψ_r of the PMSM. θ_e denotes the angle between the d-axis and the α-axis and the q-axis is 90 degrees leading to d-axis as normal.

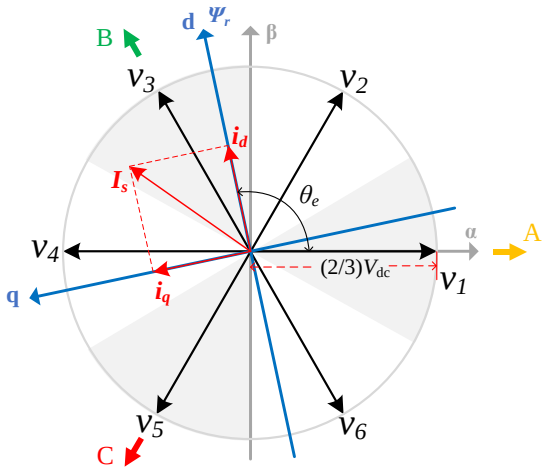

Fig. 2.7 Spatial distribution of the basic voltage vectors in different coordinate frames.

According to Faraday's Law and the theory of the coordinate transformation, the time domain stator voltage equations of the PMSM in d-q frame is modeled as:

$$\begin{cases} v_d(t) = R_s i_d(t) + L_d \frac{di_d(t)}{dt} - \omega_e(t) L_q i_q(t) \\ v_q(t) = R_s i_q(t) + L_q \frac{di_q(t)}{dt} + \omega_e(t) L_d i_d(t) + \omega_e(t) \psi_r \end{cases} \tag{2.4}$$

where $\omega_e(t)$ represents the rotor electrical speed, $i_d(t)$ and $i_q(t)$ denote the d-axis and q-axis stator currents while $v_d(t)$ and $v_q(t)$ denote the d-axis and q-axis voltage in same rotor synchronous frame, respectively. Furthermore, R_s denotes the stator winding resistance, Ψ_r denotes the flux linkage of the permanent magnet, L_d and L_q represent the direct and quadrature stator inductance, respectively. For the interior permanent magnet (IPM) machine that is considered, L_d is smaller than L_q due to the saliency of the motor.

Furthermore, the prediction model with the FCS can be established by discretizing (2.4) via forward Euler derivative as:

$$\begin{cases} i_d^p(k+1) = \left(1 - \frac{R_s T_s}{L_d}\right) i_d(k) + \frac{T_s}{L_d}\left[v_d^i(k) - e_d(k)\right] \\ i_q^p(k+1) = \left(1 - \frac{R_s T_s}{L_q}\right) i_q(k) + \frac{T_s}{L_q}\left[v_q^i(k) - e_q(k)\right] \end{cases} \tag{2.5}$$

$$\begin{cases} e_d(k) = -\omega_e(k) L_q i_q(k) \\ e_q(k) = \omega_e(k) L_d i_d(k) + \omega_e(k)\psi_r \end{cases} \tag{2.6}$$

where T_s and k represent the sampling period and the k^{th} discrete control interval. i_d^p (k+1) and i_q^p(k+1) denote the predicted d- and q- axis current at (k+1)th instant while i_d(k) and i_q(k) are the actual stator current on d- and q- axis at k^{th} instant, respectively. Moreover, v_d^i(k) and v_q^i(k) represent the projected terms of the ith basic voltage vector (v_i) on the d- and q- axis at k^{th} instant.

With the aim to minimize the tracking error between the output stator current and the reference current, the cost function with the prediction horizon of N_p is established as:

$$J(N_p) = \sum_{j=1}^{N_p} [i_d^{ref} - i_d^p(k+j)|v_i]^2 + [i_q^{ref} - i_q^p(k+j)|v_i]^2 \tag{2.7}$$

where i_d^{ref} and i_q^{ref} denote the reference stator currents on d- and q- axis. i_d(k+j)|v_i and i_q(k+j)|v_i represent the predicted d- and q-axis current at (k+j)th step, which are obtained by applying the i^{th} of the eight basic voltage vectors (v_i) in (2.3) at (k+j-1)th step within the prediction horizon N_p. The cost function J, that corresponds to each possible control

sequence, is obtained by enumerating the eight voltage vectors in (2.5) and (2.7) based on an iteration-based manner. The relationship between N_p and the enumeration times is shown in Fig. 2.8.

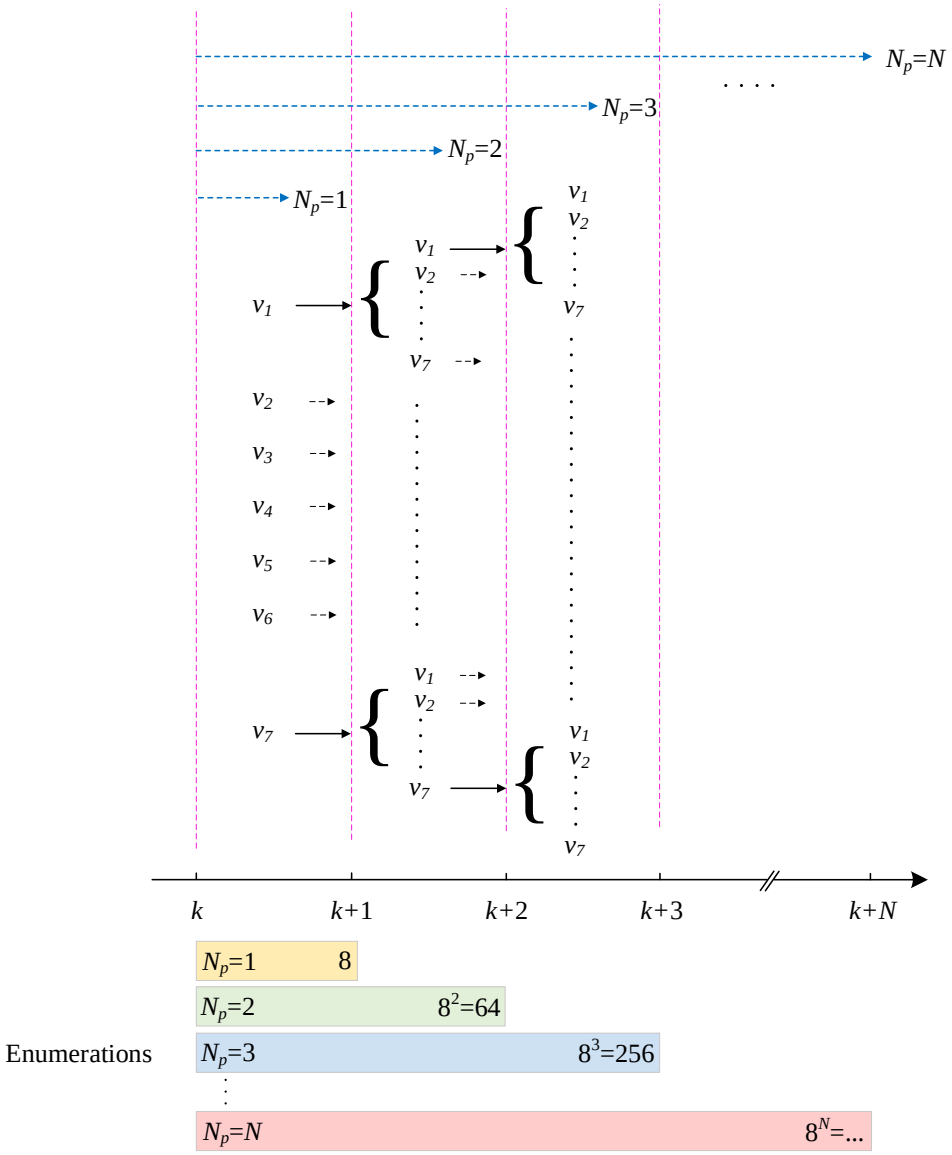

Fig. 2.8 The schematic of enumerations vs. the steps of the prediction horizon.

It is seen that, each one of the calculations that is made in the current prediction step will be followed by eight enumerations of the voltage vectors at the next prediction step. In other words, each one additional step inside the prediction horizon will lead to eight times more of the calculation burden. Long prediction horizon is able to provide more accurate data basis for the decision of the best control sequence, which delivers better control performance. However, it greatly complicates the calculation process and brings much heavier computational burden on the digital processor [57] . Considering the complexity and the computational ability of the modern microprocessor, the application of the long prediction horizon (N_p>1) is limited in the normal cases of the FCSMPC controlled system. Therefore, N_p=1 is adopted in the following analysis of the FCSMPC strategy.

By concluding the prediction model and the cost function (N_p=1) with FCS, the principle of the FCSMPC-based control system for PMSM drive could be represented as:

$$\min_{v_i(k)} \quad J = [i_d^{ref} - i_d^p(k+1)|v_i]^2 + [i_q^{ref} - i_q^p(k+1)|v_i]^2$$

subject to

$$\begin{cases} i_d^p(k+1) = \left(1 - \frac{R_s T_s}{L_d}\right) i_d(k) + \frac{T_s}{L_d}\left[v_d^i(k) - e_d(k)\right] \\ i_q^p(k+1) = \left(1 - \frac{R_s T_s}{L_q}\right) i_q(k) + \frac{T_s}{L_q}\left[v_q^i(k) - e_q(k)\right] \end{cases} \tag{2.8}$$

$$v_i(k) = v_d^i(k) + j v_q^i(k)$$

It is seen from (2.8) that the optimization principle of the FCSMPC is actually a combination of the enumerations of the voltage vectors plus the minimization of the cost function. First, the d- and q- axis currents at $(k+1)^{th}$ instant are predicted corresponding to the eight basic voltage vectors (v_0~v_7), based on the sampled values of the stator current, DC voltage and the rotor angular position at k^{th} instant. Then, the predicted $i_d^p(k+1)$ and $i_q^p(k+1)$ are substituted into the cost function and the corresponding voltage vector which produces the minimum J will be selected as the optimal control output. The flow chart of the principle of the basic FCSMPC is presented in Fig. 2.9.

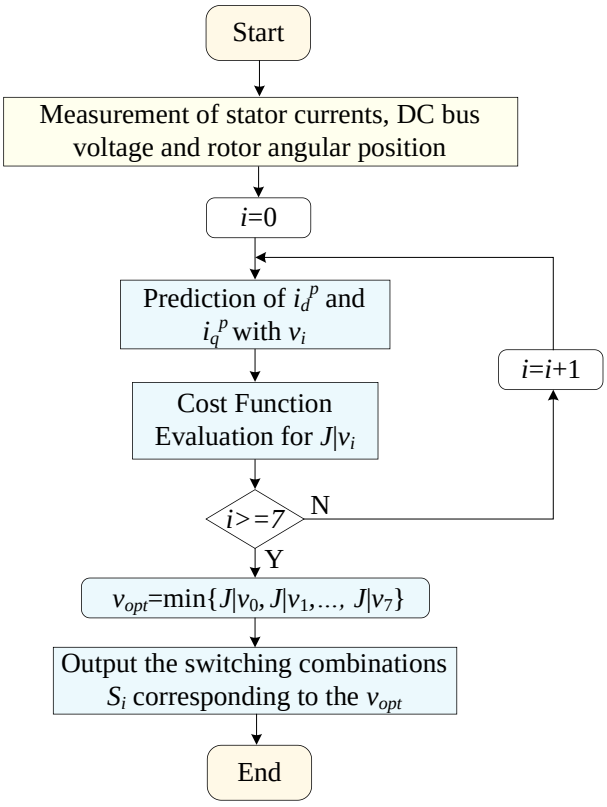

Fig. 2.9 Flow chart of the principle of the basic FCSMPC.

2.4.2 ONE-STEP DELAY COMPENSATION FOR FCSMPC

According to the basic principle of FCSMPC as illustrated in section 2.4.1, the FCSMPC is a discrete controller. Theoretically, when there is no delay in the control system, the selection and implementation of the optimal control output can be done right at the sampling instant, which will present a satisfactory tracking performance on the control system. However, in practice, the output of the FCSMPC controller usually lags behind the variation of the control objective due to various delay factors, such as the calculation time needed for the optimization algorithm, sampling delay and filters delay [58] . In other words, the optimal control voltage vector obtained at k^{th} sampling instant is not applied until after the $(k+1)^{th}$ instant, which will lead to the deviation between the predicted values and actual values of the control objective and hence affect the tracking performance of the control system. Moreover, the impact on the prediction caused by the one step delay becomes even worse when the one-sample prediction horizon is considered [59] . Therefore, it is necessary to compensate the one-step delay for the FCSMCP controlled system [60] . A simple and effective method, which utilizes one additional prediction before the optimization process of FCSMPC, is widely used to compensate the one-step delay. Fig. 2.10 shows the timing diagram of the FCSMPC with the one-step compensation.

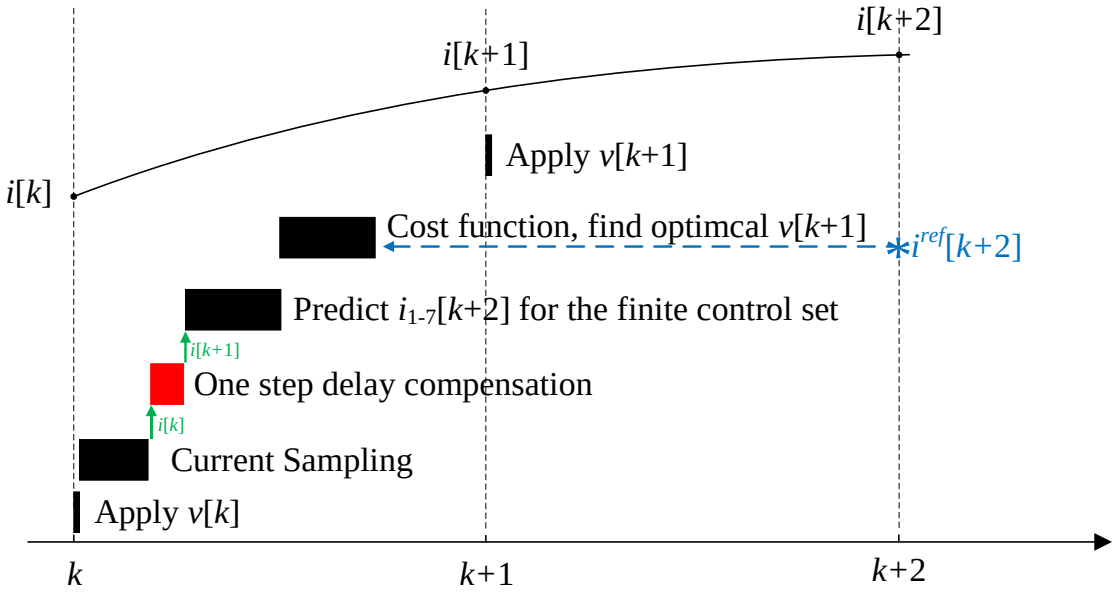

Fig. 2.10 The timing diagram of the FCSMPC with one-step compensation.

As shown in the figure, the control output obtained at $(k\text{-}1)^{th}$ instant is first applied to the system physically at k^{th} instant. Then, the current at $(k+1)^{th}$ instant ($i_{dq}^{p}(k+1)$) is predicted mathematically by substituting the currently applied vector into the prediction model (2.5). Next, $i_{dq}^{p}(k+1)$ is used to predict the currents at $(k+2)^{th}$ instant ($i_{dq}^{p}(k+2)$) with respect to the eight basic voltage vectors. Finally, the corresponding voltage vector which minimizes the error between $i_{dq}^{p}(k+2)$ and the reference current will be determined as the optimal voltage vector, and then applied at $(k+1)^{th}$ instant. As a result, the one step lag between the controller output and the variation of current is compensated and the effect of the one-step delay is eliminated. By integrating the algorithm of the one-step delay compensation with

(2.8), the principle of the FCSMPC for the PMSM drive control system could be updated as:

$$\min_{v_i(k+1) \text{ from FCS}} \quad J = [i_d^{ref} - i_d^p(k+2)|v_i]^2 + [i_q^{ref} - i_q^p(k+2)|v_i]^2$$

subject to

$$\begin{cases} i_d^p(k+2) = \left(1 - \frac{R_S T_S}{L_d}\right) i_d^p(k+1) + \frac{T_S}{L_d}\left[v_d^i(k+1) - e_d(k+1)\right] \\ i_q^p(k+2) = \left(1 - \frac{R_S T_S}{L_q}\right) i_q^p(k+1) + \frac{T_S}{L_q}\left[v_q^i(k+1) - e_q(k+1)\right] \end{cases}$$

$$\begin{cases} i_d^p(k+1) = \left(1 - \frac{R_S T_S}{L_d}\right) i_d(k) + \frac{T_S}{L_d}\left[v_d(k) - e_d(k)\right] \\ i_q^p(k+1) = \left(1 - \frac{R_S T_S}{L_q}\right) i_q(k) + \frac{T_S}{L_q}\left[v_q(k) - e_q(k)\right] \end{cases} \tag{2.9}$$

$$\begin{cases} e_d(k+1) = -\omega_e(k) L_q i_q^p(k+1) \\ e_q(k+1) = \omega_e(k) L_d i_d^p(k+1) + \omega_e(k)\psi_r \end{cases}$$

$$v_i(k+1) = v_d^i(k+1) + j v_q^i(k+1)$$

It should be noted that $\omega_e(k)$ is considered unchanged in the optimization process due to the short sampling period.

2.5 CURRENT RIPPLES BY FCSMPC

FCSMPC enjoys the merit of quick dynamic response by directly controlling the switching states of the inverter. However, the basic FCSMPC suffers from a certain problem, which

is the unsatisfactory steady-state performance with large current ripples. The current ripples produced by the basic FCSMPC are mainly resulted from the discrete nature of the FCS. As illustrated in 2.2, the FCS is constituted of eight discrete voltage vectors, which will provide only eight discrete current response possibilities at next sampling instant as obtained in (2.5). The optimal voltage vector is selected based on the principle of minimizing the cost function. However, it probably cannot reduce the function to zero. In other words, the current response generated by applying the selected voltage vector may still have difference with the reference current due to the limited voltage vector candidates. The current error exists for each sampling interval and then the current ripples start to show up. Fig. 2.11 shows an example of the FCSMPC-controlled system behavior regarding d- and q-axis current, where the mechanism of the current ripples could be demonstrated clearly.

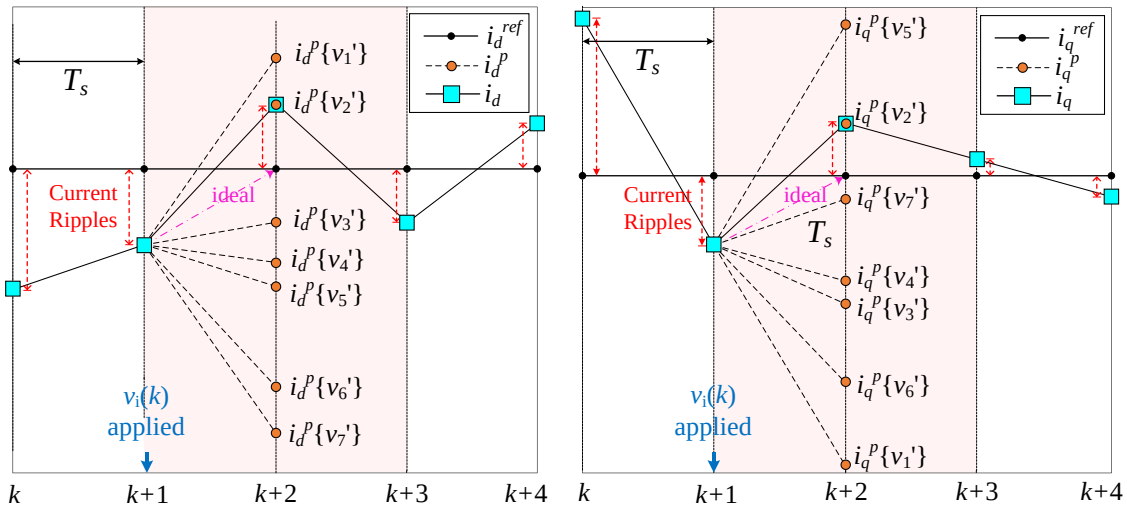

Fig. 2.11 The schematic of the current behavior of a FCSMPC controlled system.

The $i_{dq}(k)$ is sampled at k^{th} instant and predicted to $i_{dq}(k+1)$ for the one-step compensation. v_i' (i=0, 1, …, 7) denote the seven voltage vector candidates from the FCS (since the current variations caused by v_0 and v_7 are the same, they are demonstrated as one vector candidate in the figure). The corresponding seven current responses resulted from the seven voltage vector candidates are shown in the figure, among which v_2' delivers the minimum value of the cost function compared to other voltage vector candidates and therefore selected as the control output. The distinct error between the actual current and the reference current exists because v_2' is the optimal choice among FCS but not the ideal vector that eliminates the current error. Therefore, it is easily understood that the current error will exist at each sampling instant due to implementation of the inaccurate voltage vector selected from the limited and fixed discrete control voltage choices in the FCS. The current errors at each step are marked using red lines in the figure, which are added up to present as the current ripples of the FCSMCP.

In addition to the analyzation based on the current response demonstration, the mechanism of the large current ripples of FCSMPC could also be explained in the vectorial scheme with the same theory. The eight basic voltage vectors are presented in Fig. 2.12 while the ideal voltage vector as demonstrated in Fig. 2.11 is also depicted in the same figure. It is seen that the eight available control voltage vectors provided by FCS could not perfectly match the ideal voltage vector, which will result in the current error at each step and hence the current ripples.

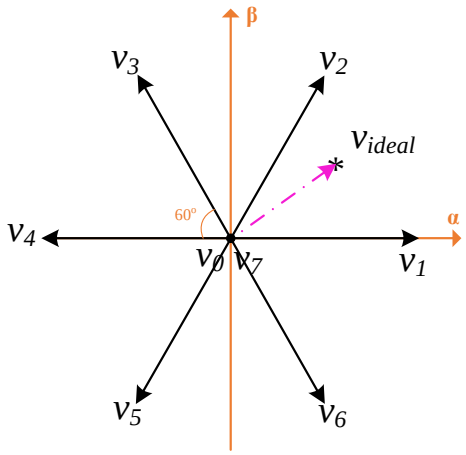

Fig. 2.12 The vectorial diagram for explaining current ripples of FCSMPC.

In conclusion, the current ripples of the FCSMPC are constituted of the errors between the actual current and the reference current at each sampling instant. This drawback is attributed to the limited voltage vector candidates provided by the FCS.

2.6 PERFORMANCE OF THE BASIC FCSMPC IN EXPERIMENTS

In this section, the steady-state performance and the transient current response of the basic FCSMPC will be presented in a few experimental results for an interior permanent magnet synchronous machine. Through the experimental curves, the current ripples of the basic FCSMPC are demonstrated vividly.

2.6.1 EXPERIMENTAL SETUP

The photograph of the IPMSM drives test bench is depicted in Fig. 2.13. The dyno on the test bench is a 5kW induction motor with Yaskawa A-1000 AC Drives as the controller. The dyno is back-to-back coupled with the reference IPM motor which is driven by the Silicon Carbide MOSFET inverter with dSPACE MicroAutobox II DS1401/1513, in which different motor control methods are implemented. The parameters of the IPM motor is specified in Table 2.2. In the experiment, the dyno machine is configured in speed control mode while the reference IPM motor is controlled in torque control mode. Moreover, the current references for the control of the IPM motor are generated based on the MTPA criteria corresponding to different torque references. The sampling frequency of the drive system is 10 kHz and the applied DC link voltage is 300V.

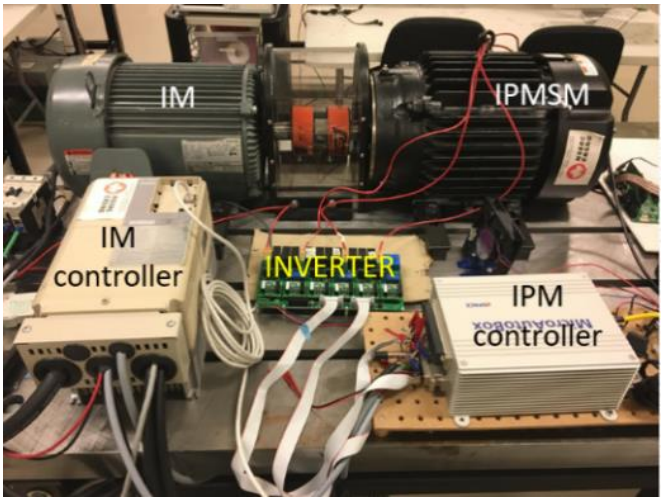

Fig. 2.13 Experimental bench of the PMSM drive system.

Table 2.2 Parameters of the PMSM

Parameters	Value
Number of poles	10
Rated current	9.4 A
Rated torque	29.7 Nm
Rated speed	600 r/min
Nominal d-axis inductance	11 mH
Nominal q-axis inductance	14.3 mH
Nominal PM flux linkage	0.3333 Wb
Nominal stator resistance	400 mΩ

2.6.2 PERFORMANCE OF FCSMPC IN EXPERIMENT

First, the dynamic performance of the basic FCSMPC is demonstrated in Fig. 2.14 and Fig. 2.15. In each figure, the d- and q-axis currents are provided in two separate subfigures (a) and (b) respectively. Fig. 2.14 shows the dynamic performance of d- and q- axis currents with the rotor speed transient from standstill to rated speed at 0.05s with no load for the basic FCSMPC. It is found that the FCSMPC presents a stable control performance against the step change of speed. However, it delivers distinct current ripples on both d- and q-axis as analyzed previously in 2.5. Fig. 2.15 shows the current transient responses to a stepped change from no load to full load at 0.05s with the machine speed of 100 r/min. It is seen in the results that the actual current shows a rapid response when the load suddenly

changes, through which the tracking performance of the FCSMPC is validated. Nevertheless, large current ripples are evidently seen in both d- and q- axis currents, which is in consistent with the theoretical analysis as shown in the previous section.

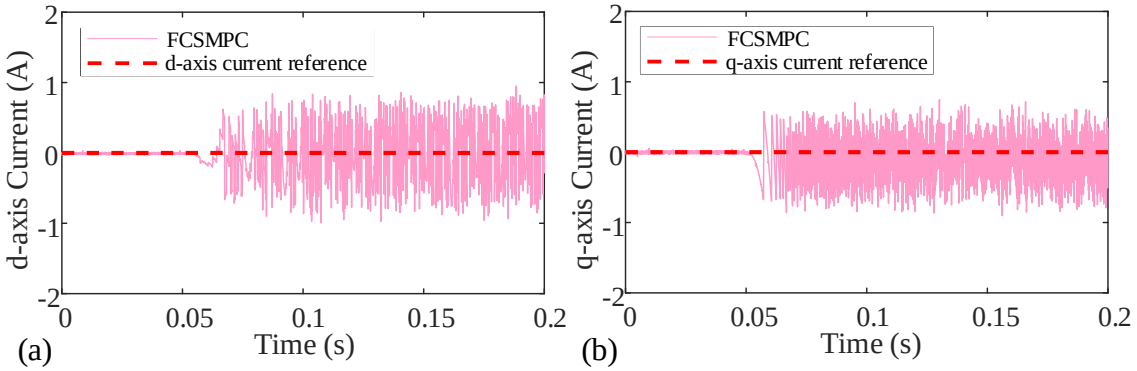

Fig. 2.14 Experimental results of the current responses (a) d-axis and (b) q-axis when speed steps from 0 r/min to 600 r/m at no load for the basic FCSMPC.

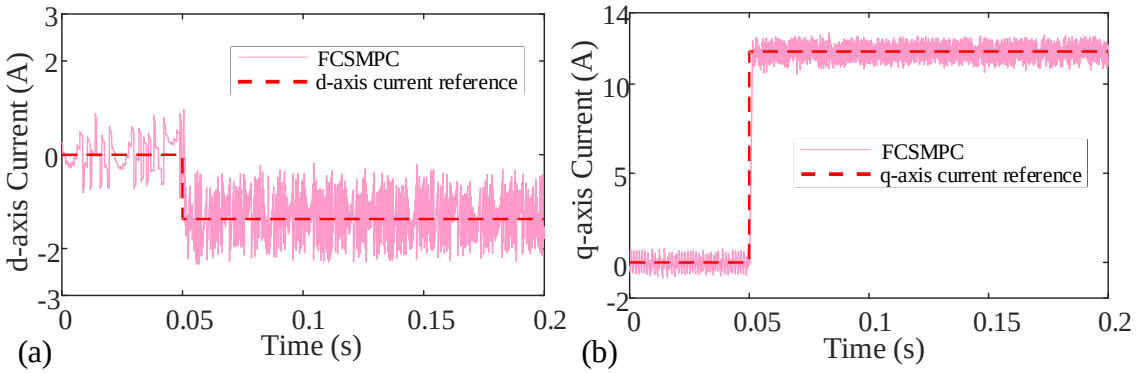

Fig. 2.15 Experimental results of the current responses (a) d-axis and (b) q-axis for step change from no load to full load at 100 r/min for the basic FCSMPC.

Then, the steady-state performance of the basic FCSMPC at rated speed with rated load is exhibited in Fig. 2.16, where the phase-a current and the corresponding harmonic spectrum are clearly depicted. As shown in the figure, the distortion of the stator current is easily observed, which further reflects the current ripple problem of the FCSMPC. The THD of the stator current is 5.05% according to the FFT analysis.

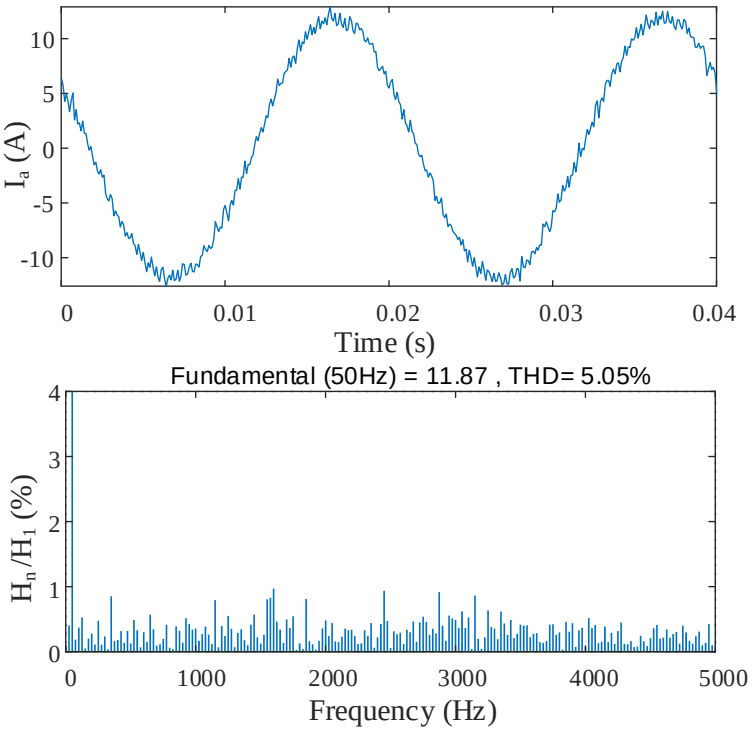

Fig. 2.16 Stator current and the corresponding harmonic spectrum at 600 r/min with rated load for the basic FCSMPC.

Chapter 3

CONVENTIONAL TECHNIQUES FOR CURRENT RIPPLE MINIMIZATION

3.1 INTRODUCTION

As analyzed in 2.5, due to the limited available voltage vector candidates and the fixed mode of applying only one voltage vector in a sampling interval, the basic FCSMPC suffers from large current ripples. The current ripples impact the steady-state performance of the system and therefore must be given enough attention. In this chapter, two conventional FCSMPC-based methods which are aiming on the reduction on current ripples are introduced. The FCSMPC with virtual voltage vectors is presented in 3.2 while the FCSMCP with duty cycle control is introduced in 3.3. The principle and the mechanism of reducing current ripples of the two conventional methods are elaborated in details. Moreover, both steady-state and transient performance of the two conventional methods are tested and demonstrated through the experimental results in the corresponding section.

3.2 FCSMPC WITH VIRTUAL VOLTAGE VECTORS

3.2.1 PRINCIPLE OF THE METHOD

Considering that the limited voltage vector candidates provided by basic FCS is one of the main sources of the large current ripples by the basic FCSMPC, the first typical technique (i.e. virtual voltage vectors) is introduced in FCSMPC. This method (FCSMPC with virtual voltage vectors) reduces the current ripples by increasing the available vector candidates in the control set. For demonstration convenience, the method of FCSMPC with virtual voltage vectors is referred as FCSMPC-I in the following content. The diagram of the FCSMPC-I is shown in Fig. 3.1, in which the key functional blocks are finite control set with virtual voltage vectors and optimal voltage vector selection. By elaborating these two blocks, the principle of the FCSMPC-I will be clearly depicted.

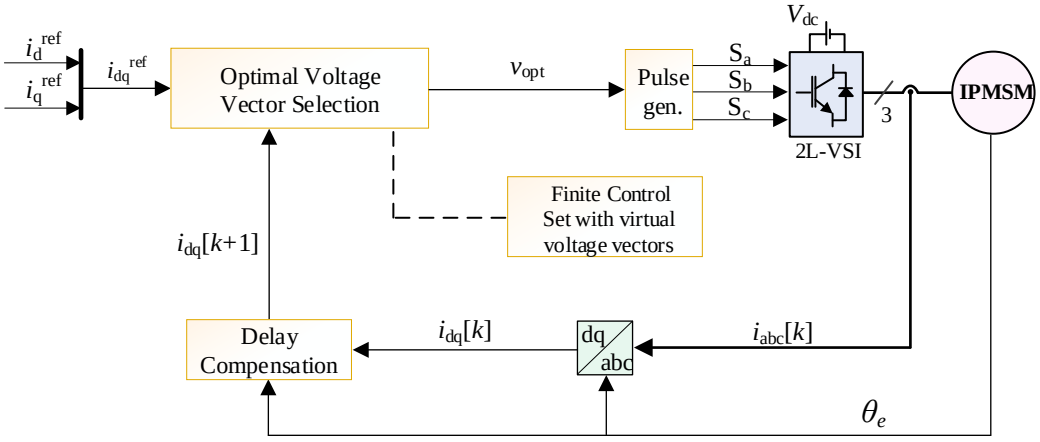

Fig. 3.1 The diagram of FCSMPC-I.

A. finite control set with virtual voltage vectors

To be consistent with the whole control scheme and the prediction model of the PMSM, the eight basic voltage vectors in stationary frame (v_0 to v_7) are transformed into the synchronous rotating coordinate (denoted as $v_{dq}0$ to $v_{dq}7$) as shown in Fig. 3.2, where θ_e is the electrical angular position of the rotor. To realize more available voltage vector candidates besides the eight basic voltage vectors in the basic FCS, the concept of virtual voltage vector is adopted. In FCSMPC-I, six additional virtual voltage vectors are introduced to expand the conventional FCS.

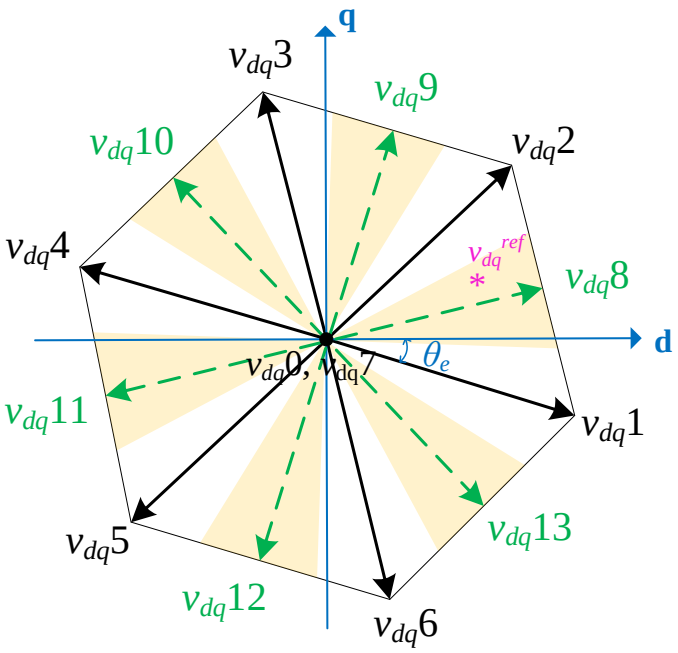

Fig. 3.2 Vectorial diagram of the voltage vectors in dq frame for FCSMPC-I.

As shown in Fig. 3.2, the six virtual voltage vectors are symmetrically distributed in the vector diagram and each of them is pre-synthesized by the two adjacent active voltage vectors with equal duty ratio of 50% [61] . For example, the virtual voltage vector $v_{dq}8$ is synthesized by applying each of the basic voltage vectors $v_{dq}1$ and $v_{dq}2$ with $0.5T_s$ in sequence in a sampling period. The correspondence between the virtual voltage vectors and the basic voltage vectors is concluded in Table 3.1.

Table 3.1 Correspondence between virtual voltage vectors and basic voltage vectors

Virtual voltage vectors	Pre-synthesized by	Gating signal
$v_{dq}8$	$v_{dq}1 + v_{dq}2$	(1, 0.5, 0)
$v_{dq}9$	$v_{dq}2 + v_{dq}3$	(0.5, 1, 0)
$v_{dq}10$	$v_{dq}3 + v_{dq}4$	(0, 1, 0.5)
$v_{dq}11$	$v_{dq}4 + v_{dq}5$	(0, 0.5, 1)
$v_{dq}12$	$v_{dq}5 + v_{dq}6$	(0.5, 0, 1)
$v_{dq}13$	$v_{dq}6 + v_{dq}1$	(1, 0, 0.5)

As compared to the basic FCSMPC, the actual control set utilized in this method is enlarged by introducing six more voltage vector candidates, which provides more available choices in the selection of the optimal voltage vector and hence achieves the reduction of the current ripples. The effect of the additional virtual voltage vectors on the reduction of the current ripples will be further analyzed in details in 3.2.2.

B. Optimal voltage vector selection

According to the principle of FCSMPC as illustrated in 2.4, the optimal voltage vector is such selected that the cost function is minimized. For the FCSMPC-I which has six additional virtual voltage vectors, the optimal voltage vector is selected among the total fourteen available voltage vector candidates through thirteen enumerations (the two null vectors are considered as one valid vector candidate in the selection process as they produce the same current variation). Considering the large computational resources required by the normal enumeration-based optimal voltage vector selection method, a quick optimal voltage vector selection strategy is adopted in FCSMPC-I. The quick selection method avoids the enumerations by integrating the concept of dead beat, which has been widely utilized in nowadays literatures [62] [63] [64] [65] . As been clearly illustrated for the FCSMPC, the cost function is minimized by the optimal voltage vector selected from the control set. Obviously, the theoretical minimum value of the cost function is zero if the predicted current equals the reference current at each sampling interval. According to the deadbeat, the reference voltage vector (v_{dq}^{ref}) which guarantees the zero error between the predicted current and the reference current could be calculated by replacing $i_{dq}(k+2)$ with i_{dq}^{ref} in (2.5):

$$\begin{cases} i_d^{ref} = \left(1 - \frac{R_s T_s}{L_d}\right) i_d^p(k+1) + \frac{T_s}{L_d}\left[v_d^{ref}(k+1) - e_d(k+1)\right] \\ i_q^{ref} = \left(1 - \frac{R_s T_s}{L_q}\right) i_q^p(k+1) + \frac{T_s}{L_q}\left[v_q^{ref}(k+1) - e_q(k+1)\right] \end{cases} \tag{3.1}$$

Next, the vector scheme is equally divided into twelve sectors, where the 12 active voltage vectors (including six basic active voltage vectors and six virtual vectors) are located in the middle of the corresponding sectors as shown in Fig. 3.2. Apparently, the control accuracy is higher if the applied voltage vector is closer to the reference voltage vector [62] [64] . Therefore, the active voltage vector which locates in the same sector with the reference voltage vector is determined as a preliminary optimal voltage vector. Finally, the optimal voltage vector is selected among the preliminary optimal voltage vector candidate and the null voltage vector according to the principle of cost function minimization. For example in Fig. 3.2, the reference voltage vector is located in the same sector with the $v_{dq}8$. Thereby, $v_{dq}8$ and one null vector are evaluated by the cost function and the one who presents a smaller value of the cost function will be selected as the optimal voltage vector.

3.2.2 MECHANISM ON REDUCING THE CURRENT RIPPLES

The benefits on the current ripple reduction by the FCSMPC-I is attributed to the increased available voltage vector candidates. For example, the v_{dq}^{ref} is located in the position as demonstrated in Fig. 3.2. For the basic FCSMPC, the basic voltage vector $v_{dq}2$ is determined as the optimal voltage vector and applied in the next step. However, by introducing six extra virtual voltage vectors, a more accurate choice $v_{dq}8$ is available for the FCSMPC-I, which will lead to less current error and hence lower current ripples at next step. Fig. 3.3 depicts an example of the q-axis current response of the FCSMPC-I, by which

the mechanism of the current ripple reduction could be exhibited in a more straightforward way.

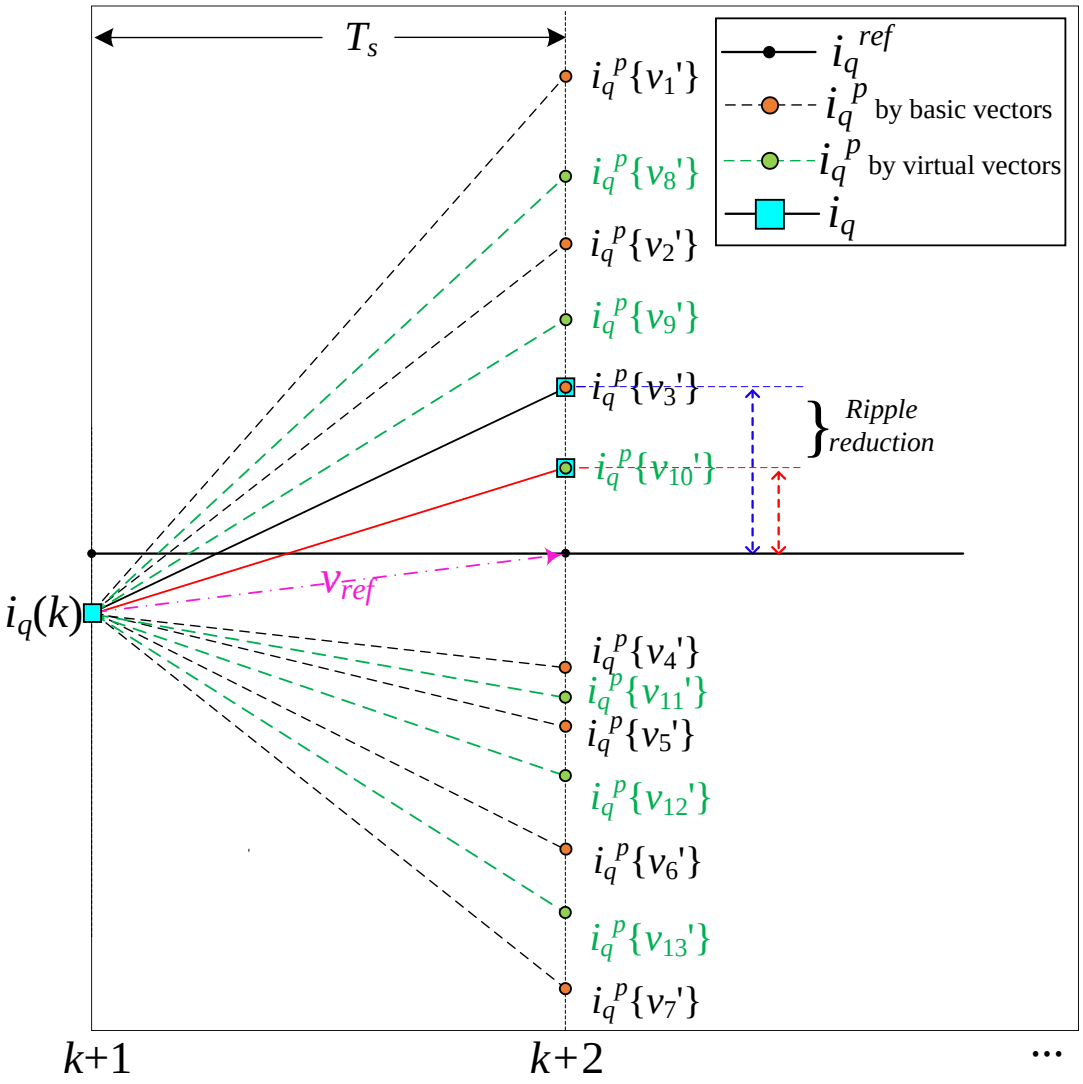

Fig. 3.3 The schematic of the current behavior by FCSMPC-I.

As shown in the figure, v_1' to v_7' denote seven basic voltage vector candidates from FCS (the two basic null vectors are considered as one valid vector candidate) while v_8' to v_{13}' represent six virtual voltage vector candidates. For the basic FCSMPC, the vector candidate v_3' is selected as the optimal voltage vector among all the basic voltage vectors as it provides the minimum error between the predicted current and the reference current. However, for the FCSMPC-I, a more accurate vector candidate v_{10}' is available for application at next step, which will present less current error and hence lower current ripples than v_3' as clearly shown in the figure. By adopting the concept of virtual voltage vectors, the actual control set utilized in this method is enlarged compared to the basic FCS, which provides more available choices in the selection of the optimal voltage vector and hence achieves the reduction of the current ripples. The effect of the current ripple reduction will be verified in the experimental results in 3.2.4.

3.2.3 LIMITATION

The FCSMPC-I achieves current ripple reduction by introducing six virtual voltage vectors. However, the reduction effect of FCSMPC-I is limited under the condition of low rotor speed, which is clearly demonstrated in the diagram as shown in Fig. 3.4. For example, the reference voltage vector v_{dq}^{ref} is located in the same sector with the virtual voltage vector $v_{dq}8$. When the motor runs at high speed, the back EMF is large, which means the magnitude of the reference voltage vector v_{dq}^{ref} is relatively large according to (3.1). By selecting the virtual voltage vector $v_{dq}8$ as the optimal voltage vector, the current ripples of

FCSMPC-I will be distinctly reduced as $v_{dq}8$ is located much closer to v_{dq}^{ref} than the basic voltage vectors $v_{dq}1$ and $v_{dq}2$. However, when the rotor rotates at low speed, the magnitude of v_{dq}^{ref} is relatively smaller due to the small back emf, as clearly shown in Fig. 3.4. Under this circumstance, the advantage of virtual voltage vectors cannot be evidently exhibited because all the vector candidates (including basic and virtual voltage vectors) are located far away from the reference voltage vector, which will significantly limit the current ripple reduction effect of the FCSMPC-I. This limitation of the FCSMPC-I will be verified and demonstrated in the experimental results in 3.2.4.

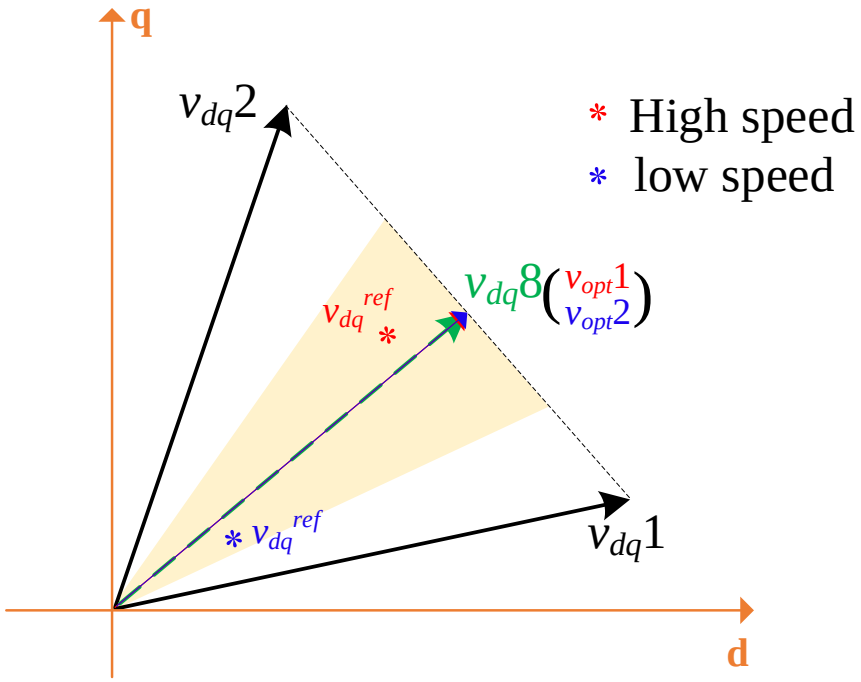

Fig. 3.4 Diagram for demonstrating the limitation of FCSMPC-I.

3.2.4 PERFORMANCE OF FCSMPC-I IN EXPERIMENT

The dynamic and steady-state performance of the FCSMPC-I are shown in the following experimental results, where the effect of the current ripple reduction of the FCSMPC-I can also be observed. For comparison purpose, the experiments for the FCSMPC-I are carried out under the same conditions as for the basic FCSMPC in 2.6.

The dynamic performance of FCSMPC-I is demonstrated in Fig. 3.5 and Fig. 3.6. Fig. 3.5 shows the dynamic performance of d- and q- axis currents with the rotor speed transient from standstill to rated speed at 0.05s with no load. By keeping the merit of the basic FCSMPC, the FCSMPC-I presents a stable control performance against the step change of speed. Moreover, it delivers smaller current ripples than the basic FCSMPC as presented in 2.6, which is observed more clearly on the d-axis current. Fig. 3.6 shows the current transient responses to a stepped change from no load to full load at 0.05s with the machine speed of 100 r/min. It is seen that the actual current tracks the reference current closely when the load suddenly changes, which is similar to the dynamic response of the FCSMPC. However, the effect of the current ripple reduction is not distinct for the FCSMPC-I as shown in the results, which reflects the limitation of the FCSMPC-I at low speed as analyzed in 3.2.3.

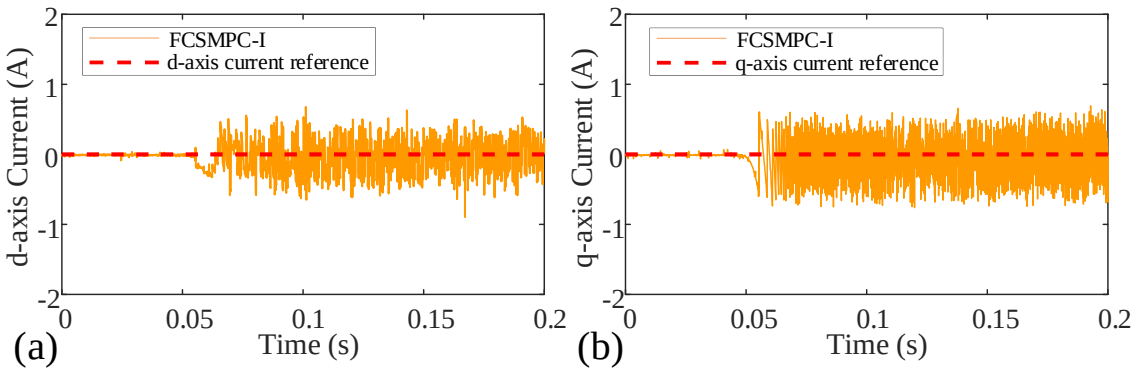

Fig. 3.5 Experimental results of the current responses (a) d-axis and (b) q-axis when speed steps from 0 r/min to 600 r/m at no load for FCSMPC-I.

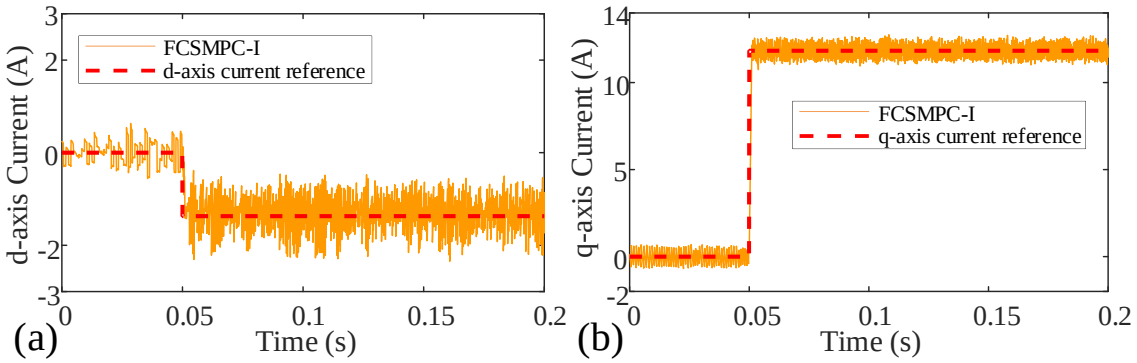

Fig. 3.6 Experimental results of the current responses (a) d-axis and (b) q-axis for step change from no load to full load at 100 r/min for FCSMPC-I.

The steady-state performance of the FCSMPC-I at rated speed with rated load is demonstrated in Fig. 3.7, where the phase-a current and the corresponding harmonic spectrum are clearly depicted. As shown in the figure, the harmonics on the stator current are easily seen. However, a lower THD of 4.31% is observed for the FCSMPC-I as

compared to the 5.01% of the FCSMPC as previously presented, which validates the improved steady-state performance by the FCSMPC-I.

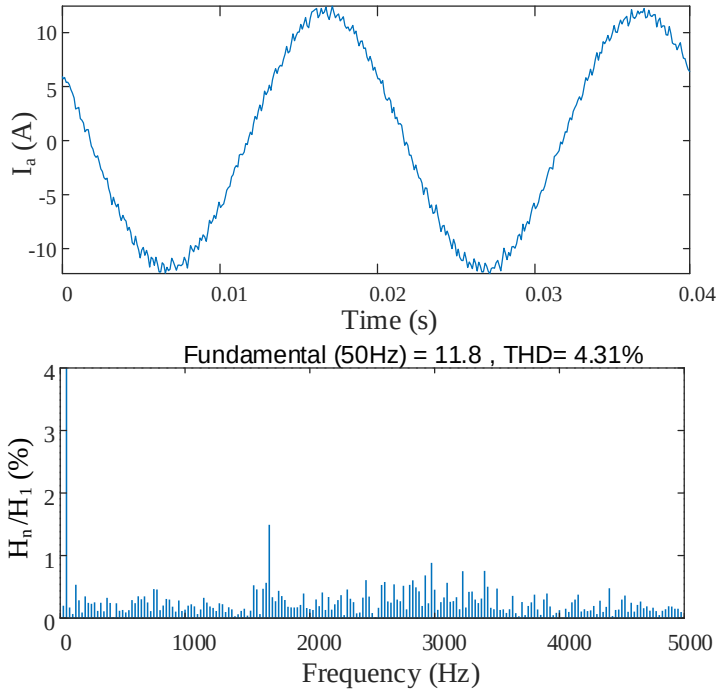

Fig. 3.7 Stator current and the corresponding harmonic spectrum at 600 r/min with rated load for FCSMPC-I.

3.3 FCSMPC WITH BASIC DUTY CYCLE CONTROL

3.3.1 PRINCIPLE OF THE METHOD

For the basic FCSMPC, only one of the eight basic voltage vectors is selected and applied during a control period, which may not reduce the cost function to a minimal value and therefore causes large current ripples. Regarding this, the second typical technique (i.e.

duty cycle control) is introduced to FCSMPC, which improves the steady-state performance by adopting the concept of duty cycle. In other words, this method (FCSMPC with duty cycle control) utilizes a more flexible control mode of applying two voltage vectors in a sampling period- one active voltage vector together with one null voltage vector [65] . For demonstration convenience, the method of FCSMPC with duty cycle control is referred as FCSMPC-II in the following content. Fig. 3.8 shows the diagram of the FCSMPC-II.

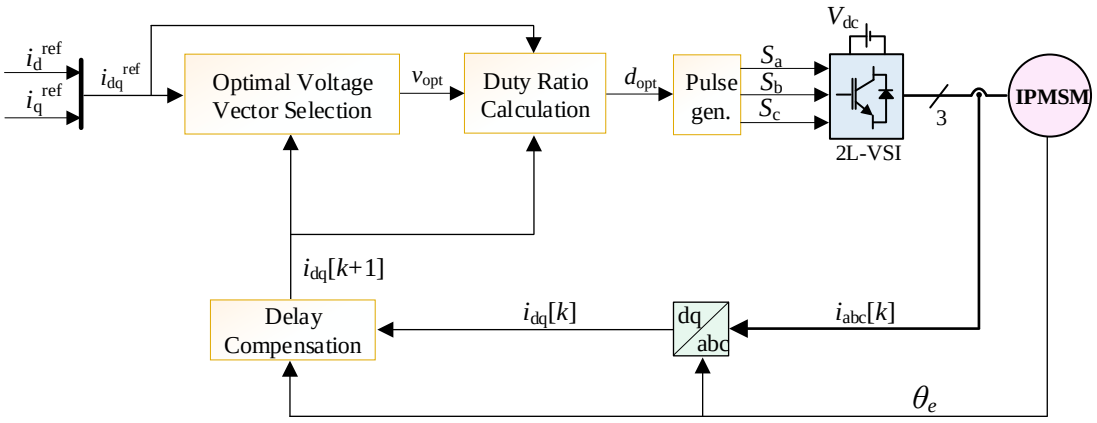

Fig. 3.8 The diagram of FCSMPC-II.

Based on the diagram, the basic principle of the FCSMPC-II is simply described by the main functional blocks: 1) Selection of optimal voltage vector among the six basic active voltage vectors; 2) Calculation of the duration time of the optimal voltage vector. By elaborating these two key blocks, the principle of the FCSMPC-II will be clearly depicted.

A. optimal voltage vector selection

For the FCSMPC-II, the quick optimal voltage vector selection method is adopted for a similar concern of avoiding the high computational load brought by the enumerations. Similar to the theory presented in 3.2.1-B, the vector scheme is equally divided into six sectors, where the six active voltage vectors are located in the middle of the corresponding sectors as shown in Fig. 3.9.

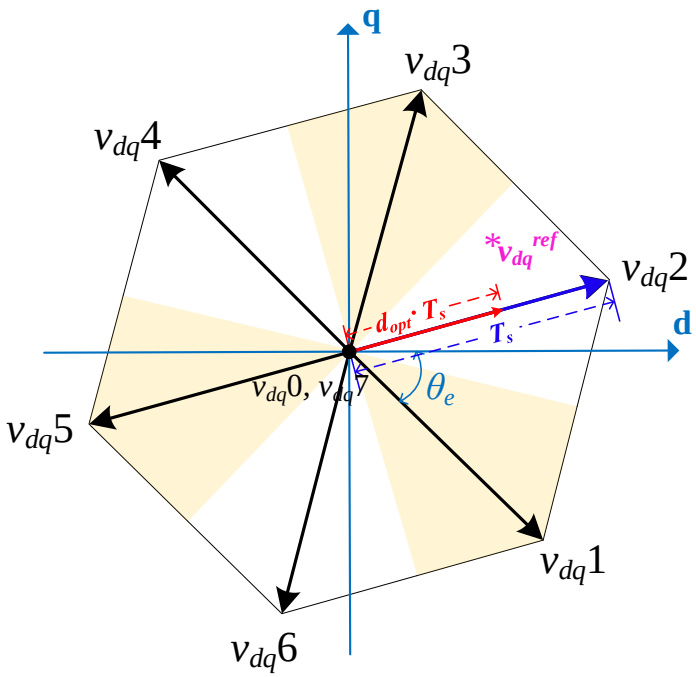

Fig. 3.9 Vectorial diagram of FCSMPC-II.

The reference voltage vector is calculated and located in the vector-sector scheme in the similar way as previously illustrated. The active voltage vector, which locates in the same

sector with the reference voltage vector, will be selected as the optimal active voltage vector. The further comparison between the selected active voltage vector and the null vectors are no longer required, as the null voltage vectors are utilized together with the selected active voltage vector in every sampling interval. Since there are two null vectors available (i.e. v_0(000) and v_7(111)), it is worth discussing which one of the null vectors is going to be selected as a companion to the optimal active vector. As acknowledged, the switching state is updated every time when the applied voltage vector is changed. Moreover, the frequent and unnecessary switching will increase the switching loss of the system and shorten the life span of the power switches. Given to this fact, the selection of the null vectors is based on the principle that the switching commutations are minimized between the optimal active voltage vector and the null voltage vector in a sampling interval [66] [67] . For example, when the optimal active voltage vector is determined as v_1(100), the application of the null vector v_0(000) will lead to only one switching while v_7(111) will result in the switching on two phases. Therefore, v1 will be selected as the companion null vector with the optimal active vector. In conclusion, the active voltage vectors v_1(100), v_3(010) and v_5(001) will be followed by the null vector v_0(000), while the active voltage vectors v_2(110), v_4(011) and v_6(101) will be accompanied by the null vector v_7(111). According to this principle, the switching frequency and hence the switching loss will be effectively reduced.

B. duty ratio calculation of the optimal voltage vector

In FCSMPC-II, the selected optimal active voltage vector will be applied in a certain duration of a sampling period and the null voltage vectors will be applied for the rest of the time in the same sampling interval. The duty ratio is defined as the division of the duration time of the optimal voltage vector by the sampling period T_s. Considering that the reference voltage vector guarantees the zero error between the predicted current and the reference current, the duty ratio for the FCSMPC-II is calculated based on the principle that the error between the reference voltage vector and the optimal active voltage vector is minimized [63] [64] . Thereby, the duty ratio of FCSMPC-II is calculated as:

$$d_{opt} = \frac{v_{dq}^{ref} \cdot v_{opt}}{|v_{opt}|^2} \tag{3.2}$$

Definitely, the optimal active voltage vector will be applied in a duration of $d_{\text{opt}} \cdot T_s$ and the null voltage vector is applied during the rest time $(1\text{-}d_{\text{opt}}) \cdot T_s$. By concluding the effect of both the null vector and the optimal active voltage vector in a control interval, the actual voltage vector applied at next control step can be represented as:

$$v_{act} = d_{opt} \cdot v_{opt} + (1 - d_{opt}) \cdot \ v_{null} \tag{3.3}$$

The mechanism of implementing the duty cycle control on the reduction of the current ripples will be elaborated in the next section.

3.3.2 MECHANISM ON REDUCING THE CURRENT RIPPLES

The benefits on the current ripple reduction by the FCSMPC-II is attributed to the flexible control mode, which adopts the concept of duty cycle control by applying one null voltage vector together with one active voltage vector in a sampling interval. By introducing the null voltage vectors, the optimal voltage vector can be flexibly applied in the right proportion of the sampling interval, which actually provides more accurate control choices in each control interval. For example, v_{dq}^{ref} is located in the position as demonstrated in Fig. 3.9. For the basic FCSMPC, the active voltage vector $v_{dq}2$ is selected and directly applied in a full sampling interval, which significantly deviates from the reference voltage vector and hence results in low control accuracy with large current ripples. However, by adopting the concept of duty cycle control, the optimal voltage vector $v_{dq}2$ is only applied in a regulated proportion of the sampling period when the null voltage vector occupies the rest of the time. The actual applied voltage vector is demonstrated using the red vector as shown in Fig. 3.9. Obviously, it locates closer to the reference voltage vector and therefore results in higher control accuracy and presents lower current ripples.

The effect of adopting the duty cycle control could be demonstrated through another perspective by analyzing the current response caused by the null voltage vectors. According to the prediction model in (2.4), the current variations caused by the null voltage vectors can be represented as:

$$\begin{cases} \frac{di_d(t)}{dt} = -R_s i_d(t) - e_d(k) \\ \frac{di_q(t)}{dt} = -R_s i_q(t) - e_d(k) \end{cases} \tag{3.4}$$

It is clearly seen that the current will always decrease by applying the null voltage vectors. Therefore, the null voltage vectors could be used to adjust the extra current variation caused by the active voltage vectors. Fig. 3.10 depicts an example of the q-axis current response of the FCSMPC-II, by which the mechanism of the current ripple reduction could be exhibited in a straightforward way.

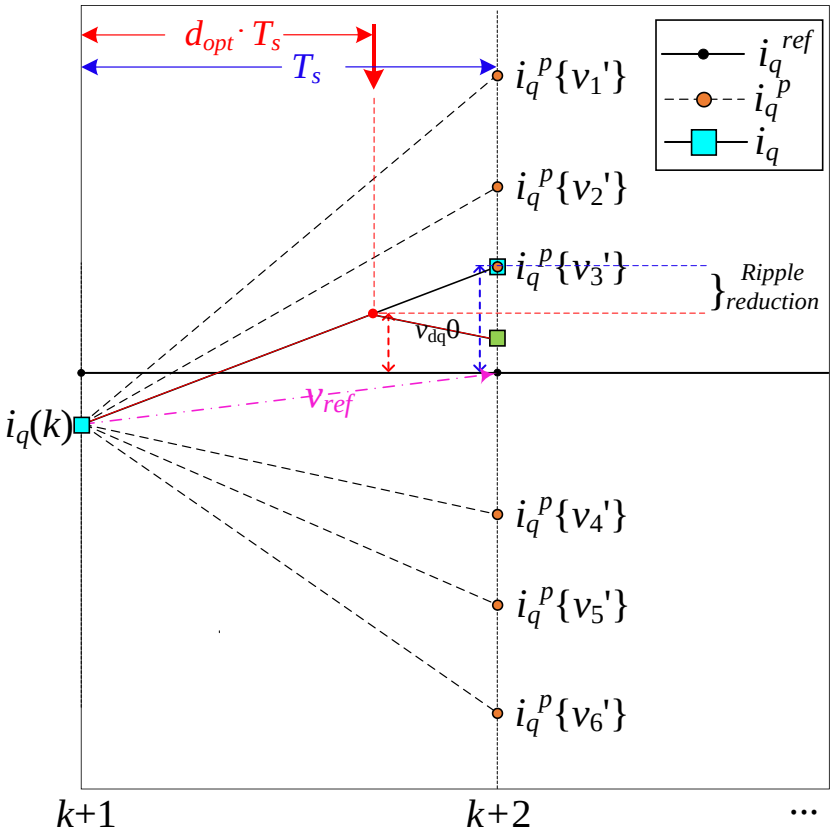

Fig. 3.10 The schematic of the current behavior by FCSMPC-II.

As shown in the figure, v_1' to v_7' denote seven basic voltage vector candidates from FCS (the two basic null vectors are considered as one valid vector candidate). According to the principle of the basic FCSMPC, the vector candidate v_3' is selected as the optimal voltage vector. By applying v_3' in a full sampling period, the q-axis current reaches the reference value first, however continuously rises up and finally exceeds the reference current with a large error at next instant. On the contrary, by adjusting the current variation using the null voltage vectors, the q-axis current of FCSMPC-II achieves mild variation and hence presents smaller current ripples as clearly shown in the figure. By adopting the concept of duty cycle control, the application duration of the optimal voltage vector can be flexibly adjusted in this method as compared to the basic FCSMPC, which achieves mild current variations and hence reduces the current ripples.

3.3.3 LIMITATION

By utilizing one null voltage vector and one active voltage vector in a sampling period, the current ripples by FCSMPC-II are effectively reduced. However, the ripple reduction effect of FCSMPC-II is limited at high rotor speed, which is clearly demonstrated in the diagram as shown in Fig. 3.11. For example, the reference voltage vector v_{dq}^{ref} is located between the basic voltage vectors $v_{dq}1$ and $v_{dq}2$, among which the $v_{dq}1$ is selected as the optimal voltage vector as it locates closer to v_{dq}^{ref}. When the motor runs at low speed, the back EMF is small, which means the magnitude of the reference voltage vector v_{dq}^{ref} is relatively small according to (3.1). By properly calculating the duty ratio of the optimal voltage vector $v_{dq}1$

in (3.2), the actually applied voltage vector $v_{opt}1$ could be located very close to v_{dq}^{ref} as shown in the figure, which will lead to higher control performance with distinct reduction on the current ripples. However, when the rotor rotates at high speed, the magnitude of v_{dq}^{ref} is relatively larger due to the large back emf, as clearly shown in Fig. 3.11. Under this circumstance, the advantage of utilizing the null voltage vectors cannot be fully exhibited. Even by regulating $v_{dq}1$ with a properly calculated duty ratio, the actually applied voltage vector $v_{opt}2$ is far away from the reference voltage vector, which will greatly limit the current ripple reduction effect of FCSMPC-II. This limitation of FCSMPC-II will be verified and demonstrated in the experimental results in 3.3.4.

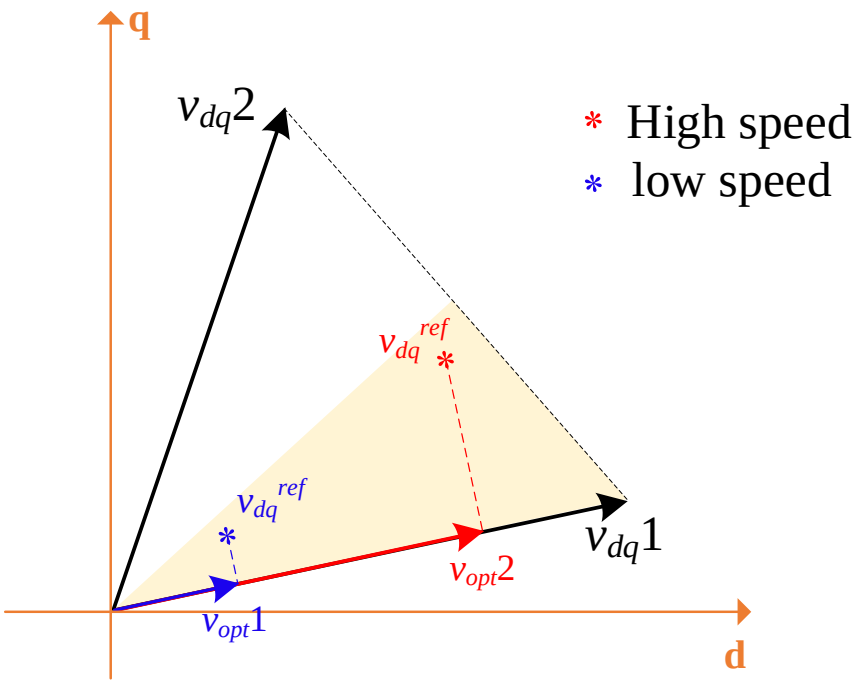

Fig. 3.11 Diagram for demonstrating the limitation of FCSMPC-II.

3.3.4 PERFORMANCE OF FCSMPC-II IN EXPERIMENT

The dynamic and steady-state performance of the FCSMPC-II are demonstrated in the following experimental results, where the effect of the current ripple reduction of the FCSMPC-II can also be observed. For comparison purpose, the experiments for the FCSMPC-II are carried out under the same conditions as for the basic FCSMPC in 2.6.

The dynamic performance of FCSMPC-II is demonstrated in Fig. 3.12 and Fig. 3.13. Fig. 3.12 shows the dynamic performance of d- and q- axis currents with the rotor speed transient from standstill to rated speed at 0.05s with no load. As compared to the basic FCSMPC as presented in 2.6, the FCSMPC-II shows a similar dynamic control performance against the step change of speed while effectively reduces the current ripples. However, the current ripples on the d-axis are still large, which is mainly due to the limitation of the FCSMPC-II at high speed as analyzed in 3.3.3. Fig. 3.13 shows the current transient responses to a stepped change from no load to full load at 0.05s with the machine speed of 100 r/min. As shown in the figure, the FCSMPC-II shows good tracking performance when the load changes, while it presents an overshoot on the d-axis current which may come from uncertain vibration on the motor. Moreover, an obvious current ripple reduction is clearly observed on both d- and q- axis for the FCSMPC-II as compared to the basic FCSMPC.

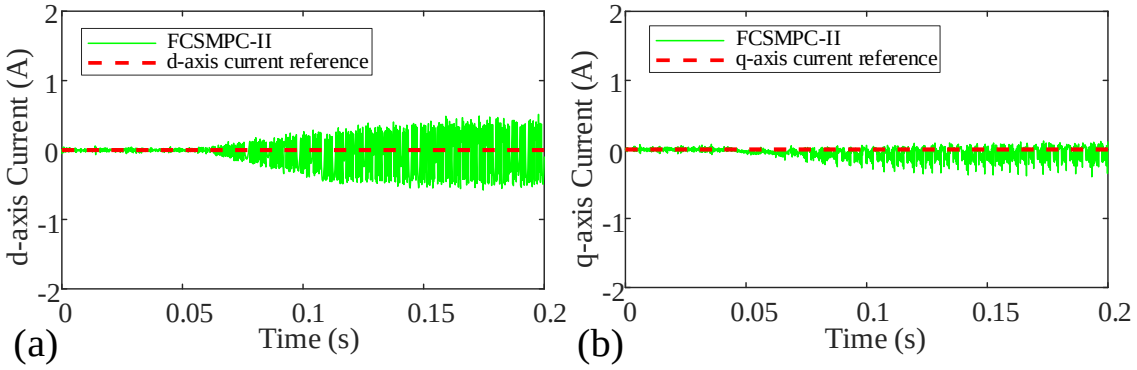

Fig. 3.12 Experimental results of the current responses (a) d-axis and (b) q-axis when speed steps from 0 r/min to 600 r/m at no load for FCSMPC-II.

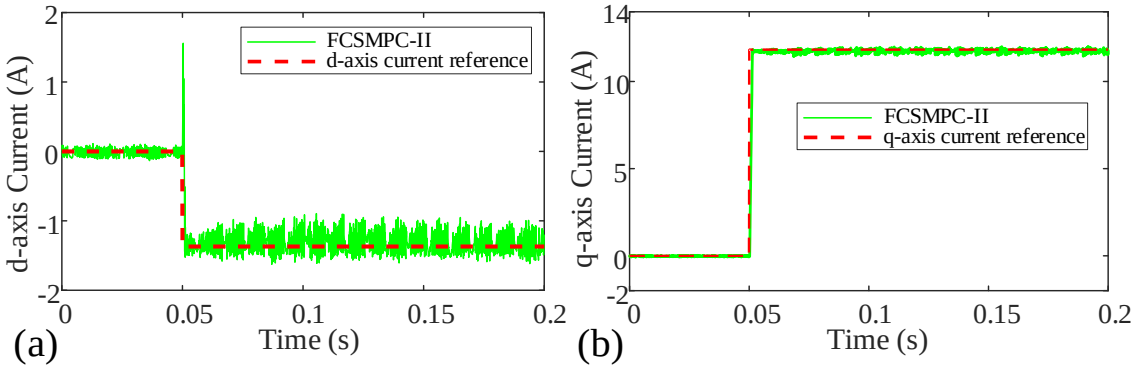

Fig. 3.13 Experimental results of the current responses (a) d-axis and (b) q-axis for step change from no load to full load at 100 r/min for FCSMPC-II.

The steady-state performance of the FCSMPC-II at rated speed with rated load is presented in Fig. 3.14, where the phase-a current and the corresponding harmonic spectrum are clearly depicted. As compared to the basic FCSMPC as shown in 2.6.2, the stator current of FCSMPC-II is observed to be more sinusoidal with less distortion. According to the FFT

analysis, a lower THD of 3.40% is observed for the FCSMPC-II as compared to the 5.01% of the basic FCSMPC as previously presented, which validates the improved steady-state performance by the FCSMPC-II.

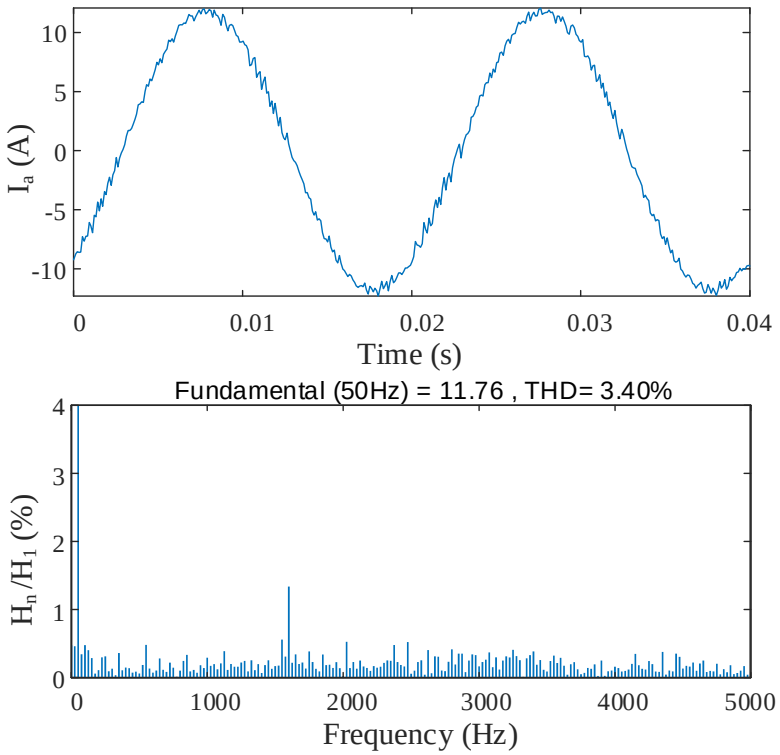

Fig. 3.14 Stator current and the corresponding harmonic spectrum at 600 r/min with rated load for FCSMPC-II.

Chapter 4

PROPOSED INTEGRATED DUTY CYCLE AND FINITE VIRTUAL VOLTAGE VECTOR TECHNIQUE

4.1 INTRODUCTION

As illustrated before, FCSMPC is a simple and effective control scheme for PMSM drives. However, it faces certain problem such as large current ripples and unsatisfactory steady-state performance. To reduce the current ripples, the concept of duty cycle is introduced in FCSMPC-II as presented in 3.3. In this method, one null voltage vector is applied in company with one active voltage so that the active voltage vector is applied in the right proportion of the sampling period. It achieves moderate current variations than that of the basic FCSMPC. However, relatively large current ripples still exist, because, the duty ratio is only applied to the six basic active voltage vectors as adopted in the basic FCSMPC, so that the choices of the output voltage candidates are still limited. To obtain more output voltage vector candidates, the available control vectors are expanded in FCSMPC-I, as

presented in 3.2. However, it does not take the full advantage of duty cycle and therefore fails to achieve distinct improvement on the current ripple reduction.

This chapter proposes an improved FCSMPC method with integrated duty cycle and finite virtual voltage vector technique to achieve current ripple minimization for high performance control of PMSM drives. In the proposed method, six symmetrically located virtual voltage vectors are generated and then introduced in addition to the six original active voltage vectors to expand the finite control set. Then, one optimal voltage vector is selected according to the enumeration-based principle of current cost function minimization. Compared to the basic FCSMPC, the proposed method is proven to cause no additional computation load but can deliver higher control accuracy. Finally, the corresponding duty ratio of the optimal voltage vector is decided based on a straightforward principle with a computationally efficient algorithm. The principle of the proposed method is introduced in 4.2. The mechanism of the proposed method on reducing current ripples is elaborated in 4.3. In 4.4, the performance of the proposed method is verified through the results in MATLAB Simulink. Furthermore in 4.5, the proposed method is comparatively studied with FCSMPC-I and FCSMPC-II and its benefits are confirmed by the experimental results for the reference IPMSM drive system. Finally, a supplementary analysis is given on the difference between the proposed optimal vector selection method and the conventional quick selection method, which will further prove the higher accuracy of the proposed method.

4.2 PRINCIPLE OF THE METHOD

The control diagram of the proposed method is shown in Fig. 4.1, which mainly comprises of current prediction, finite control set expansion, cost function minimization/optimal voltage vector selection, duty ratio calculation and pulse generation. The torque reference is given to calculate the d-axis and q-axis current reference based on the criteria of maximum torque per ampere (MPTA). Moreover, all the variables in the control scheme are transformed into the synchronous rotating frame to perform field-oriented control. For demonstration convenience, the proposed method is referred as Proposed-I in the following content. The detailed introduction of the main functional blocks of Proposed-I are elaborated as follows.

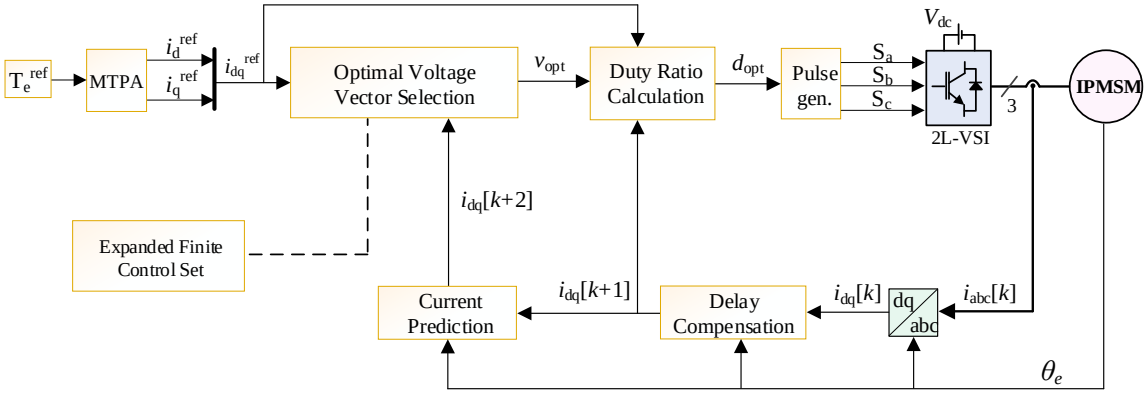

Fig. 4.1 The diagram of Proposed-I.

A. Expansion of the basic FCS

For a two-level voltage source inverter, there are eight basic switching states (including six active voltage vectors and two null voltage vectors), which constitute the conventional finite control set of FCSMPC as illustrated in Chapter 2. The eight basic voltage vectors in the stationary reference frame (v_0 to v_7) are transformed in the rotor synchronous frame (denoted as $v_{dq}0$ to $v_{dq}7$) as shown in Fig. 4.2, where the angle between $v_{dq}1$ and the d-axis is denoted as θ, which represents the electrical angular position of the rotor. Since the basic FCSMPC adopts only the eight basic voltage vectors in each sampling interval, it inevitably leads to poor approximation of the exact voltage required to precisely track the reference current (such as in vector control), and therefore results in large current ripples.

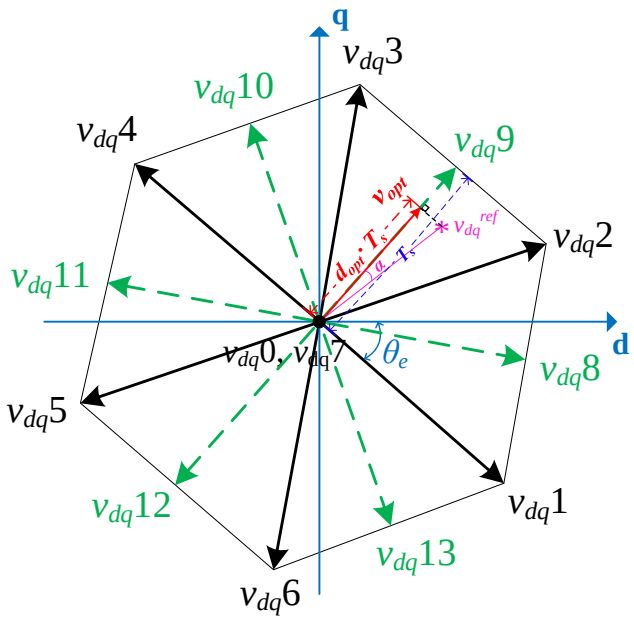

Fig. 4.2 Vectorial diagram of Proposed-I.

To realize more available voltage vector candidates, the conventional finite control set is expanded by introducing six additional virtual voltage vectors (denoted as $v_{dq}8$ to $v_{dq}13$) as shown in Fig. 4.2. The six virtual vectors are symmetrically distributed in the vector diagram and each of them is pre-synthesized by the two adjacent active voltage vectors with equal duty ratio of 50%. The enlarged control set provides more choices of the control voltage when evaluating the objective cost function, which will definitely improve the control accuracy.

B. Optimal voltage vector selection

With the aim to minimize current ripples, the principle of the Proposed-I is to select one voltage vector which minimizes the current-error-based cost function (4.1). Considering the one-step delay compensation, the currents predicted at $(k+2)^{th}$ step are used in the calculation.

$$J = \left| i_{dq}^{ref} - i_{dq}(k+2) \right|^2 \tag{4.1}$$

where

$$i_{dq}^{ref} = \begin{bmatrix} i_d^{ref} \\ i_d^{ref} \end{bmatrix} \tag{4.2}$$

$$i_{dq}(k+2) = \begin{bmatrix} i_d(k+2) \\ i_q(k+2) \end{bmatrix} \tag{4.3}$$

For the proposed method, six $i_{dq}(k+2)$ are first predicted for the six basic active voltage vectors, among which the two voltage vectors that present the minimum and subminimum values of the cost function J will be selected as the optimal vector candidates. Then, the virtual voltage vector that locates between these two optimal vector candidates is selected as the third optimal vector candidate and evaluated by (4.1). Finally, the optimal vector candidate that presents the minimal value of the cost function J is selected as the optimal non-zero voltage vector. It should be noted that the null vector is not enumerated in the optimal vector selection since it is applied in each sampling period to adjust the amplitude of the optimal voltage vector, which will be elaborated in part C of this sub-section. For Proposed-I, the optimal voltage vector is selected among fourteen voltage vector candidates through only seven enumerations while the conventional FCSMPC also requires the same number of enumerations to evaluate eight voltage vectors. Compared to the basic FCSMPC, the Proposed-I causes no computational load but exhibits higher control accuracy and much better steady-state performance.

C. Duty cycle calculation

In the proposed method, a null vector is applied in combination with the optimal voltage vector in each sampling period to achieve further improvement on the steady-state performance. After obtaining the optimal non-zero voltage vector, the next step is the determination of its optimal duty ratio.

As shown in the part B, the optimal voltage vector (v_{opt}) is selected such as the cost function (4.1) is minimized. Obviously, the theoretical minimal value of (4.1) is zero and it can be achieved by applying a reference voltage vector, which is obtained according to the same equation as presented in (3.1). Then, the duty ratio of the optimal voltage vector is calculated based on the principle that the error between the reference voltage vector and the optimal voltage vector is minimal. Instead of utilizing vector calculations as in FCSMPC-II, a more concise and efficient way is adopted to obtain the duty ratio for the Proposed-I. As shown in Fig. 4.2, a line from the reference voltage vector is projected vertically to the optimal voltage vector. The division of the corresponding projection of v_{dq}^{ref} by the magnitude of the optimal voltage vector is determined as the optimal duty ratio:

$$d_{opt} = \frac{\left|v_{dq}^{ref}\right| \cdot cos\alpha}{|v_{opt}|} \tag{4.4}$$

where α is defined as the angle between the reference voltage vector and the optimal non-zero voltage vector.

4.3 MECHANISM ON REDUCING THE CURRENT RIPPLES

By integrating the merits of both virtual voltage vectors and duty cycle control, the Proposed-I achieves distinct current ripple reduction. By introducing the virtual voltage vectors, the actual control set is expanded, which provides more available voltage vector candidates for the optimal vector selection. With the further integration of duty cycle

control, the optimal voltage vector selected from the enlarged control set can be flexibly applied in the optimal proportion of the sampling interval, which further improves the control accuracy. For example, v_{dq}^{ref} is located in the position as demonstrated in Fig. 4.2. For the basic FCSMPC, the basic voltage vector $v_{dq}2$ is selected as the optimal voltage vector and applied at next step. However, for Proposed-I, a more accurate choice $v_{dq}9$ is first selected as the substitute for the $v_{dq}2$, and then applied in an optimal proportion of the sampling period. The actual applied voltage vector is demonstrated using the red vector as shown in Fig. 4.2. Obviously, it locates closer to the reference voltage vector and therefore results in higher control accuracy.

Fig. 4.3 depicts an example of the q-axis current response of the Proposed-I, by which the mechanism of the current ripple reduction could be exhibited in a more straightforward way. To demonstrate the better performance of the Proposed-I, the mechanisms of the conventional techniques are also presented in the figure. As shown in the figure, v_1' to v_4' denote four basic voltage vector candidates, while v_5' to v_7' represent three virtual voltage vector candidates. Moreover, the current predictions corresponding to the voltage vector candidates are clearly shown in the figure. For the basic FCSMPC, the vector candidate v_3' is selected as the optimal voltage vector among all the basic voltage vectors as it provides the minimum error between the predicted current and the reference current. However, for FCSMPC-I, a more accurate voltage vector v_6' would be selected as the optimal voltage vector instead, which provides less current error and lower current ripples. For the case of

FCSMPC-II, the vector candidate v_3' is selected as the optimal voltage vector as similar to the basic FCSMPC, while it is only applied in a regulated proportion of a sampling interval. As shown in Fig. 4.3, the current ripple presented by FCSMPC-II is even lower than the previous two methods. Finally, for Proposed-I, the more accurate vector candidate v_6' is first selected as the optimal voltage vector, and then applied in the right proportion of a sampling period according to an optimal duty ratio. Obviously, the current error and current ripples are further reduced for Proposed-I as compared to the previous techniques as clearly demonstrated in Fig. 4.3.

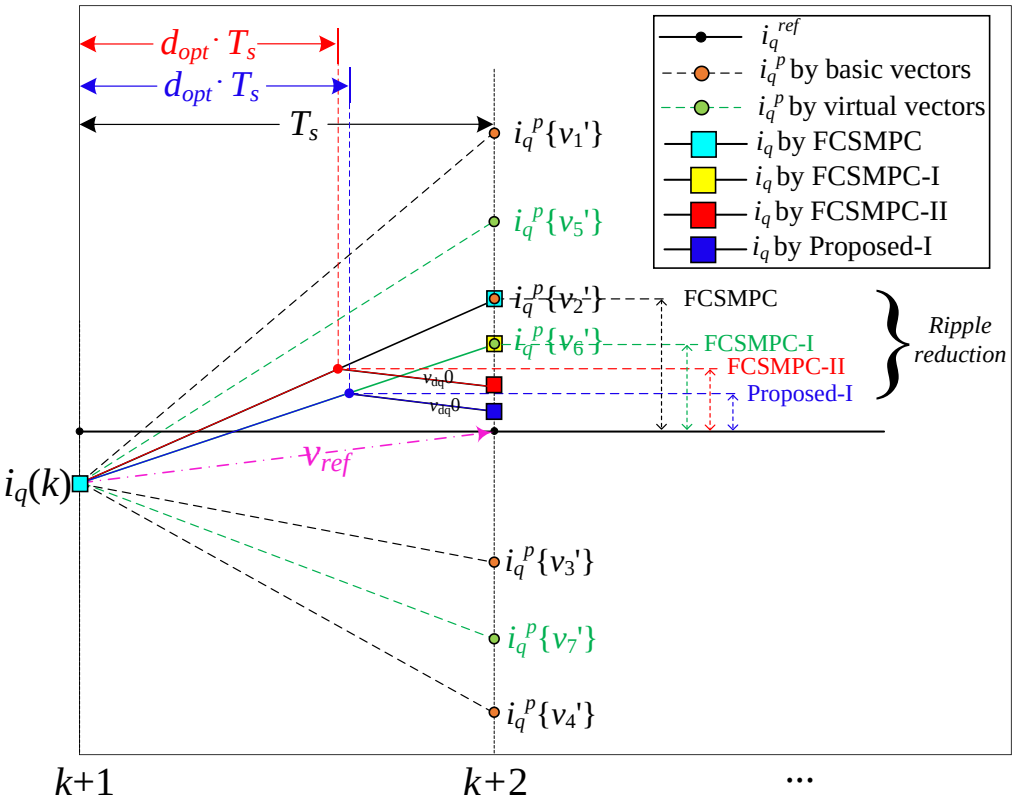

Fig. 4.3 The mechanism of the current ripple reduction by Proposed-I.

Unlike FCSMPC-I and FCSMPC-II whose performance are limited at low speed and high rotor speed respectively, the Proposed-I presents effective current ripple reduction effect at whole speed range as shown in Fig. 4.4. When the motor runs at low speed, the effect of implementing the duty ratio is more distinct, which will effectively regulate the magnitude of the applied voltage vector to an optimal value. When the rotor speed is high, the advantage of the introduced virtual voltage vector will exhibit more evidently, which provides more accurate vector candidates so that the current ripples could be further reduced, as clearly shown in Fig. 4.4. By integrating the virtual voltage vectors and the concept of duty cycle control, the Proposed-I achieves higher control accuracy with distinct current ripple reduction, which will be verified through simulation and experimental results in 4.4 and 4.5.

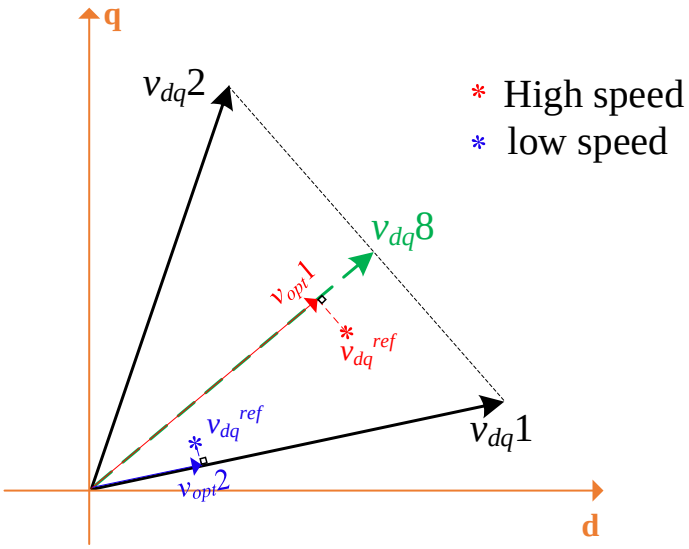

Fig. 4.4 Diagram for Proposed-I under high speed and low speed conditions.

4.4 SIMULATION RESULTS

The performance of the Proposed-I for a PMSM drive is first verified through simulations in MATLAB Simulink. The mathematical model of the IPM machine is built in Simulink by strictly following the parameters as shown in Table 2.2. To be consistent with the experimental environment as presented in 2.6.1, the sampling frequency of the simulation is configured as 10 kHz and the applied DC link voltage value is set as 300 V.

Fig. 4.5 shows the dynamic performance of d- and q- axis currents with the rotor speed transient from standstill to rated speed at 0.05s with no load. In Fig. 4.5, d-axis current and q-axis current for four methods are provided in two separate subfigures as shown in (a) and (b). It can be seen that the Proposed-I presents a stable control performance against the step change of speed, while reduces the current ripples especially on q-axis as compared to that of the basic FCSMPC as demonstrated in 2.6. Fig. 4.6 shows the current transient responses to a stepped change from no load to full load at 0.05s with the machine speed of 100 r/min. As shown in the figure, the actual current tracks the reference current closely when the load suddenly changes, which proves the dynamic response of the Proposed-I. Moreover, very small current ripples are observed for both d- and q-axis currents, by which the current ripple reduction effect is verified for the Proposed-I.

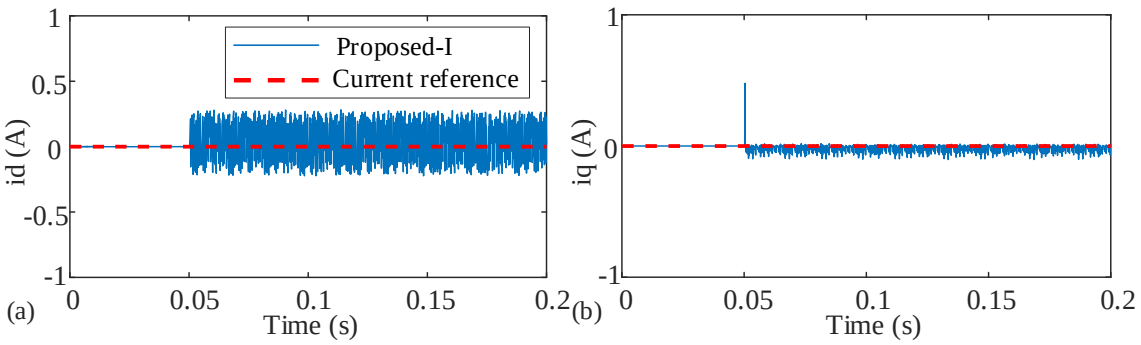

Fig. 4.5 Simulation results of the current responses (a) d-axis and (b) q-axis when speed steps from 0 r/min to 600 r/min at no load for Proposed-I.

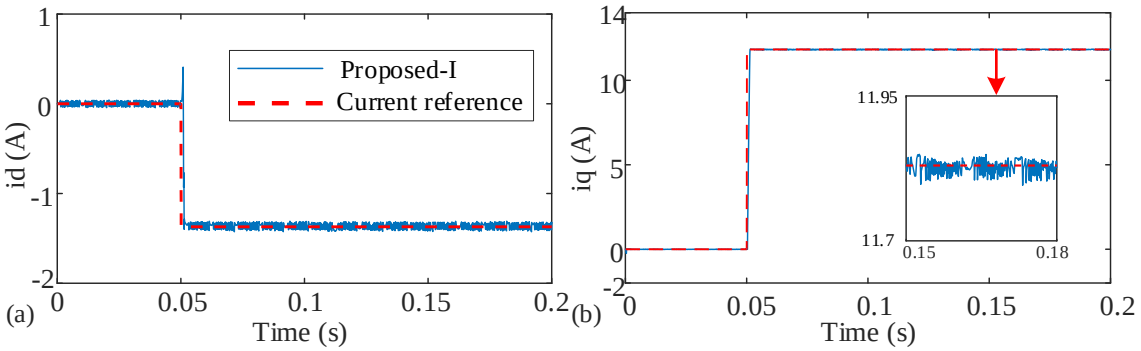

Fig. 4.6 Simulation results of the current responses (a) d-axis and (b) q-axis for the step change from no load to full load at 100 r/min for Proposed-I.

The performance of the Proposed-I will be further validated through experimental results in the next section, where more test conditions are applied and more analysis are given.

4.5 EXPERIMENTAL RESULTS

4.5.1 TRANSIENT AND STEADY-STATE PERFORMANCE

In this section, the steady-state and transient performance of the Proposed-I is validated through experiments under different conditions. Moreover, the basic FCSMPC, FCSMPC-I and FCSMPC-II are also experimentally tested as the comparisons for the Proposed-I under the same conditions. The experimental results for the four techniques are comparatively studied and analyzed, through which the effectiveness of the Proposed-I is confirmed. The experimental environment and the configurations are exactly the same as presented in 2.6.1.

First, the response of d- and q-axis currents with speed transient from 0 r/min to the rated speed at 0.05s with no load for the basic FCSMPC, FCSMPC-I, FCSMPC-II and Proposed-I are illustrated in Fig. 4.7. In Fig. 4.7, d-axis current and q-axis current for four methods are provided in two separate subfigures as shown in (a) and (b). It is seen that the current ripples delivered by the Proposed-I in experiment are consistent with simulation results as shown in Fig. 4.5. Moreover, compared to the basic FCSMPC, FCSMPC-I and FCSMPC-II, the Proposed-I shows similar dynamic performance while presents much lower current ripples. Similar results can also be observed in Fig. 4.8, where the rotor speed steps from 300 r/min to 600 r/min at 0.1s with 25% load on the machine. There is no distinct difference in dynamic performance of the Proposed-I, basic FCSMPC, FCSMPC-I and FCSMPC-II,

while obvious reduction on the current ripples is easily seen for the Proposed-I, which leads to a considerable improvement on the steady-state performance. Fig. 4.9 shows the transient responses for speed reversion at ±300 rpm at 0.1s when there is 25% load on the machine. It is demonstrated that the dynamic performance of the basic FCSMPC, FCSMPC-I, FCSMPC-II and the Proposed-I are very similar to each other, while the proposed method still delivers more satisfied steady-state performance than the other three FCSMPC methods in terms of lower current ripples.

Second, the current transient responses against step change of load for the four methods are investigated and shown in Fig. 4.10 and Fig. 4.11. Fig. 4.10 shows the dynamic responses to a step change from no load to full load at 0.05s where the machine runs at a low speed of 100 r/min. As shown in the figure, the Proposed-I presents similar current ripples as compared to the simulation results shown in Fig. 4.6. Moreover, it could be observed more distinctly than the previous results that the dynamic performance for the three methods are very close to each other. Nevertheless, it should be also noted that the Proposed-I has much smaller overshoot on the currents when the load changes, and it also presents lower current ripples. Similar results are also found in Fig. 4.11, which shows the current transient responses of load reversion at negative and positive half load at 0.1s where the machine still runs at 100 r/min. The Proposed-I presents obvious reduction on current ripples while maintains similar dynamic response to that of other methods. These results validate that the proposed method achieves better steady-state performance with low

current ripples than the conventional FCSMPC and FCSMPC with duty cycle without affecting the dynamic performance.

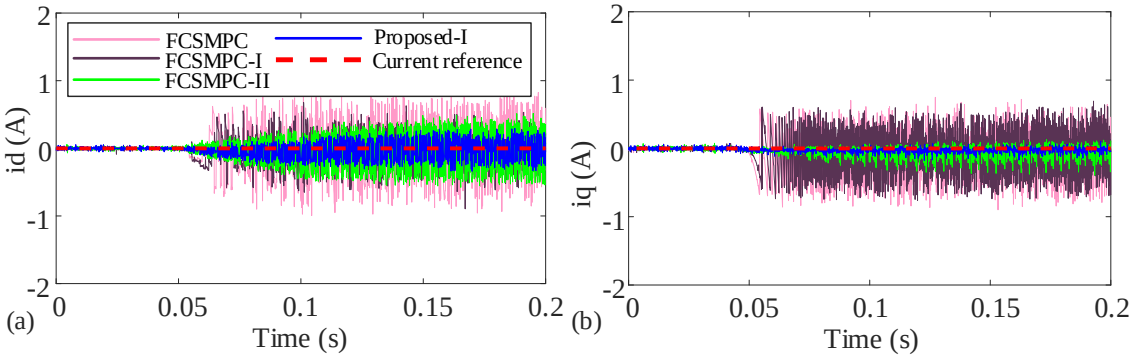

Fig. 4.7 Experimental results of the current responses (a) d-axis and (b) q-axis when speed steps from 0 r/min to 600 r/min at no load for Proposed-I.

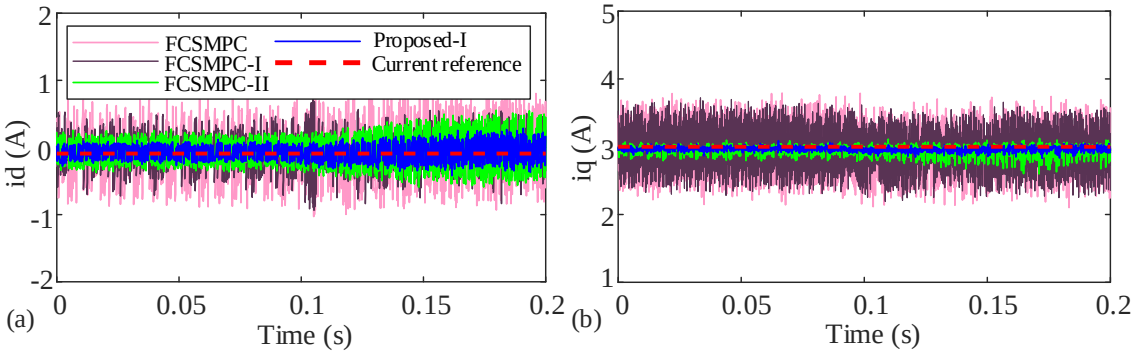

Fig. 4.8 Experimental results of the current responses (a) d-axis and (b) q-axis when speed steps from 300 r/min to 600 r/min at 25% load for Proposed-I.

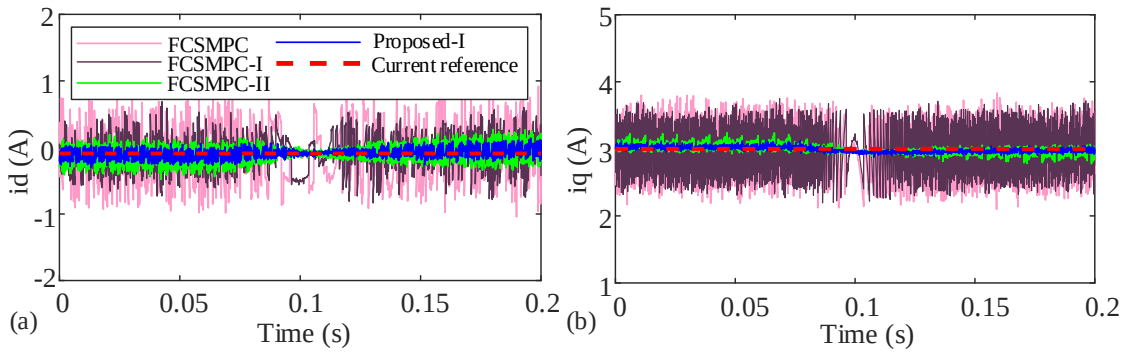

Fig. 4.9 Experimental results of the current responses (a) d-axis and (b) q-axis when speed steps from -300 r/min to 300 r/min at 25% load for Proposed-I.

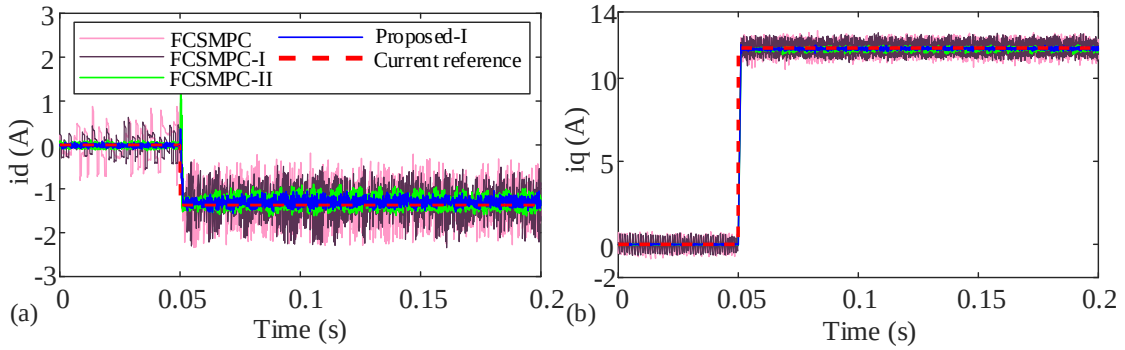

Fig. 4.10 Experimental results of the current responses (a) d-axis and (b) q-axis for the step change from no load to full load at 100 r/min for Proposed-I.

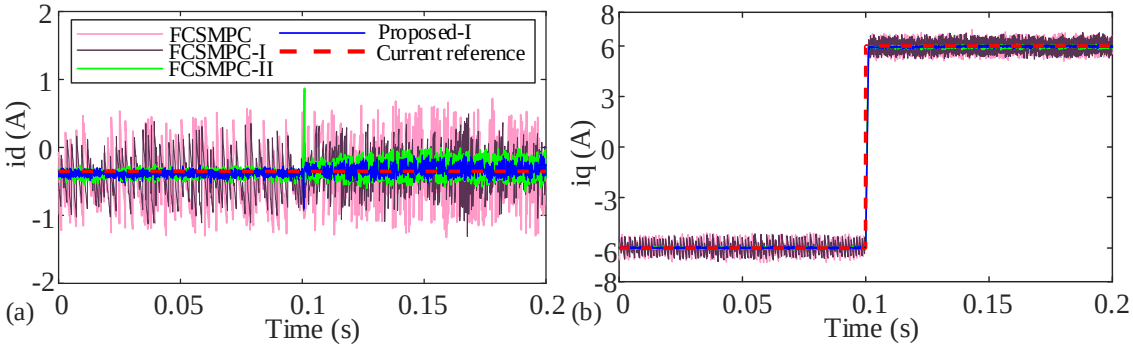

Fig. 4.11 Experimental results of the current responses (a) d-axis and (b) q-axis for the step change from negative half load to positive half load at 100 r/min for Proposed-I.

Finally, the phase-a current and the corresponding harmonic spectrum of the Proposed-I is demonstrated in Fig. 4.12, by which the steady-state performance of the Proposed-I at rated speed with rated load is further tested. It is observed in the figure that the stator current of the Proposed-I shows a much lower THD of only 2.10% than the 5.05% presented by the basic FCSMPC as shown in Fig. 2.16. Moreover, the THD of the stator current of the different techniques will be fully analyzed and compared in Chapter 5.

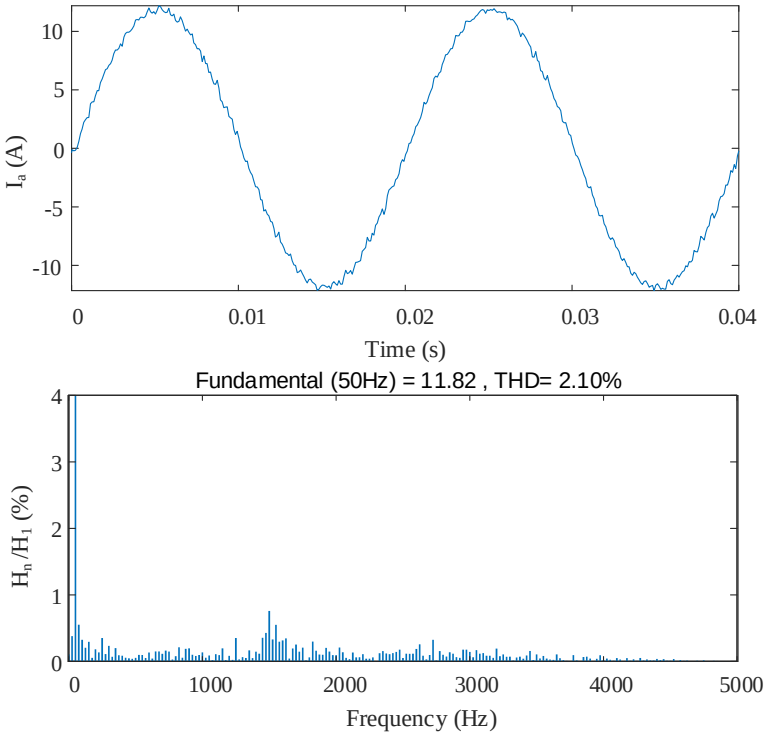

Fig. 4.12 Stator current and the corresponding harmonic spectrum at 600 r/min with rated load for Proposed-I.

4.5.2 PARAMETER SENSITIVITY ANALYSIS

In this subsection, the effect of the parameter variations on the proposed method is experimentally verified and presented in Fig. 4.13 to Fig. 4.16. These variations are made on the nominal values of the parameters used in the prediction model of the reference IPM machine. The d- and q-axis current responses to the variations in the parameters are demonstrated at 100 r/min with half the rated load reversal. As seen in Fig. 4.13, the variations in d-axis inductance by ±25% do not have any significant effects on both the d- and q- axis current responses as compared to the nominal case. It is found in Fig. 4.14 that an increase of q-axis inductance by 25% shows no distinct effects on the q-axis current while decreases the d-axis current by approximately 0.06 A. Moreover, the decrease of q-axis inductance by 25% does not cause much effect on the q-axis current while rises the d-axis current by around 0.06 A. As shown in Fig. 4.15, the variations in resistance by ±50% exhibits negligible influence on both d- and q-axis current. As presented in Fig. 4.16, the effect of the variations in permanent magnet flux by ±25% is negligible on the d-axis current response. On the contrary, deviations in the q-axis current with respect to nominal case are clearly seen. Apart from slight offset and increase in current ripples, the proposed method shows robust control performance with variations in parameters.

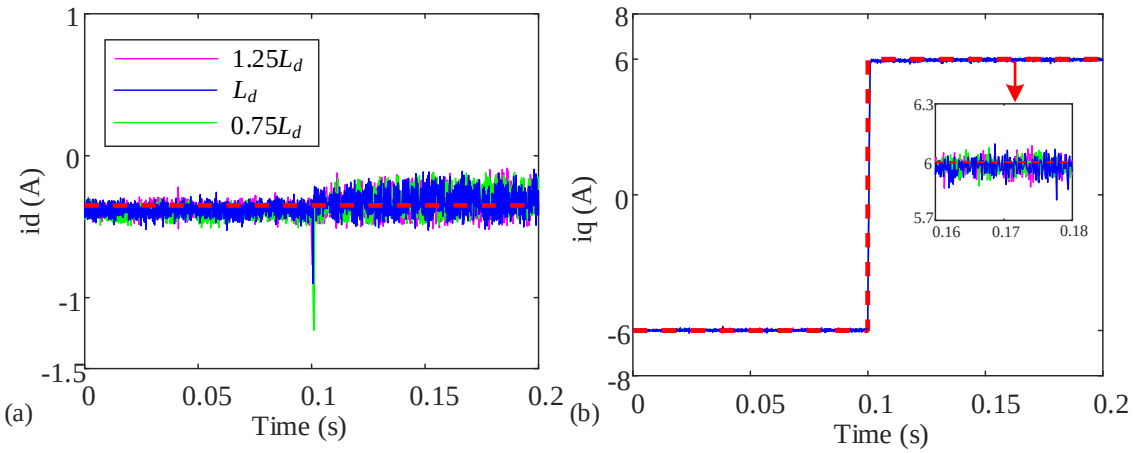

Fig. 4.13 Experimental results of the current responses (a) d-axis and (b) q-axis against ±25% variation in L_d for the step change from negative half load to positive half load at 100 r/min for Proposed-I.

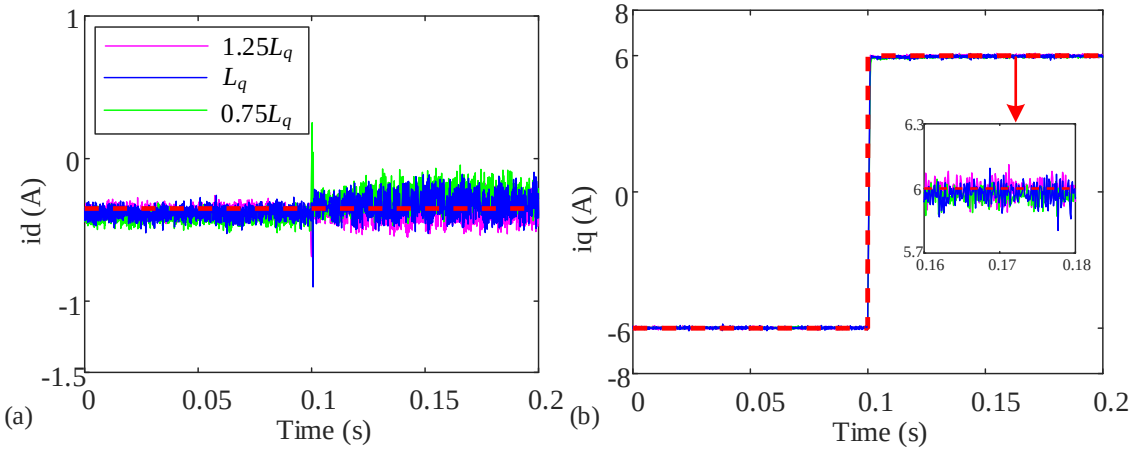

Fig. 4.14 Experimental results of the current responses (a) d-axis and (b) q-axis against ±25% variation in L_q for the step change from negative half load to positive half load at 100 r/min for Proposed-I.

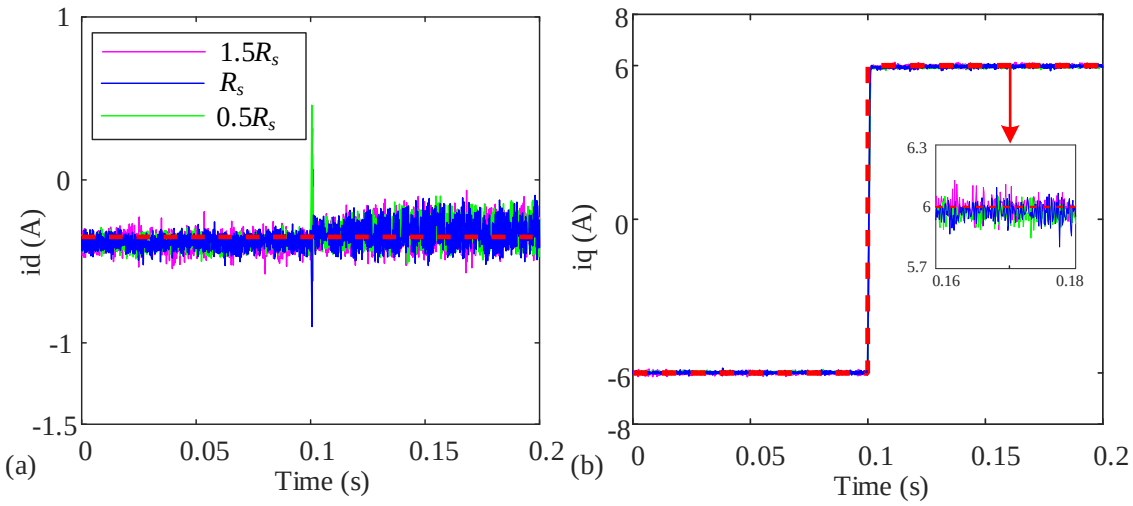

Fig. 4.15 Experimental results of the current responses (a) d-axis and (b) q-axis against ±50% variation in R_s for the step change from negative half load to positive half load at 100 r/min for Proposed-I.

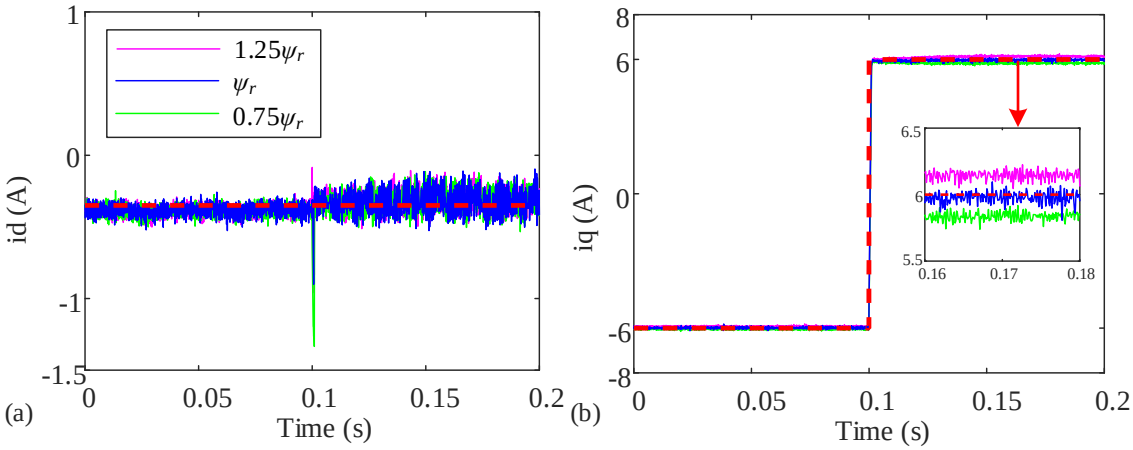

Fig. 4.16 Experimental results of the current responses (a) d-axis and (b) q-axis against ±25% variation in ψ_r for the step change from negative half load to positive half load at 100 r/min for Proposed-I.

4.6 DIFFERENCE BETWEEN THE OPTIMAL VOLTAGE VECTOR AND THE ADJACENT VOLTAGE VECTOR

It is noted that the enumeration-based optimal voltage vector selection method is used for Proposed-I, instead of the quick optimal vector selection method as illustrated in 3.2. The difference between the two optimal vector selection methods is studied and analyzed in this subsection, through which the enumeration-based method is proved to provide higher accuracy for Proposed-I for the IPM machine.

For the enumeration-based optimal voltage vector selection method that is adopted in Proposed-I, the active voltage vector which minimizes the current-error-based cost function will be selected as the optimal non-zero voltage vector. For the quick optimal voltage vector selection method which adopts the concept of deadbeat, the active voltage vector which is located in the same sector with the reference voltage vector will be directly selected as the optimal non-zero voltage vector. In other words, the voltage vector that is located most adjacent to the reference voltage vector is quickly chosen as the optimal one. Considering the aim of current ripple minimization, the selected optimal voltage vector in a sampling interval should always be the one that could minimize the error between the predicted current and the reference current among the whole control set. Given to this principle, the voltage vector selected by the enumeration-based method is always the optimal vector while the adjacent voltage vector selected by the quick selection method is not guaranteed at all conditions. Firstly, the theoretical analyzation is conducted.

According to (2.9) and (3.1), the current-error-based cost function (4.1) of the Proposed-I could be rewritten as:

$$J = \left|i_{dq}^{ref} - i_{dq}(k+2)\right|^2 = \left\| \begin{bmatrix} i_d^{ref} - i_d(k+2) \\ i_q^{ref} - i_q(k+2) \end{bmatrix} \right\|^2 \tag{4.5}$$

where

$$\left(i_d^{ref} - i_d(k+2)\right) = \left(v_d^{ref}(k+1) - v_d\right) T_s / L_d \tag{4.6}$$

$$\left(i_q^{ref} - i_q(k+2)\right) = \left(v_q^{ref}(k+1) - v_q\right) T_s / L_q \tag{4.7}$$

Therefore, the following equation is obtained:

$$\left\| \begin{bmatrix} i_d^{ref} - i_d(k+2) \\ i_q^{ref} - i_q(k+2) \end{bmatrix} \right\|^2 = \left\| \begin{bmatrix} \frac{T_s}{L_d} & 0 \\ 0 & \frac{T_s}{L_q} \end{bmatrix} \cdot \begin{bmatrix} v_d^{ref}(k+1) - v_d \\ v_q^{ref}(k+1) - v_q \end{bmatrix} \right\|^2 \tag{4.8}$$

For a SPM machine where L_d=L_q=L_s, the equation (4.8) could be further simplified as:

$$\left\| \begin{bmatrix} i_d^{ref} - i_d(k+2) \\ i_q^{ref} - i_q(k+2) \end{bmatrix} \right\|^2 = \left(\frac{T_s}{L_s}\right)^2 \cdot \left\| \begin{bmatrix} v_d^{ref}(k+1) - v_d \\ v_q^{ref}(k+1) - v_q \end{bmatrix} \right\|^2 \tag{4.9}$$

Apparently for an SPM machine according to (4.9), the active voltage vector that locates the most adjacent to the reference voltage vector is the optimal non-zero voltage vector that minimizes the current-error-based cost function. At this situation, the optimal voltage vector selected by the quick selection method will be the same as that by the enumeration-

based voltage vector selection method. However, for the IPM machine where L_d and L_q are not equal, the active voltage vector that locates the most adjacent to the reference voltage vector may not be the optimal voltage vector that can present the minimal error between the reference current and the actual predicted current according to (4.8). Thereby, for the application of IPM machine, the quick selection method may not provide as high accuracy as the enumeration-based method in selecting the optimal voltage vector.

The difference between the two selection methods for SPM and IPM machine is further revealed and validated through the simulation in MATLAB Simulink. The simulation environment and configurations are kept the same as previously presented in 4.4. The mathematical model of the IPM machine is built in Simulink by strictly following the parameters as shown in Table 2.2. For the purpose of comparison, the mathematical model of the SPM machine is built with the same parameters as of the IPM except that the L_d and L_q are set with the same value of 14.3 mH for the SPM. The two selection methods are tested for the IPM and SPM machine under the same condition of rated speed with rated load. Fig. 4.17 shows the simulation results of the optimal vector index that are presented by the two selection methods for the SPM machine. It is clearly shown in the figure that the voltage vector selected by the quick selection method is always the same with the enumeration-based selection method, which means the adjacent voltage vector to the reference voltage vector is the exactly the optimal voltage vector for the application in SPM machine. Fig. 4.18 shows the simulation results of the optimal vector index that are

presented by the two selection methods for the IPM machine. It is found that there exist certain instants that the voltage vector selected by the quick selection method is different from that by the enumeration-based selection method, which means that the adjacent voltage vector to the reference voltage vector is not guaranteed to be the optimal voltage vector for the application in IPM machine.

Based on the theoretical analysis and the validation in Simulink, the enumeration-based optimal voltage vector selection method is proved to provide higher accuracy for the Proposed-I for the IPM machine.

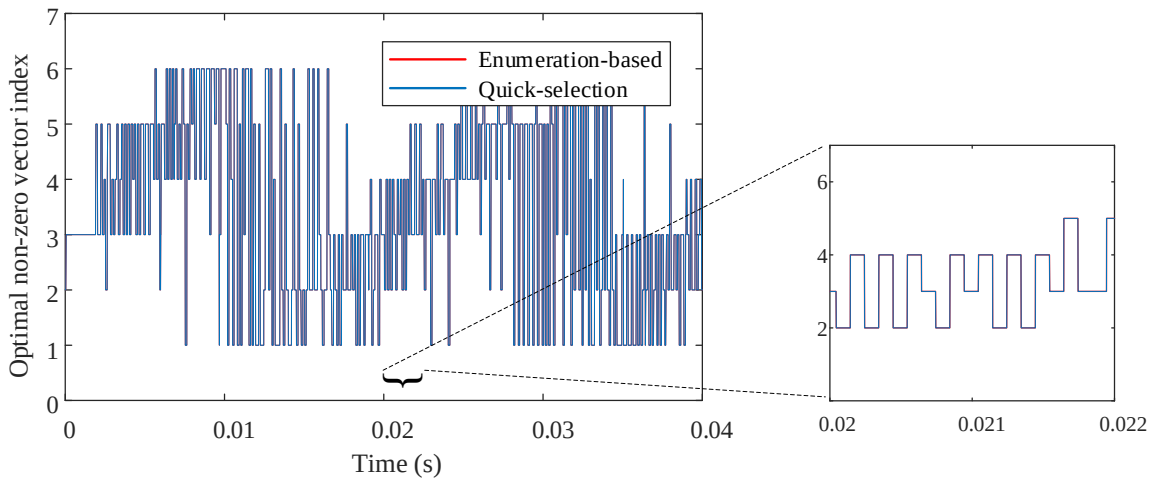

Fig. 4.17 Comparison between the enumeration-based method and quick-selection methods in selecting optimal voltage vectors for the application for SPM motor drive.

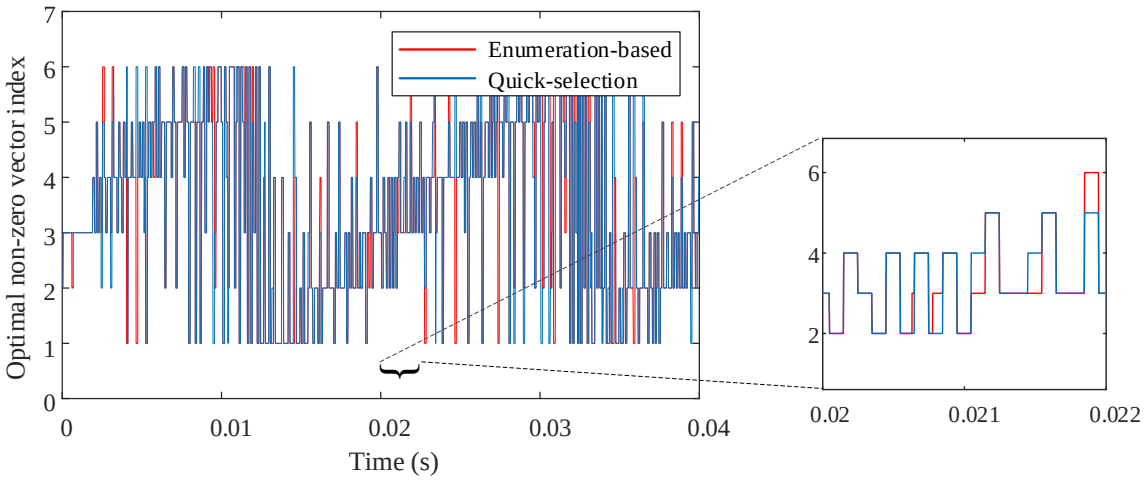

Fig. 4.18 Comparison between the enumeration-based method and quick-selection methods in selecting optimal voltage vectors for the application for IPM motor drive.

Chapter 5

PROPOSED CONTINUOUS VIRTUAL VOLTAGE VECTOR TECHNIQUE

5.1 INTRODUCTION

To reduce the large current ripples and improve the steady-state performance, various techniques have been presented for the FCSMPC in the previous chapters. FCSMPC-I reduces the current ripples by providing more available voltage vector candidates through introducing six additional virtual voltage vectors. Moreover, the concept of duty cycle control is introduced in FCSMPC-II by utilizing the null voltage vector as the second voltage vector to apply the active voltage vector in the right proportion of the sampling period, which effectively improves the steady-state performance as compared to the basic FCSMPC. To further reduce the current ripples, the Proposed-I integrates the concept of virtual voltage vectors and duty cycle control in the FCSMPC control scheme, which achieves higher control accuracy and better current ripple reduction effect as compared to the conventional techniques. Nevertheless, none of the FCSMPC-I, FCSMPC-II or the Proposed-I could really achieve error-free tracking of the reference current. Therefore, three-vector-based FCSMPC is proposed to further reduce the current ripples. A method is

proposed in [68] to eliminate the error between the reference stator currents and the actual currents by using three-vector based FCSMPC. However, it uses complex interpolation polynomials to simulate the variations of the cost function, which couldn't achieve absolute error-free as the algorithms are built based on approximations.

This chapter proposes an improved FCSMPC method with continuous virtual voltage vector technique in a three-vector-based control scheme. It applies a continuous virtual voltage vector at every sampling interval that reduces the current ripples by successfully eliminating the error between the reference value and the actual value of the current. The continuous virtual voltage vector is realized by at the most three vectors, including one null voltage vector and two suboptimal basic non-zero voltage vectors which are chosen based on the MPC's principle of minimizing the cost function. Moreover, the corresponding duty ratios are obtained based on two factors, k_1 and k_2, which could be calculated in an efficient way with low computational requirement. The principle of the proposed method is introduced in 5.2. The mechanism of the proposed method on reducing current ripples is elaborated in 5.3. In 5.4, the performance of the proposed method is verified through the results in MATLAB Simulink. Furthermore in 5.5, the proposed method is comparatively studied with the basic FCSMPC, FCSMPC-II and Proposed-I, where its benefits are confirmed by the experimental results for the referenced IPMSM drive system.

5.2 PRINCIPLE OF THE METHOD

The control diagram of the proposed method is shown in Fig. 5.1, which mainly comprises of the delay compensation, optimal virtual voltage vector determination, cost function minimization/suboptimal voltage vectors selection, duty ratio calculation and pulse generation. The reference currents on d-axis and q-axis are calculated based on the criteria of maximum torque per ampere (MPTA) according to the torque reference. Moreover, all the variables in the control scheme are transformed into the synchronous rotating frame to perform field-oriented control. For demonstration convenience, the proposed method is referred as Proposed-II in the following content. The detailed introduction of the main functional blocks of Proposed-II are elaborated as follows.

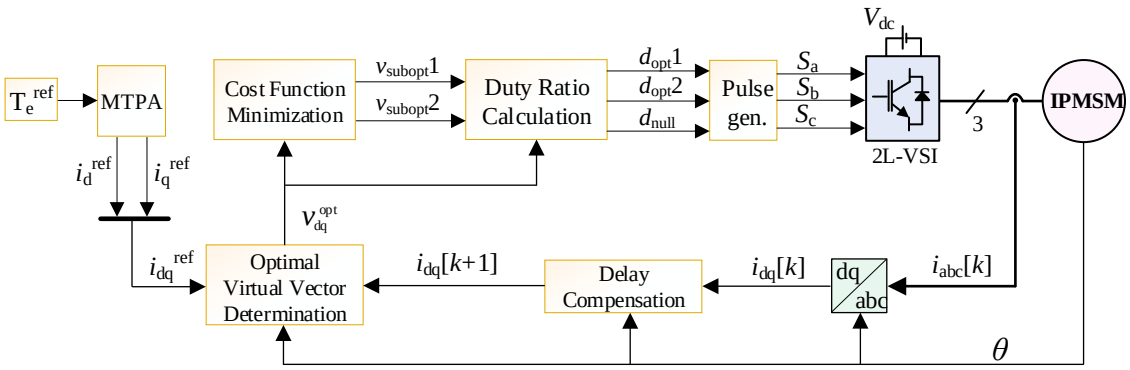

Fig. 5.1 The diagram of Proposed-II.

A. Optimal virtual voltage vector determination

With the aim to minimize current ripples, the basic principle of FCSMPC is to find one of the eight vectors which minimizes the cost function (5.1). Considering the one-step delay compensation, the currents predicted at (k+2)th step are used in the calculation.

$$J = \left| i_{dq}^{ref} - i_{dq}(k+2) \right|^2 \tag{5.1}$$

where

$$i_{dq}^{ref} = \begin{bmatrix} i_d^{ref} \\ i_d^{ref} \end{bmatrix} \tag{5.2}$$

$$i_{dq}(k+2) = \begin{bmatrix} i_d(k+2) \\ i_q(k+2) \end{bmatrix} \tag{5.3}$$

To eliminate the error between the reference current and the actual current, the Proposed-II realizes i_{dq}^{ref} at (k+2)th instant by applying an optimal voltage vector (v_{dq}^{opt}) that is obtained by simply replacing $i_{dq}(k+2)$ with i_{dq}^{ref} and substituting v_{dq} by v_{dq}^{opt} in (2.5):

$$\begin{cases} i_d^{ref} = \left(1 - \frac{R_s T_s}{L_d}\right) i_d^p(k+1) + \frac{T_s}{L_d}\left[v_d^{opt}(k+1) - e_d(k+1)\right] \\ i_q^{ref} = \left(1 - \frac{R_s T_s}{L_q}\right) i_q^p(k+1) + \frac{T_s}{L_q}\left[v_q^{opt}(k+1) - e_q(k+1)\right] \end{cases} \tag{5.4}$$

It is apparent from (5.4) that v_{dq}^{opt} is applied at (k+1)th instant and the corresponding i_{dq}^{ref} is obtained at (k+2)th instant. Moreover, it is noted that the effect presented by the v_{dq}^{opt} is the same with the reference voltage vector as calculated in (3.1), both of which guarantee the

zero error between the reference current and the actual current at each sampling instant. In other words, the Proposed-II adopts the reference voltage vector as the optimal voltage vector and applies it at every sampling interval to eliminate the current error. Obviously, this optimal voltage vector for Proposed-II is a virtual voltage vector with infinite possibilities. It is realized by at the most three basic voltage vectors with corresponding duty ratios, which will be illustrated in the following of this subsection. The benefits brought by the optimal voltage vector on the current ripple reduction for Proposed-II will be further demonstrated in 5.3.

B. Suboptimal active voltage vector selection

As demonstrated in Section III-A, the optimal vector v_{dq}^{opt} is no longer limited to only the eight basic voltage vectors but become a flexible virtual voltage vector that is realized by at most two suboptimal active voltage vectors and a null vector selected from the conventional finite control set. In Proposed-II, the six active voltage vectors at $(k+1)^{\text{th}}$ sampling instant are calculated and enumerated in the following cost function:

$$G = \left| v_{dq}^{opt}(k+1) - v_{dq}(k+1) \right|^2 \tag{5.5}$$

Then, the two active voltage vectors that present the minimum and subminimum values of (5.5) will be selected as the suboptimal voltage vectors. It should be noted that the suboptimal voltage vector selection is only regarding the active voltage vectors since the

null vector is applied in every control interval as an adjustment vector to assist realizing v_{dq}^{opt}, which will be elaborated in Part-C.

C. Duty ratio calculation

After obtaining the two suboptimal voltage vectors as discussed in Part-B, the next step is to determine their duty ratios to realize v_{dq}^{opt}. v_{dq}^{opt} is a virtual voltage vector which could be located anywhere inside the voltage hexagon. For example, v_{dq}^{opt} is located between $v_{dq}1$ and $v_{dq}2$ at a certain instant as demonstrated in Fig. 5.2. α_{opt} is defined as the angle between v_{dq}^{opt} and $v_{dq}1$.

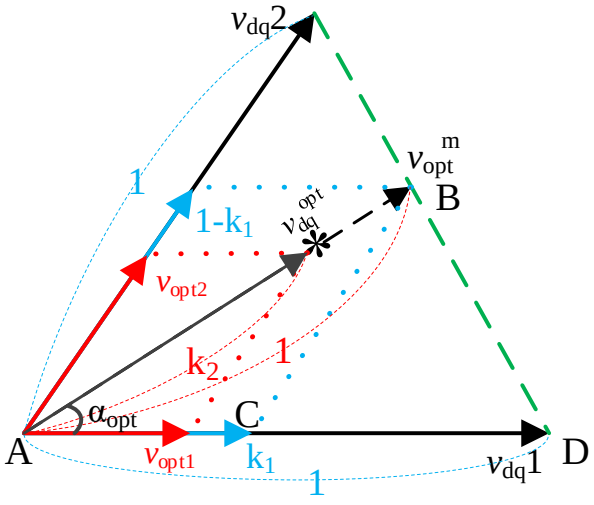

Fig. 5.2 Duty ratio calculation scheme for Proposed-II.

As shown in Fig. 5.2, the maximum optimal voltage vector v_{opt}^{m} is the maximum voltage which can be applied by synthesizing two suboptimal voltage vectors $v_{dq}1$ and $v_{dq}2$ with

full duty cycle. However, only the optimal direction can be accomplished by applying v_{opt}^{m}, not the optimal magnitude as shown in Fig. 5.2. In order to achieve the optimal magnitude $|v_{dq}^{opt}|$, the concept of duty cycle is applied to v_{opt}^{m} and hence the two suboptimal voltage vectors as selected in Part-B. As shown in Fig. 5.2, a straight line in parallel to $v_{dq}2$ is projected from v_{opt}^{m} to $v_{dq}1$, and similarly, another line in parallel to $v_{dq}1$ is projected to $v_{dq}2$. The magnitudes of these projected lines are fractions k_1 and 1- k_1 of $|v_{dq}1|$ (=$|v_{dq}2|$). The fraction k_1 is found based on the sine theorem applied to triangle ABC as:

$$k_1 = \frac{1}{1+\frac{\sin(\alpha_{opt})}{\sin(\frac{\pi}{3}-\alpha_{opt})}} \tag{5.6}$$

The maximum optimal voltage vector v_{opt}^{m} is achieved by applying $v_{dq}1$and $v_{dq}2$ for k_1 and (1- k_1) of a control interval. In addition, another factor k_2 is introduced to realize the actual optimal voltage vector v_{dq}^{opt}. The factor k_2 is found as:

$$k_2 = \frac{\left|v_{dq}^{opt}\right|}{\left|v_{opt}^{m}\right|} \tag{5.7}$$

Where $|v_{opt}^{m}|$ is found by applying sine theorem in triangle ABD as:

$$\left|v_{dq}^{m}\right| = \left|v_{dq}1\right| \cdot \frac{\sin(\frac{\pi}{3})}{\sin(\frac{2\pi}{3}-\alpha_{opt})} \tag{5.8}$$

Finally, to apply the optimal virtual voltage vector v_{dq}^{opt}, the duty ratios of the two suboptimal voltage vectors and one null vector could be summarized as:

$$\begin{cases} d_{opt}1 = k_1 \cdot k_2 \\ d_{opt}2 = (1 - k_1) \cdot k_2 \\ d_{null} = 1 - k_2 \end{cases} \tag{5.9}$$

5.3 MECHANISM ON REDUCING THE CURRENT RIPPLES

The mechanism of Proposed-II on the current ripple reduction is fully discussed in this subsection, where the Proposed-II is further proved to provide higher accuracy with lower current ripples than the conventional techniques and even Proposed-I. Fig. 5.3 shows the optimal voltage vector scheme adopted by the different techniques.

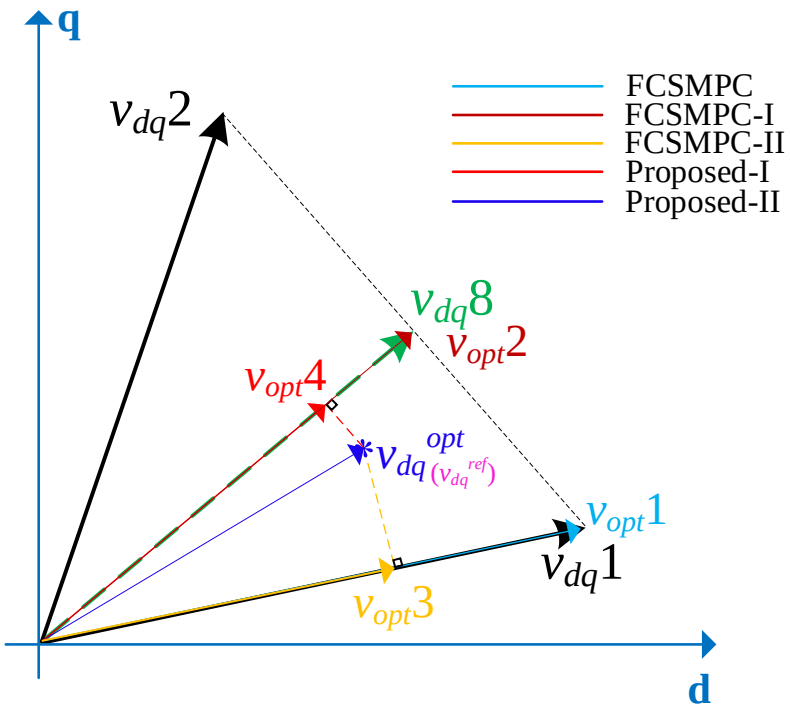

Fig. 5.3 Optimal voltage vector scheme of different techniques.

As shown in the figure, the basic voltage vector $v_{dq}1$ is selected as the voltage vector for the basic FCSMPC, while a more accurate choice- the virtual voltage vector $v_{dq}8$ is available for utilization for the FCSMPC-I. By introducing the concept of duty cycle control in FCSMPC-II, the $v_{dq}1$ is first selected as the optimal voltage vector and then applied in a right proportion of a sampling period, which is represented as $v_{opt}3$ as shown in Fig. 5.3. The current ripples are effectively reduced due to the flexible mode of applying voltage vectors. For the case of the Proposed-I, the concept of virtual voltage vector and duty cycle control are combined, which provides more accurate choice of the applied voltage vector and presents more distinct reduction effect on the current ripples. Finally, for the Proposed-II, the optimal voltage vector is such selected that the error between the actual current and the reference current is zero at each sampling instant. It definitely achieves much higher control accuracy than the conventional techniques and the Proposed-I, which will evidently achieve much better effect on the current ripple reduction. Fig. 5.4 depicts an example of the q-axis current response of the Proposed-II, by which the mechanism of the current ripple reduction could be exhibited in a more straightforward way. Since the Proposed-I is already validated to present lower current ripples than the conventional techniques, the mechanism of FCSMPC-I and FCSMPC-II are not shown in the figure. More details on the mechanism of the conventional techniques could refer to the previous chapters.

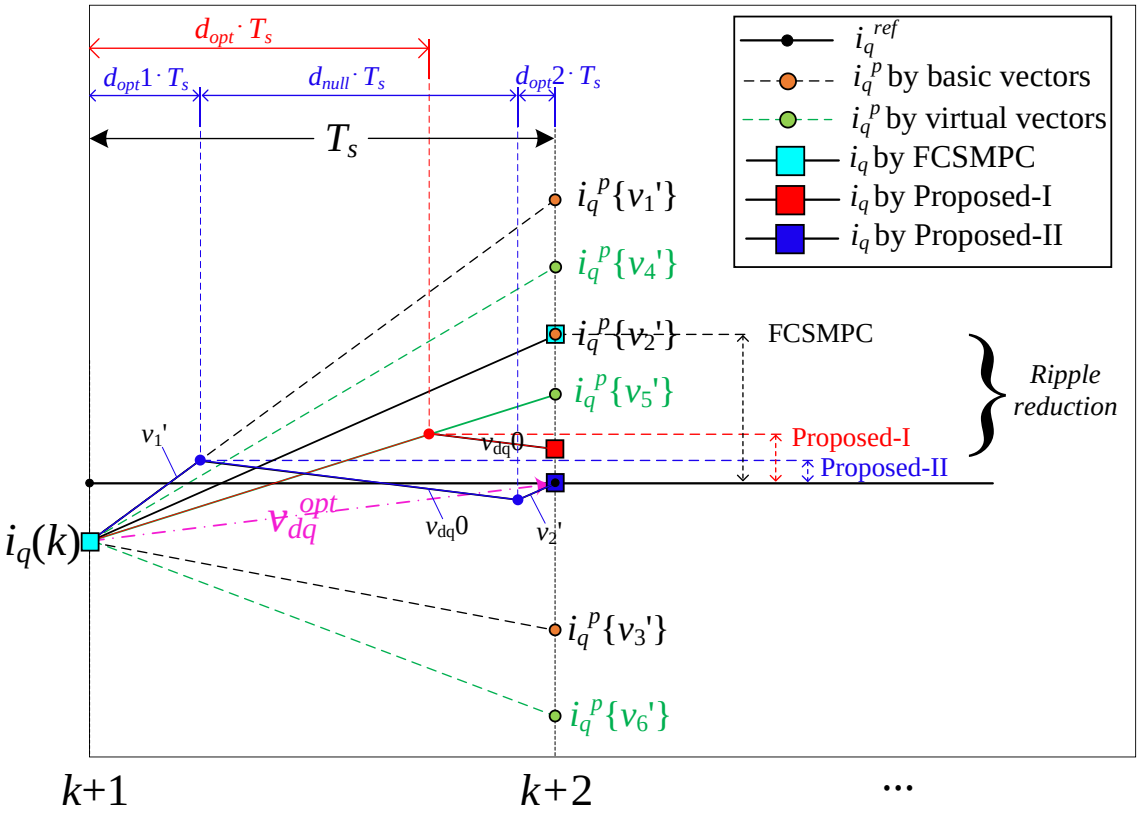

Fig. 5.4 The mechanism of the current ripple reduction by Proposed-II.

As shown in the figure, v_1' to v_3' denote three basic voltage vector candidates, while v_4' to v_6' represent three virtual voltage vector candidates. Moreover, the current predictions corresponding to the voltage vector candidates are clearly shown in the figure. For the basic FCSMPC, the vector candidate v_2' is selected as the optimal voltage vector among all the basic voltage vectors as it provides the minimum error between the predicted current and the reference current. For the case of Proposed-I, the more accurate virtual voltage vector v_5' is first selected as the optimal voltage vector, and then applied in the right proportion of

a sampling period according to an optimal duty ratio. It presents effective reduction on the current ripples as shown in the figure. However, the error between the reference current and the actual current still exits while the current ripples are not small enough, which means the effect could be further improved. For the Proposed-II, the concept of virtual voltage vectors and duty cycle control are deeply integrated in a three-vector-based control scheme. The optimal voltage vector is no longer limited to the basic voltage vectors or the virtual voltage vectors with fixed duty ratio, but becomes a more flexible virtual voltage vector with infinite possibilities which could be easily realized by only the basic voltage vector candidates. As demonstrated in Fig. 5.4, the vector candidates v_1' and v_2' are selected as the suboptimal active voltage vectors and then applied in the regulated proportion of a sampling period according to the corresponding duty ratios, while the null voltage vector will be applied in rest of the time in the sampling period. It can be seen the Proposed-II eliminates the current error at next sampling instant while achieves much lower current ripples as compared to that of the basic FCSMPC and even Proposed-I.

5.4 SIMULATION RESULTS

The performance of the Proposed-II for a PMSM drive is first verified through simulations in MATLAB Simulink. The mathematical model of the IPM machine is accurately built in Simulink by strictly following the parameters as shown in Table 2.2. To be consistent with the experimental environment as presented in 2.6.1, the sampling frequency of the simulation is configured as 10 kHz and the applied DC link voltage value is set as 300 V.

Fig. 5.5 shows the dynamic performance of d- and q- axis currents with the rotor speed transient from standstill to rated speed at 0.05s with no load. It can be seen that Proposed-II presents a stable control performance against the step change of speed. Moreover, the current ripples on both d- and q-axis are barely seen under the simulation condition, which proves the great current ripple reduction effect by Proposed-II. Fig. 5.6 shows the current transient responses to a stepped change from no load to full load at 0.05s with the machine speed of 100 r/min. As shown in the figure, the actual current tracks the reference current closely when the load suddenly changes, which proves the dynamic response of the Proposed-II. Furthermore, it presents very small ripples on both d- and q-axis currents, by which the current ripple reduction effect is verified for the Proposed-II.

The performance of the Proposed-II will be further validated through experimental results in 5.5, where more test conditions are applied and more analysis are given.

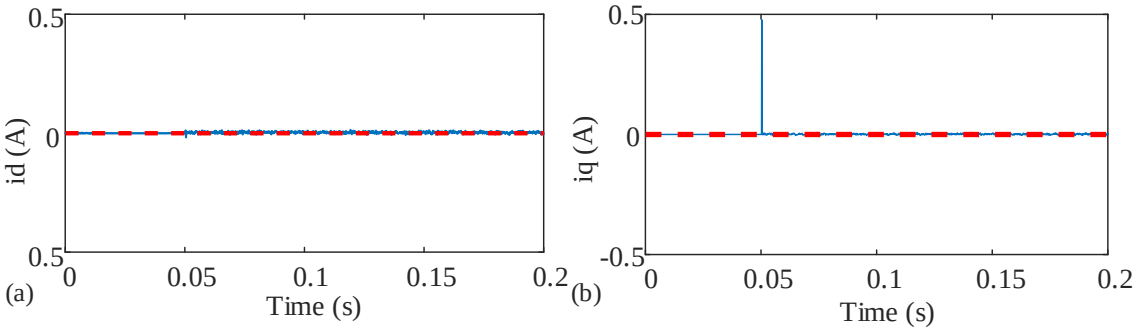

Fig. 5.5 Simulation results of the current responses (a) d-axis and (b) q-axis when speed steps from 0 r/min to 600 r/min at no load for Proposed-II.

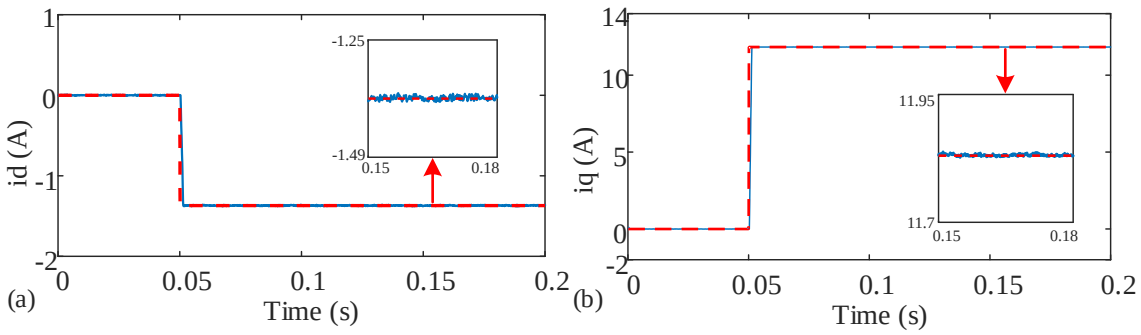

Fig. 5.6 Simulation results of the current responses (a) d-axis and (b) q-axis for the step change from no load to full load at 100 r/min for Proposed-II.

5.5 EXPERIMENTAL RESULTS

5.5.1 TRANSIENT AND STEADY-STATE PERFORMANCE

In this subsection, the steady-state and transient performance of the Proposed-II is validated through experiments under different conditions. Moreover, the basic FCSMPC, FCSMPC-II and Proposed-I are also experimentally tested as the comparisons for the Proposed-I under the same conditions (Since FCSMPC-II presents a better current ripple reduction effect than the other conventional technique FCSMPC-I as validated through the figures in 4.5, only FCSMPC-II is presented in this subsection for better comparison effect). The experimental results for the four techniques are comparatively studied and analyzed, through which the effectiveness of the Proposed-I is confirmed. The experimental environment and the configurations are exactly the same as presented in 2.6.1.

First, the response of d- and q-axis currents with speed transient from 0 r/min to the rated speed at 0.05s with no load for the basic FCSMPC, FCSMPC-I, FCSMPC-II and Proposed-I are illustrated in Fig. 5.7. In Fig. 5.7, d-axis current and q-axis current for four methods are provided in two separate subfigures as shown in (a) and (b). It is shown that the dynamic response of the Proposed-II is similar to that of the basic FCSMPC, FCSMPC-II and Proposed-I. The current ripples presented by Proposed-II in experiment are larger than the corresponding simulation results under the same condition as illustrated in 5.4. However, the Proposed-II still presents much lower current ripples and hence better steady-state performance as compared to the previous techniques as shown in Fig. 5.7. Similar conclusions can also be reached according to the results in Fig. 5.8, where the rotor speed steps from 300 r/min to 600 r/min at 0.1s with 25% load on the machine. It is seen that the difference in the dynamic response between the four methods is negligible, while substantial reduction on the current ripples exists for the Proposed-II. Fig. 5.9 shows the transient responses for the speed reversion at ±300 rpm at 0.1s with 25% load on the machine. As compared to the basic FCSMPC, FCSMPC-II and Proposed-I, the Proposed-II delivers similar dynamic response while presents more satisfied steady-state performance in terms of lower current ripples.

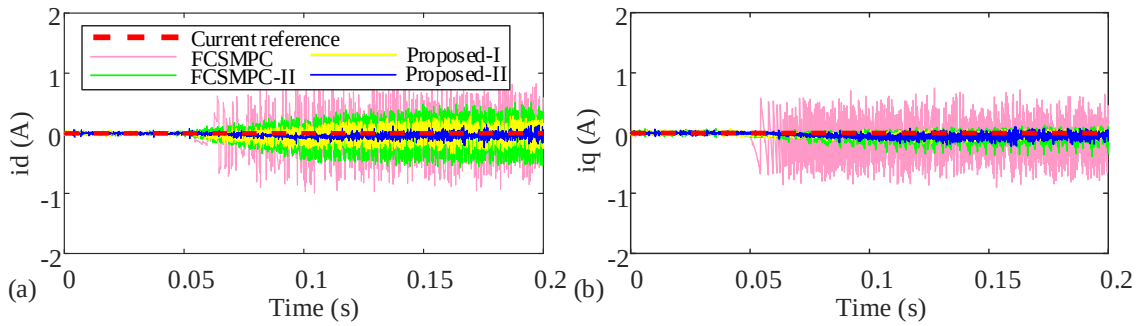

Fig. 5.7 Experimental results of the current responses (a) d-axis and (b) q-axis when speed steps from 0 r/min to 600 r/min at no load for Proposed-II.

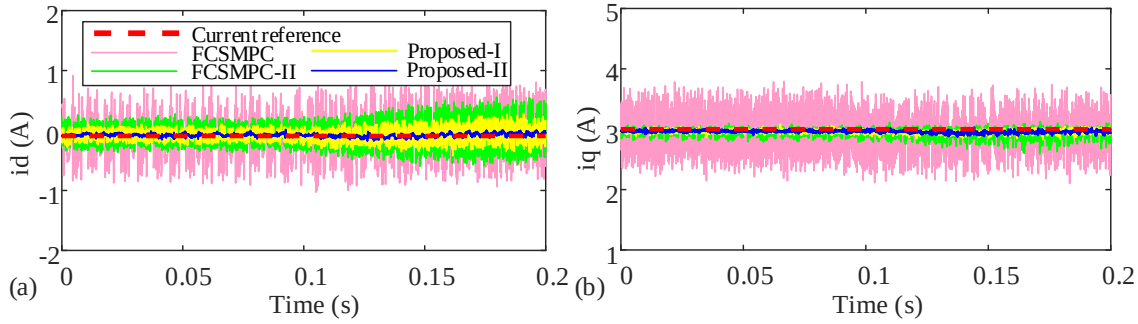

Fig. 5.8 Experimental results of the current responses (a) d-axis and (b) q-axis when speed steps from 300 r/min to 600 r/min at 25% load for Proposed-II.

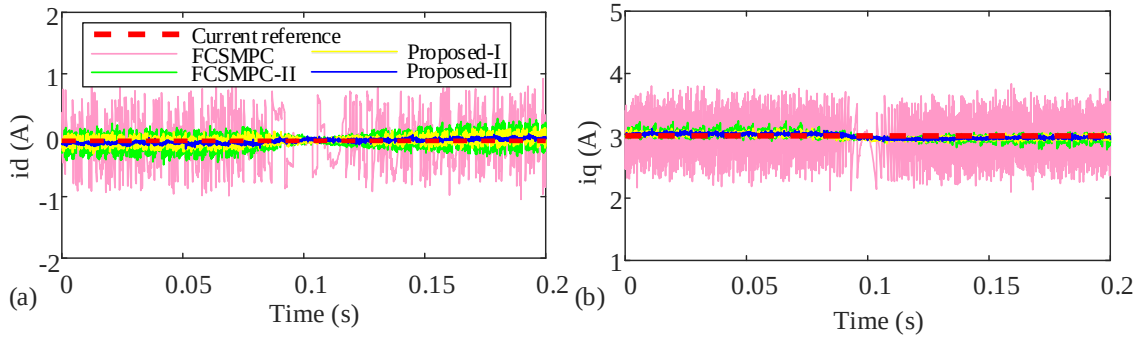

Fig. 5.9 Experimental results of the current responses (a) d-axis and (b) q-axis when speed steps from -300 r/min to 300 r/min at 25% load for Proposed-II.

Second, the current transient responses against load change for three methods are investigated and shown in Fig. 5.10 and Fig. 5.11. Fig. 5.10 shows the dynamic responses to a stepped change from no load to full load at 0.05s with the machine speed of 100 r/min. As shown in the figure, the current ripples presented by Proposed-II in experiment are similar to the simulation results as shown in Fig. 5.6. Moreover, the results presented in this figure provide more evidence that the dynamic process for the four methods are very close to each other. Nevertheless, it is clearly seen that the Proposed-II causes nearly no overshoot on the currents when the load changes while delivers much lower current ripples as compared to the basic FCSMPC, FCSMPC-II and Proposed-I.

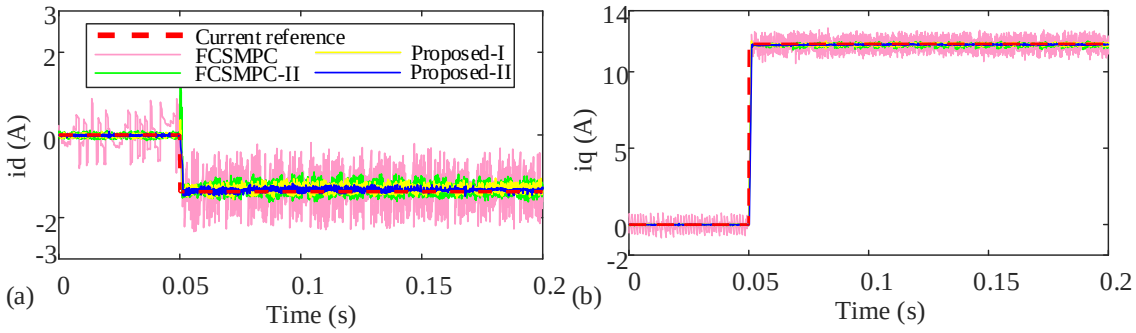

Fig. 5.10 Experimental results of the current responses (a) d-axis and (b) q-axis for the step change from no load to full load at 100 r/min for Proposed-II.

Similar results can also be seen in Fig. 5.11, which shows the current responses of load reversion at negative and positive half load at 0.1s with the machine speed of 100 r/min. The Proposed-II exhibits significant reduction on current ripples, while maintains similar dynamic responses as compared to the other techniques. All the experimental results

presented before prove that Proposed-II delivers much better steady-state performance with low current ripples than the basic FCSMPC, FCSMPC-II and Proposed-I without affecting the dynamic performance.

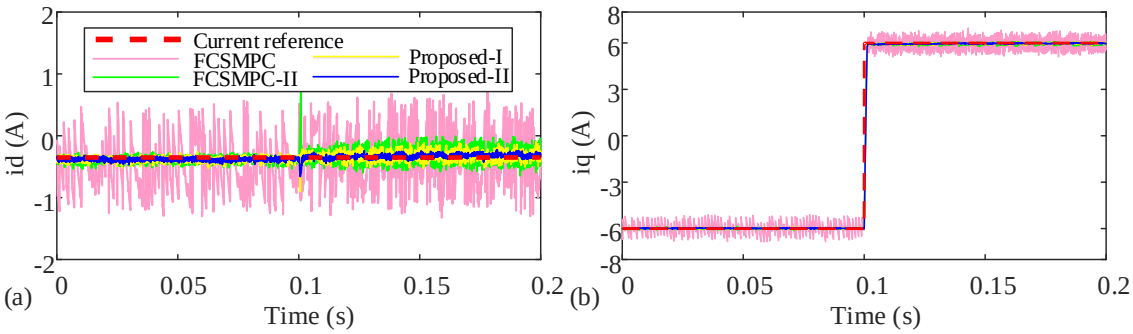

Fig. 5.11 Experimental results of the current responses (a) d-axis and (b) q-axis for the step change from negative half load to positive half load at 100 r/min for Proposed-II.

Finally, the conclusion of the better steady-state performance of the Proposed-II can be further supported by the THD of the phase current. The phase-a current of the Proposed-II at rated speed with rated load is demonstrated in Fig. 5.12. It is found that the phase current by Proposed-II is basically a sinusoidal wave with a low THD of only 1.82%. Moreover, the THD of the stator current of the different techniques under the condition of rated speed with rated load are compared and concluded as shown in Fig. 5.13. It is seen that the FCSMPC-I shows a lower THD of 4.31% than the 5.05% of the basic FCSMPC, while the FCSMPC-II presents even better performance with a lower THD of 3.40% on the current. For Proposed-I, the THD of the stator current is further reduced to a smaller value of 2.10%, which proves the better effect of Proposed-I than the conventional techniques on reducing

the current ripples. Finally, for Proposed-II, a smallest THD of 1.82% is presented among all the THD values presented by the previous methods, by which the better steady-state performance of the Proposed-II is evidently validated.

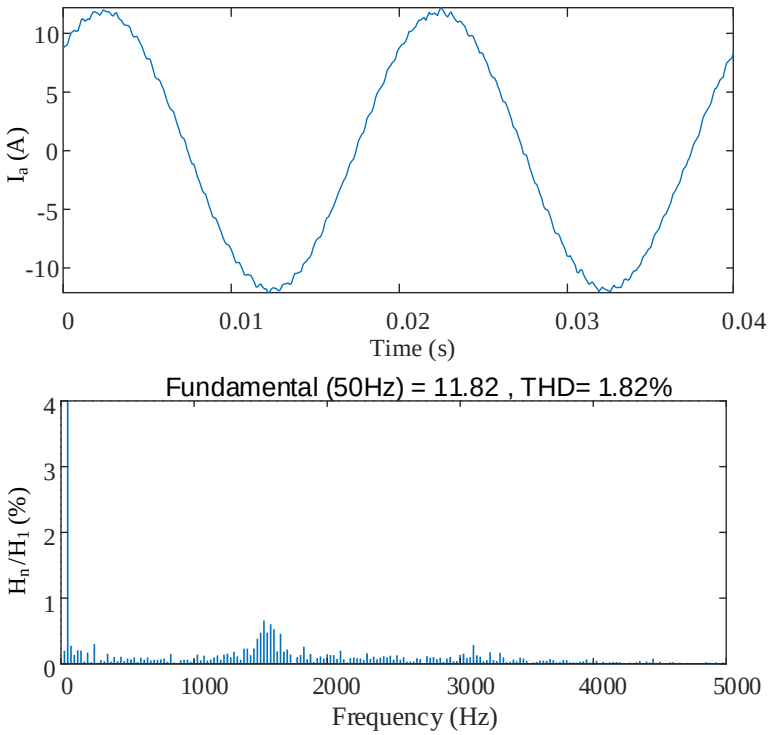

Fig. 5.12 Stator current and the corresponding harmonic spectrum at 600 r/min with rated load for Proposed-II.

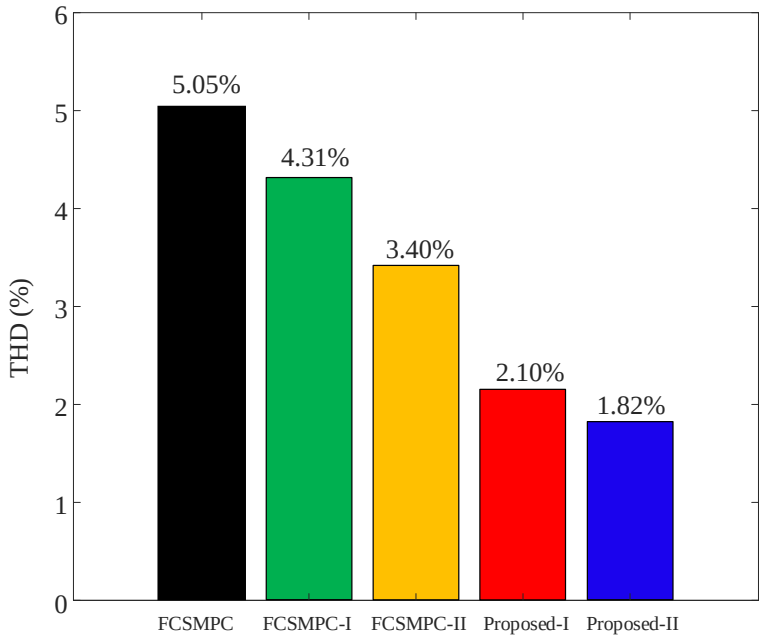

Fig. 5.13 THD of the stator current of the different techniques at rated speed with rated load in experiment.

5.5.2 PARAMETER SENSITIVITY ANALYSIS

In this subsection, the effect of the parameter variations on the proposed-II is experimentally verified and presented in Fig. 5.14 to Fig. 5.17. These variations are made on the nominal values of the parameters used in the prediction model of the reference IPM machine. The d- and q-axis current responses with respect to the variations in the parameters are demonstrated at 100 r/min with half the rated load reversal. As seen in Fig. 5.14, the variations in d-axis inductance by ±25% do not have any significant effects on both the d- and q- axis current responses as compared to the nominal case. It is found in Fig. 5.15 that an increase of q-axis inductance by 25% decreases the d-axis current by

approximately 0.07A while producing larger q-axis current ripples with respect to the nominal case. The decrease of q-axis inductance by 25% presents larger q-axis current ripples while rises the d-axis current by around 0.07A. The variations in resistance by ±50% exhibits negligible influence on the d-axis current while results in slight ripples on the q-axis current as shown in Fig. 5.16. Moreover, slight offset in q-current response is also seen as compared to nominal case. As shown in Fig. 5.17, the effect of the variations in permanent magnet flux by ±25% is negligible on the d-axis current response. On the contrary, deviations in the q-axis current with respect to nominal case are clearly seen. Apart from slight offset and increase in current ripples, the proposed-II shows robust control performance with variations in parameters.

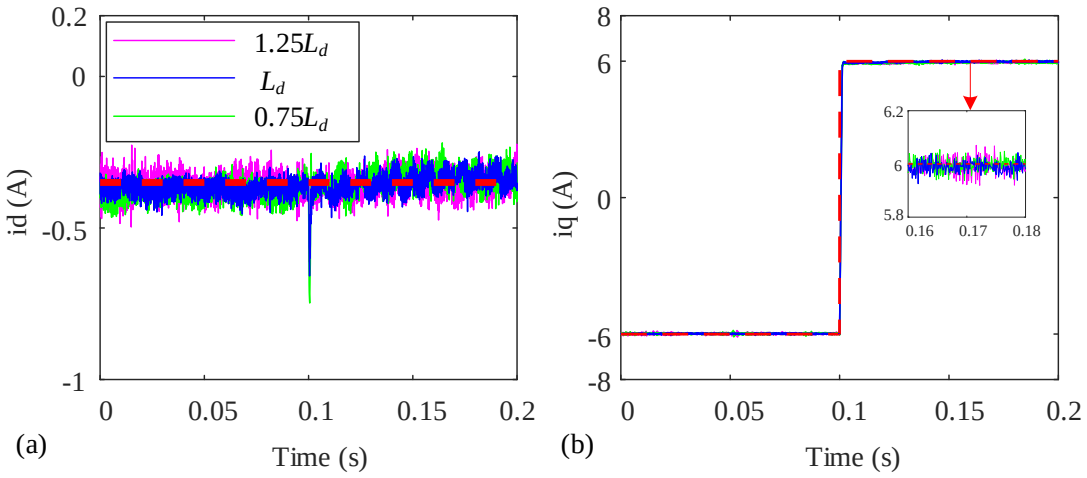

Fig. 5.14 Experimental results of the current responses (a) d-axis and (b) q-axis against ±25% variation in L_d for the step change from negative half load to positive half load at 100 r/min for Proposed-II.

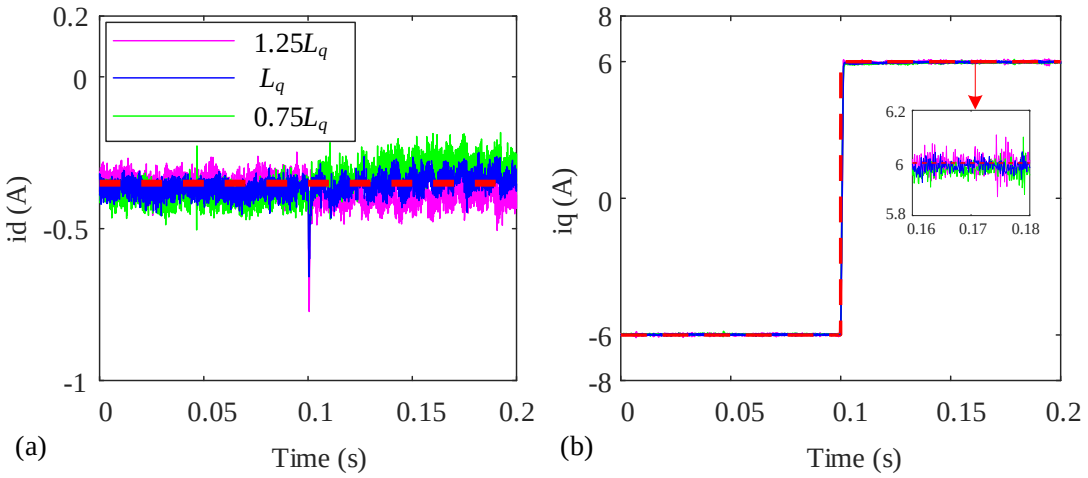

Fig. 5.15 Experimental results of the current responses (a) d-axis and (b) q-axis against ±25% variation in L_q for the step change from negative half load to positive half load at 100 r/min for Proposed-II.

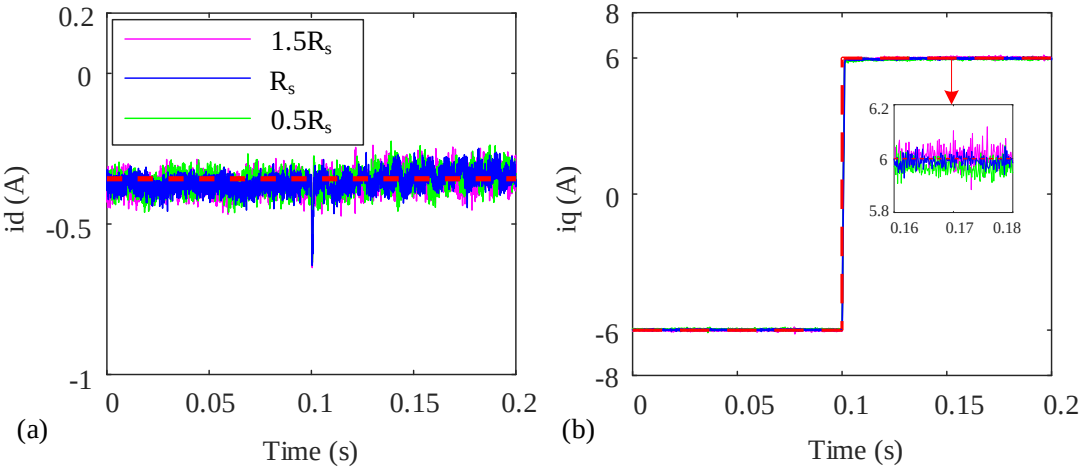

Fig. 5.16 Experimental results of the current responses (a) d-axis and (b) q-axis against ±50% variation in R_s for the step change from negative half load to positive half load at 100 r/min for Proposed-II.

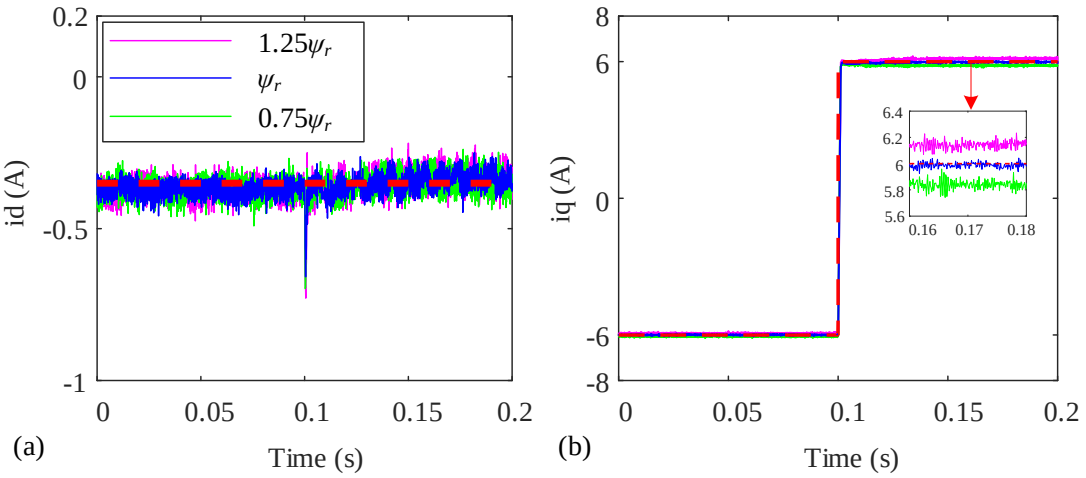

Fig. 5.17 Experimental results of the current responses (a) d-axis and (b) q-axis against ±25% variation in ψ_r for the step change from negative half load to positive half load at 100 r/min for Proposed-II.

5.6 COMPREHENSIVE ANALYSIS ON THE CURRENT RIPPLE REDUCTION

A comprehensive analysis of the current ripple minimization is introduced in this section, where the dominating advantages and the accompanied drawbacks are discussed. As previously demonstrated through the experimental results, the current ripples of the proposed methods are effectively reduced under different conditions. Under the certain condition of rated speed and rated load, the RMS current on d-axis for the Proposed-I and Proposed-II are 5.1% and 5.98% smaller than that of the basic FCSMPC. The percentage of the q-axis currents are 0.079% and 0.083%, respectively. The smaller current ripples will bring the benefit of smaller torque ripples, which will effectively improve the control performance of the system. This has great practical significance in various industrial

applications. Moreover, the vibration and noise of the machine are also reduced given to the smaller torque ripples.

The proposed methods achieve distinct current ripple reduction while slightly increasing the switching frequency. For the basic FCSMPC, one voltage vector is applied during a sampling interval and there are possibilities that it applies same vectors in the adjacent sampling intervals. Therefore, the switching frequency of the basic FCSMPC could be lower than the sampling frequency. With the introduction of the virtual voltage vectors and duty cycle, the switching frequency could be increased since two switching states might be employed in one sampling interval. The switching frequency of the proposed-I is slightly increased as compared to that of the conventional techniques because three switching states might be utilized in the control scheme. Furthermore, the proposed-II utilizes the three-vector-scheme and consequently increases the switching frequency as compared to proposed-I and the conventional methods. Therefore, the current ripple minimization is the trade-off against the increase in the switching frequency.

The loss of the machine is also briefly analyzed. The copper loss of the proposed-I and proposed-II are 0.3% and 0.34% smaller than that of the basic FCSMPC. Furthermore, due to the lower phase current harmonic for the proposed methods, the core loss might be also lower than the basic FCSMPC. Due to the fact that the experimental setup is not equipped with torque sensor, the total loss is not analyzed here.

Chapter 6

Conclusion and Future Work

In this thesis, two FCSMPC methods with improved techniques have been presented to achieve current ripple minimization for high-performance control of PMSM drives.

The mechanism of the current ripples by FCSMPC has been carefully analyzed. The conventional techniques for reducing the current ripples of the FCSMPC-controlled PMSM drives have been fully discussed. Additionally, the FCSMPC with the conventional techniques have been implemented with the referenced IPMSM drive system, which provide significant benchmark references for the proposed methods.

An improved FCSMPC method with integrated duty cycle and finite virtual voltage vector technique has been proposed for the PMSM drives. In the proposed method, the finite control set is properly expanded by introducing six symmetrically located virtual voltage vectors in addition to the six basic active voltage vectors. The optimal voltage vector is selected among all the non-zero voltage vector candidates according to MPC's principle of minimizing the current-error-based cost function. Moreover, the corresponding duty ratio of the optimal voltage vector is calculated based on a straightforward principle with great computational efficiency. The proposed method is first validated in the simulation and then comparatively studied with the conventional methods through experiments with the

referenced IPMSM drive system. It is found in the experimental results that the FCSMPC with the proposed technique achieves better steady-state performance and low current ripples while maintains similar transient responses as compared to the FCSMPC with conventional techniques.

To further reduce the current ripples, an improved FCSMPC method with continuous virtual voltage vector technique has been proposed for the PMSM drives. In the proposed method, an optimal voltage vector is identified at first. This optimal voltage vector cannot be effectively applied to the electric machine by the basic FCSMPC or the FCSMPC with conventional techniques as it is a continuous voltage vector. In the proposed method, the optimal voltage vector is realized by at most two suboptimal voltage vectors and a null vector with corresponding duty cycle ratios. Moreover, the two suboptimal voltage vectors are found based on MPC's principle of minimizing the cost function and the corresponding duty ratios are calculated based on simple and computationally efficient mathematical relationships. The proposed method is first validated in the simulation and then comparatively studied with the conventional methods and the first proposed method through experiments with the referenced IPMSM drive system. It is found in the experimental results that the FCSMPC with the proposed technique significantly improves the steady-state performance with much lower current ripples while maintains similar transient responses as compared to the FCSMPC with conventional techniques and even with the first proposed technique.

This thesis has proposed two FCSMPC methods with improved techniques which achieve convincing effects on the current ripple reduction for the PMSM drives. However, there are interesting topics which can be further investigated based on the research in this thesis. More flexible virtual voltage vector injection schemes could be investigated to further improve the control precision and reduce the current ripples. Moreover, switching frequency could be investigated and concerned in the current ripple reduction control scheme of FCSMPC. Besides, the inverter nonlinearity may affect control accuracy and generate unexpected current ripples, which could be investigated in future work.

REFERENCES

[1] P. Waide and C. U. Brunner, *Energy-Efficiency Policy Opportunities for Electric Motor-Driven Systems.* Cedex, France: Int. Energy Agency, 2011.

[2] R. Saidura, S. Mekhilef, M. B. Ali, A. Safari, and H. A. Mohammed, "Applications of variable speed drive (VSD) in electrical motors energy savings," *Renew. Sustain. Energy Rev.*, vol. 16, no. 1, pp. 543–550, 2012.

[3] Y. Niwa and Y. Akiyama, "Propositions for the analysis of commutation phenomenon and the modeling of universal motors based on introducing the state function method into FEM electromagnetic field analysis," in *Proc. IEEE ECCE*, San Jose, CA, USA, Sept. 2009, pp.226-233.

[4] A. E. Fitzgerald, C. Kingsley, and S. D. Umans, *Electric Machinery.* New York: McGraw-Hill, 2003.

[5] S. Morimoto, Y. Tong, Y. Takeda, and T. Hirasa, "Loss minimization control of permanent magnet synchronous motor drives," *IEEE Trans. Ind. Electron.*, vol. 41, no. 5, pp. 511–517, Oct. 1994.

[6] J. Rodriguez and P. Cortes, *Predictive Control of Power Converters and Electrical Drives.* Hoboken, NJ, USA: Wiley, 2012.

[7] M. S. Merzoug and F. Naceri, "Comparison of field-oriented control and direct torque control for Permanent Magnet Synchronous Motor (PMSM)," *World Acad. Sci., Eng. Technol.*, vol. 45, pp. 300–305, Nov. 2008.

[8] Q. Liu and K. Hameyer, "A finite control set model predictive direct torque control for the PMSM with MTPA operation and torque ripple minimization," in *Proc. IEEE Int. Elect. Mach. Drives Conf.*, May 2015, pp. 804–810.

[9] X. Garcia, B. Zigmund, A. Terlizzi, R. Pavlanin, and L. Salvatore. (2011). Comparison between FOC and DTC strategies for permanent magnet synchronous motors. *Adv. Elect. Electron. Eng. [Online]*. 5 (1–2). Available: http://advances.utc.sk/index.php/AEEE/article/view/179

[10] C. Mademlis and V. G. Agelidis, "On considering magnetic saturation with maximum torque to current control in interior permanent magnet synchronous motor drives," *IEEE Trans. Energy Convers.*, vol. 16, no. 3, pp. 246–252, Sep. 2001.

[11] F. Blaschke, "The principle of field orientation as applied to the transvector closed-loop control system for rotating-field machines," *Siemens Rev.*, vol. 34, pp. 217–220, 1972.

[12] D. Casadei, F. Profumo, G. Serra, and A. Tani, "FOC and DTC: Two viable schemes for induction motors torque control," *IEEE Trans. Power Electron.*, vol. 17, no. 5, pp. 779–787, Sep. 2002.

[13] C. French and P. Acarnley, "Direct torque control of permanent magnet drives," *IEEE Trans. Ind. Applicat.*, vol. 32, pp. 1080–1088, Sept./Oct. 1996.

[14] L. Zhong, M. F. Rahman, W. Y. Hu, and K. W. Lim, "Analysis of direct torque control in permanent magnet synchronous motor drives," *IEEE Trans. Power Electron.*, vol. 12, pp. 528–536, May 1998.

[15] F. Korkmaz and R. G¨urb¨uz, “Comparative performance evaluation of FOC and DTC controlled PMSM drives,” in *Proc. 4th Int. Conf. Power Eng., Energy Elect. Drives*, Istanbul, 2013, pp. 705–708.

[16] M. Preindl and S. Bolognani, “Comparison of direct and PWM model predictive control for power electronic and drive systems,” in *Proc. IEEE App. Power Electron. Conf. Expo.*, Long Beach, CA, USA, Mar. 2013, pp. 2526–2533.

[17] C.-K. Lin, T.-H. Liu, J.-T. Yu, L.-C. Fu, and C.-F. Hsiao, “Model-free predictive current control for interior permanent-magnet synchronous motor drives based on current difference detection technique,” *IEEE Trans. Ind. Electron.*, vol. 61, no. 2, pp. 667–681, Feb. 2014.

[18] P. Cortes, M. P. Kazmierkowski, R. M. Kennel, D. Quevedo, and J. Rodriguez, “Predictive control in power electronics and drives,” *IEEE Trans. Ind. Electron.*, vol. 55, no. 12, pp. 4312–4324, Dec. 2008.

[19] T. Geyer, “Generalized model predictive direct torque control: Long prediction horizons and minimization of switching losses,” in *Proc. 48th IEEE Conf. Decision and Control (CDC) Held Jointly With 2009 28th Chin. Control Conf.*, Dec. 2009, pp. 6799–6804.

[20] J. H. Lee, “Model predictive control: Review of the three decades of development,” *Int. J. Contr. Autom. Syst.*, vol. 9, no. 3, pp. 415–424, 2011.

[21] Camacho, F. Eduardo, A. B. and Carlos. *Model Predictive Control.* Springer, London.

[22] J. A. Rossiter, Model Based Predictive Control—A Practical Approach. Boca Raton, FL: CRC Press, 2003.

[23] S. J. Qin and T. A. Badgwell, "A survey of industrial model predictive control technology," Control Eng. Pract., vol. 11, no. 7, pp. 733–764, Jul. 2003.

[24] M. H. Vafaie, B. Mirzaeian Dehkordi, P. Moallem, and A. Kiyoumarsi, "A new predictive direct torque control method for improving both steady-state and transient-state operations of PMSM," *IEEE Trans. Power Electron.*, vol. 31, no. 5, pp. 3738–3753, May 2016.

[25] M. Preindl, S. Bolognani, and C. Danielson, "Model predictive torque control with PWM using fast gradient method," in *Proc. IEEE App. Power Electron. Conf. Expo.*, Long Beach, CA, USA, Mar. 2013, pp. 2590–2597.

[26] J. Rodriguez, R. Kennel, J. Espinoza, M. Trincado, C. Silva, and C. Rojas, "High performance control strategies for electrical drives: An experimental assessment," *IEEE Trans. Ind. Electron.*, vol. 59, no. 2, pp. 812–820, Feb. 2012.

[27] P. Cortes, J. Rodriguez, D. E. Quevedo, and C. Silva, "Predictive current control strategy with imposed load current spectrum," *IEEE Trans. Power Electron.*, vol. 23, no. 2, pp. 612–618, Mar. 2008.

[28] W. Xie et al., "Finite-control-set model predictive torque control with a deadbeat solution for PMSM drives," *IEEE Trans. Ind. Electron.*, vol. 62, no. 9, pp. 5402–5410, Sep. 2015.

[29] E. J. Fuentes, C. Silva, D. E. Quevedo, and E. I. Silva, "Predictive speed control of a synchronous permanent magnet motor," in Proc. IEEE Int. Conf. Ind. Technol. ICIT 2009, 2009, pp. 1–6.

[30] M. Siami, D. A. Khaburi, and J. Rodriguez, "Simplified finite control set-model predictive control for matrix converter-fed PMSM drives," *IEEE Trans. Power Electron.*, vol. 33, no. 3, pp. 2438–2446, Mar. 2018.

[31] X. Cai, Z. Zhang, J. Wang, and R. Kennel, "Optimal control solutions for PMSM drives: A comparison study with experimental assessments," *IEEE J. Emerg. Sel. Topics Power Electron.*, vol. 6, no. 1, pp. 352–362, Mar. 2018.

[32] Y. Zhang and X. Wei, "Torque ripple rms minimization in model predictive torque control of PMSM drives," in *Proc. Int Electr. Mach. Syst. Conf.*, 2013, pp. 2183–2188.

[33] S. Nalakath, Y. Sun, M. Preindl, and A. Emadi, "Optimization-Based Position Sensorless Finite Control Set Model Predictive Control for IPMSMs," *IEEE Trans. Power Electron.*, vol. 33, no. 10, pp. 8672– 8682, 2018.

[34] M. Preindl and S. Bolognani, "Model predictive direct speed control with finite control set of PMSM drive systems," *IEEE Trans. Power Electron.*, vol. 28, no. 2, pp. 1007–1015, Feb. 2013.

[35] W. H. Kwon and S. Han, Receding Horizon Control. New York: Springer-Verlag, 2005.

[36] Y. Xu, B. Zhang, and Q. Zhou, "A model predictive current control method of PMSM based on the simultaneous optimization of voltage vector and duty cycle," in *Power Electronics and Motion Control Conference (IPEMC-ECCE Asia), 2016 IEEE 8th International*, 2016, pp. 881-884: IEEE.

[37] A. M. Bozorgi, M. Farasat, and S. Jafarishiadeh, "Model predictive current control of surface-mounted permanent magnet synchronous motor with low torque and current ripple," *IET Power Electron.*, vol. 10, no. 10, pp. 1120–1128, 2017.

[38] F. Morel, X. Lin-Shi, J.-M. Retif, B. Allard, and C. Buttay, "A comparative study of predictive current control schemes for a permanent-magnet synchronous machine drive," *IEEE Trans. Ind. Electron.*, vol. 56, no. 7, pp. 2715–2728, Jul. 2009.

[39] V. Yaramasu, M. Rivera, B. Wu, and J. Rodriguez, "Model predictive current control of two-level four-leg inverters—Part I: Concept, algorithm and simulation analysis," *IEEE Trans. Power Electron.*, vol. 28, no. 7, pp. 3459–3468, Jul. 2013.

[40] M. Rivera, V. Yaramasu, J. Rodriguez, and B. Wu, "Model predictive current control of two-level four-leg inverters—Part II: Experimental implementation and validation," *IEEE Trans. Power Electron.*, vol. 28, no. 7, pp. 3469–3478, Jul. 2013.

[41] A. A. Ahmed, B. K. Koh, H. S. Park, K. B. Lee, and Y. I. Lee, "Finite control set model predictive control method for torque control of induction motors using a state tracking cost index," *IEEE Trans. Ind. Electron.*, vol. 64, no. 3, pp. 1916–1928, Mar. 2017.

[42] P. Ramya and A. Sivaprakasam, "Model predictive direct torque control of PMSM with optimized duty cycle," IEEE 9th International Conference on Intelligent Systems and Control (ISCO), pp. 1-5, Coimbatore, 9-10 Jan., 2015.

[43] M. Leuer and J. Bocker, "Self-optimizing model predictive direct torque control for electrical drives," in *Proc. IEEE 24th Int. Symp. Ind. Electron.*, Jun. 2015, pp. 1046–1051.

[44] T. Geyer, G. Papafotiou, and M. Morari, "Model predictive direct torque control—Part 1: Concept, algorithm, and analysis," *IEEE Trans. Ind. Electron.*, vol. 56, no. 6, pp. 1894–1905, Jun. 2009.

[45] G. Papafotiou, J. Kley, K. Papadopoulos, P. Bohren, and M. Morari, "Model predictive direct torque control—Part 2: Implementation and experimental evaluation," *IEEE Trans. Ind. Electron.*, vol. 56, no. 6, pp. 1894–1905, Jun. 2009.

[46] M. Preindl and S. Bolognani, "Model predictive direct torque control with finite control set for PMSM drive systems, part 1: Maximum torque per ampere operation," *IEEE Trans. Power Electron.*, vol. 9, no. 4, pp. 1912–1921, Nov. 2013.

[47] C. Garcia, J. Rodriguez, C. Silva, C. Rojas, P. Zanchetta, and H. AbuRub, "Full predictive cascaded speed and current control of an induction machine," *IEEE Trans. Energy Convers.*, vol. 31, no. 3, pp. 1059–1067, Apr. 2016.

[48] T. Tarczewski and L. Grzesiak, "Constrained state feedback speed control of PMSM based on model predictive approach," *IEEE Trans. Ind. Electron.*, vol. 63, no. 6, pp. 3867–3875, Jun. 2015.

[49] Y. Zhang and H. Yang, “Two-vector-based model predictive torque control without weighting factors for induction motor drives,” *IEEE Trans. Power Electron.*, vol. 31, no. 2, pp. 1381–1390, Feb. 2016.

[50] Y. Zhang, J. Liu, G. Yuan, Z. Li, and H. Lou, "An improved model predictive control with duty cycle control for PMSM drives," in *Electrical Machines and Systems (ICEMS), 2016 19th International Conference on*, 2016, pp. 1-5: IEEE.

[51] K. S. Low, K. Y. Chiun, and K. V. Ling, “Evaluating generalized predictive control for a brushless dc drive,” *IEEE Trans. Power Electron.*, vol. 13, no. 6, pp. 1191–1198, Nov. 1998.

[52] R. Kennel, A. Linder,and M. Linke, “Generalized predictive control (GPC)-ready for use in drive applications?” in *Proc. 32nd Annu. IEEE PESC*, 2001, vol. 4, pp. 1839–1844.

[53] A. Linder and R. Kennel, “Model predictive control for electrical drives,” in *Proc. IEEE PESC*, Recife, Brazil, Jun. 12–16, 2005, pp. 1793–1799.

[54] J. Rodriguez et al., “State of the art of finite control set model predictive control in power electronics*,” IEEE Trans. Ind. Informat.*, vol. 9, no. 2, pp. 1003–1016, May 2013.

[55] L. Rovere, A. Formentini, A. Gaeta, P. Zanchetta, and M. Marchesoni, “Sensorless finite control set model predictive control for IPMSM drives,” *IEEE Trans. Ind. Electron.*, vol. 63, no. 9, pp. 5921–5931, Sep. 2016.

[56] S. Kouro, P. Cortes, R. Vargas, U. Ammann, and J. Rodriguez, "Model predictive control—A simple and powerful method to control power converters," *IEEE Trans. Ind. Electron.*, vol. 56, no. 6, pp. 1826–1838, Jun. 2009.

[57] T. Geyer, "A comparison of control and modulation schemes for medium-voltage drives: Emerging predictive control concepts versus PWM-based schemes," *IEEE Trans. Ind. Appl.*, vol. 47, no. 3, pp. 1380–1389, Mar. 2011.

[58] S. Bibian and H. Jin, "Time delay compensation of digital control for dc switch mode power supplies using prediction techniques," *IEEE Trans. Power Electron.*, vol. 15, pp. 835–842, Sept. 2000.

[59] P. Cortes, J. Rodriguez, C. Silva, and A. Flores, "Delay compensation in model predictive current control of a three-phase inverter," *IEEE Trans. Ind. Electron.*, vol. 59, no. 2, pp. 1323–1325, Feb. 2012.

[60] Y. Zhang, J. Zhu, and W. Xu, "Analysis of one step delay in direct torque control of permanent magnet synchronous motor and its remedies," in Proc. ICEMS, 2010, pp. 792–797.

[61] S. Chai and L. Wang, "Finite Control Set Model Predictive Control of 2LVSI-PMSM using interpolated switching states," *IECON 2012 - 38th Annual Conference on IEEE Industrial Electronics Society*, vol., no., pp.1799-1804, 25-28 Oct. 2012.

[62] Y. Zhang, D. Xu, and L. Huang, "Generalized Multiple-Vector-Based Model Predictive Control for PMSM Drives," *IEEE Transactions on Industrial Electronics*, pp. 1-1, 2018.

[63] Y. Zhang; L. Huang; L. Xu; L. Liu; L. Jin, "Performance Evaluation of Two-Vector-Based Model Predictive Current Control of PMSM Drives," *Chin. J. Electr. Eng.* 2018, 4, 65–81.

[64] Y. Zhang, D. Xu, J. Liu, S. Gao, and W. Xu, "Performance improvement of model predictive current control of permanent magnet synchronous motor drives," *IEEE Trans. Ind. Appl.*, vol. 53, no. 4, pp. 3683–3695, Jul./Aug. 2017.

[65] Y. Zhang, J. Liu, G. Yuan, Z. Li and H. Lou, "An improved model predictive control with duty cycle control for PMSM drives," in *Electrical Machines and Systems (ICEMS), 2016 International Conference on*, Chiba, 2016, pp. 1-5.

[66] Y. Zhang and J. Zhu, "A novel duty cycle control strategy to reduce both torque and flux ripples for DTC of permanent magnet synchronous motor drives with switching frequency reduction," *IEEE Trans. Power Electron.*, vol. 26, no. 10, pp. 3055–3067, Oct. 2011.

[67] Y. Zhang and J. Zhu, "Direct torque control of permanent magnet synchronous motor with reduced torque ripple and commutation frequency," *IEEE Trans. Power Electron.*, vol. 26, no. 1, pp. 235–248, Jan. 2011.

[68] Y. Zhou, H. Li, R. Liu, and J. Mao, "Continuous Voltage Vector Model-free Predictive Current Control of Surface Mounted Permanent Magnet Synchronous Motor," *IEEE Trans. Energy Convers.*, vol. 34, no. 2, pp. 899-908, June 2019.